Spring 2013

New methodologies for evaluating human biodynamic response and discomfort during seated whole-body vibration considering multiple postures

Jonathan DeShaw
University of Iowa

NEW METHODOLOGIES FOR EVALUATING HUMAN BIODYNAMIC RESPONSE AND DISCOMFORT DURING SEATED WHOLE-BODY VIBRATION CONSIDERING MULTIPLE POSTURES

by

Jonathan DeShaw

An Abstract

Of a thesis submitted in partial fulfillment of the requirements for the Doctor of Philosophy degree in Biomedical Engineering in the Graduate College of The University of Iowa

May 2013

Thesis Supervisor: Associate Professor Salam Rahmatalla

ABSTRACT

The lack of adequate equipment and measurement tools in whole-body vibration has imposed significant constraints on what can be measured and what can be investigated in the field. Most current studies are limited to single direction measurements while focusing on simple postures. Besides the limitation in measurement, most of the current biomechanical measures, such as the seat-to-head transmissibility, have discrepancies in the way they are calculated across different labs. Additionally, this field lacks an important measure to quantify the subjective discomfort of individuals, especially when sitting with different postures or in multiple-axis vibration.

This work begins by explaining discrepancies in measurement techniques and uses accelerometers and motion capture to provide the basis for more accurate measurement during single- and three-dimensional human vibration responses. Building on this concept, a new data collection method is introduced using inertial sensors to measure the human response in whole-body vibration. The results indicate that measurement errors are considerably reduced by utilizing the proposed methods and that accurate measurements can be gathered in multiple-axis vibration.

Next, a biomechanically driven predictive model was developed to evaluate human discomfort during single-axis sinusoidal vibration. The results indicate that the peak discomfort can be captured with the predictive model during multiple seated postures. The predictive model was then modified to examine human discomfort to whole-body vibration on a larger scale with random vibrations, multiple postures, and multiple vibration directions. The results demonstrate that the predictive measure can capture human discomfort in random vibration and during varying seated postures.

Lastly, a new concept called effective seat-to-head transmissibility is introduced, which describes how to combine the human body's biodynamic response to vibration from multiple directions. This concept is further utilized to quantify the human response using many different vibration conditions and seated postures during 6D vibration. The results from this study demonstrate how complicated vibrations from multiple-input and multiple-output motions can be resolved into a single measure. The proposed effective seat-to-head transmissibility concept presents an objective tool to gain insights into the effect of posture and surrounding equipment on the biodynamic response of the operators.

This thesis is timely as advances in seat design for operators are increasingly important with evolving armrests, backrests, and seat suspension systems. The utilization of comprehensive measurement techniques, a predictive discomfort model, and the concept of effective seat-to-head transmissibility, therefore, would be beneficial to the fields of seat/equipment design as well as human biomechanics studies in whole-body vibration.

Abstract Approved:

_____
Thesis Supervisor

_____
Title and Department

_____
Date

NEW METHODOLOGIES FOR EVALUATING HUMAN BIODYNAMIC RESPONSE AND DISCOMFORT DURING SEATED WHOLE-BODY VIBRATION CONSIDERING MULTIPLE POSTURES

by

Jonathan DeShaw

A thesis submitted in partial fulfillment of the requirements for the Doctor of Philosophy degree in Biomedical Engineering in the Graduate College of The University of Iowa

May 2013

Thesis Supervisor: Associate Professor Salam Rahmatalla

Graduate College
The University of Iowa
Iowa City, Iowa

CERTIFICATE OF APPROVAL

PH.D. THESIS

This is to certify that the Ph. D. thesis of

Jonathan DeShaw

has been approved by the Examining Committee
for the thesis requirement for the Doctor of Philosophy
degree in Biomedical Engineering at the May 2013 graduation.

Thesis Committee:

Salam Rahmatalla, Thesis Supervisor

Nicole Grosland

David Wilder

Fredric Gerr

Nathan Fethke

ACKNOWLEDGEMENTS

I would like to acknowledge the people in the 3D Bio-Motion research lab (3D-BMRL) at the Center for Computer Aided Design (CCAD) at the University of Iowa for their help and support with this thesis. I would like to especially thank John Meusch for his collaborations, assistance with experimentations, and spending many long hours helping with data processing. I also would like to thank Adam Scheer, Steph Swaitlo, Mike Steiff, Calvin Fehr, and Rosalind Smith for help with the experimentation setup and assistance with the motion capture and data analysis utilized in the 3D Bio-Motion research lab.

The experiment in chapter 6 was partially funded by Caterpillar Inc. of Peoria, Illinois, and was conducted at Sears Manufacturing of Davenport, Iowa. David Wilder of the Department of Biomedical Engineering and Laura Frey-Law of the Department of Physical Therapy at The University of Iowa helped in the experiment and the discussion of this article. Michael Contratto and Greg Kopp of Caterpillar, Dean Macken and Brad Parker of The University of Iowa, and Mike Drinkall and Jason Boldt of Sears Manufacturing helped in conducting the experiment.

Additionally, I would like to thank Ting Xia from the Palmer College of Chiropractic for his help with the lab setup and experimentation for the studies presented in Chapters 4 and 6. Ye Liu at CCAD assisted with MATLAB programming. The inertial sensors used in this work were provided by the U.S. Army Aberdeen Test Center (ATC).

I would also like to acknowledge and thank the members of my thesis committee, David Wilder, Nicole Grosland, Fred Gerr, and Nathan Fethke for their continual feedback and guidance during this learning process.

Furthermore, I would like to give a special thank you to Salam Rahmatalla for providing expertise and insights into human biodynamics during vibration and also for being a professional mentor over the years.

Finally, I would like to give thanks to my parents Phil and Jane DeShaw for being so patient throughout the years and keeping me focused during hectic times when managing duties between farm work, school work, and conducting research at the University of Iowa.

My sincere appreciation and thanks to all.

TABLE OF CONTENTS

LIST OF TABLES

LIST OF FIGURES

LIST OF ABBREVIATIONS

1D:..... one-dimensional

2D: .....two-dimensional

3D: .....three-dimensional

6D:..... six-dimensional

A/D:..... analog-to-digital

DC:..... direct current

deg:.....degrees

DOF:.....degrees of freedom

ESTHT:.....effective seat-to-head transmissibility

Hz:..... hertz

lb: ..... pound

m: ..... meter

m/s^2: .....meter-per-second-squared

mm: ..... millimeter

rad: ..... radian

rad/s^2.....radian-per-second-squared

RMS: ..... root-mean-square

sec: .....second

STHT:.....seat-to-head transmissibility

WBV: ..... whole-body vibration

PREFACE

This thesis is the direct result of many years of experimentation and research dealing with the question of how to effectively measure and evaluate human response to whole-body vibration. The chapters of this thesis consist of works published in many peer-reviewed journals or works that are currently submitted for review.

The thesis starts with a general introduction as to why whole-body vibration is a concern for health and safety, and what limitations are present for measuring and evaluating the human response. Because this thesis is part of many works, each chapter will have its own specific introduction as well as discussion. Chapter 1 begins by explaining discrepancies in measurement techniques using accelerometers and provides the basis of more accurate measurement for single- and three-dimensional human vibration responses. Building on this concept, Chapter 2 examines measurement discrepancies in whole-body vibration, and a new data collection method is introduced using inertial sensors from the methods presented in Chapter 1. Chapters 3 and 4 examine the role of single axis vibration on human discomfort and propose predictive equations for that discomfort. Chapter 5 modifies the methodology of Chapters 3 and 4 examining human discomfort to whole-body vibration on a larger scale with random vibrations, multiple postures, and multiple vibration directions. Chapter 6 introduces a new concept called effective-seat-to-head transmissibility, which examines how to combine the human body's response to vibration from multiple directions. Chapter 7 uses this concept to quantify the vibration response using many different vibration conditions and seated postures in 6D motion. The thesis concludes with a discussion on the specific finding of these works, the novel approaches found, and future potential applications for this work.

INTRODUCTION

The effect of vibration exposure on human discomfort, safety, and performance is a major concern in many occupations involving aircrafts, ships, automobiles, farming machinery, construction equipment, army vehicles, and other moving environments. Recent studies (Maeda et al., 2008; Schust et al., 2006; Morioka and Griffin, 2006; Rakheja et al., 2002; Subashi et al., 2009) have shown positive correlations between biomechanical responses and subjective perception and the amount of vibration transferred to the participants.

Limitations in the current research's equipment, measurements, and analysis tools in whole-body vibration (WBV) have imposed significant constraints on investigating seated human response to realistic field-motion. Most researchers acquire single axis motion platform, therefore most studies utilize artificial ride files in a single direction, mostly vertical and fore-aft (Mansfield, 2005B; Wang et al., 2004; Fairley and Griffin, 1989; Paddan and Griffin, 1988A).

In terms of measurement, accelerometers are considered the standard sensors in this field, and therefore, the measurements of the 6 degrees of freedom of the body segments become impractical. Additionally, it is very hard to use accelerometers to define the various postures that have considerable role on the human response to WBV. Besides the limitation of equipment and measurements, current analysis tools such as seat-to-head transmissibility are still suffering from several uncertainties and are still having difficulties in achieving meaningful measures in multiple-axis WBV. Additionally, the field of human biodynamic in WBV is still lacking critical discomfort

measures that can play major roles in the development of biodynamical human models and the design of effective suspension systems.

Historically, measurements in WBV are conducted using accelerometers (Griffin, 1990). Theoretically, six accelerometers should be used to describe the three-dimensional motion of each body segment. Furthermore, due to the nonlinear relationship between the linear and angular kinematics variables and the influence of the gravity-related terms and drift, nine accelerometers (Padgaonkar et al., 1975) are needed to resolve the complete kinematics. As a result, a very high number of sensors with connection wires are required for whole-body motion analysis, and this may affect a participant's normal movements.

To circumvent the accelerometers' problems, a hybrid system is presented in this work where accelerometers and motion capture data from markers are combined to get the most accurate results. In this process, one accelerometer is attached to each segment with three to four orthogonal markers placed on the accelerometer body. With this arrangement, the accelerometer's local coordinate system can be related to the global coordinate systems, making it possible to investigate the relationship between the motions of any segments of the body without worrying about their location and orientation in the space. This is crucial and could be very beneficial to any multiple-axis WBV study.

Researchers have realized there is an effect of posture on human response and risk evaluation in WBV (Kitazaki and Griffin, 1998; Paddan and Griffi, 1998; Hinz et al., 2002; Johanning et al., 2006; Okunribido et al., 2008; Wang et al., 2008; Baker and Mansfield, 2010). Wang et al. (2006B) found a significant effect of sitting posture on the biodynamic response under vertical vibration after considering 36 different sitting

postures and seat configurations. There are many occupations where people need to use non-neutral postures to monitor their equipment while both the person and the equipment are under vibration (Kittusamy and Buchholz, 2004; Rehn, Nilsson et al., 2005; Thuresson, et al., 2005; Eger et al., 2008; Newell and Mansfield, 2008). Because of the complicated vibration environments, seating configurations, posture configurations, and vehicle suspension systems it is nearly impossible to define the human response to each. Therefore, it would be extremely useful to have a measurement tool that capture human sensitivity to vibration in any condition.

Current biomechanical measures such as transmissibility (Paddan and Griffin, 1998; Paddan and Griffin, 2000; Wang et al., 2008)have shown encouraging and consistent correlations with the subjective-reported discomfort measures; however, they showed sensitivity to the body postures and to the interaction of participants with the surrounding equipment (Wang et al., 2008).

In this work, a new musculoskeletal-based predictive measure is introduced for the evaluation of discomfort in WBV during fore-aft discrete frequency rides with people taking non-neutral postures. The hypothesis behind the proposed discomfort measure is that the head-neck discomfort is sensitive to the neck posture relative to the neck neutral position (Kee and Karwowski, 2001; Kee and Karwowski, 2003) and to the rate of angular change of the head-neck motion. This biomechanically based predictive discomfort measure (Rahmatalla and DeShaw, 2011) can then be extended for the evaluation of discomfort for multiple joints (DeShaw and Rahmatalla, 2011). The predictive discomfort measure developed has the distinct advantage that it is less vulnerable to measurement locations than is other measures such as seat-to-head

transmissibility.

The seat-to-head transmissibility (STHT) is a widely used biomechanical measure in whole-body vibration (WBV) for the quantification of the energy transferred through the body (Demic and Lukic, 2009; Griffin, 1990; Jack and Eger, 2008; Wang et al., 2008). The general uncertainty in the calculation of the STHT in terms of its sensitivity to the location of the output point on the head makes it very hard to compare results between different labs and conditions. Paddan and Griffin (1992) noticed significant changes in the STHT when they used different locations for the output point on the head and showed that the pitch motion of the head-neck region considerably affects the STHT.

The STHT contains another uncertainty in the way people calculate it. In a comprehensive study on transmissibility, Paddan and Griffin (1998) calculated the STHT using only a single motion component (for example, the fore-aft) of the output point on the head and a single-input motion component (fore-aft) on the seat. Other researchers, such as Wang et al. (2008), used the norm of the motion (fore-aft, lateral, and vertical) at the output point on the head and a single direction motion of the seat to calculate the STHT. Within this context, the frequency-dependent transmissibility matrix for multiple-input/multiple-output (Preumont et al., 2006) is normally composed as the ratio between the input and output signals.

Researchers in the area of human response to whole-body vibration (WBV) would agree, in general terms, on the potential of the seat-to-head transmissibility (STHT) in capturing the perception of vibration of seated people for single-input/single-output motions (Griffin, 1990; Qiu and Griffin, 2003; Demic and Lukic, 2009; Paddan and Griffin, 1998; ISO 2631-1). This traditionally results in a single graph, which has been

used widely as a measure of seat effectiveness and as an indication of the amount of vibration transferred through the body (Demic and Lukic, 2009; Wang et al., 2008). However, for real-life scenarios the input motion normally comprises single- or multiple-axis components; likewise, the output motion on the body would normally have multiple-axis components. In such cases, the STHT matrix contains a full matrix with many out-of-diagonal cross-axis elements (Preumont et al., 2006; Smith et al., 2008; Qui and Griffin, 2004); therefore, it becomes very hard to infer the most effective information from it.

In this work, the concept of the effective seat-to-head transmissibility (ESTHT) is introduced, in which the single-input/multiple-output and multiple-input/multiple-output transmissibility matrix is transformed into a single graph, similar to those for single-input and single-output. The singular value decomposition and maximum distortion energy theory were used to achieve that goal.

Motivation:

- The lack of adequate equipment and measurement tools in WBV has imposed significant constraints, limitations on what can be measured, and what can be investigated in this field. For example, most current studies are limited to single direction WBV with the participant taking simple postures.
- Besides the limitation in measurements, most of the current biomechanical measures such as the seat-to-head transmissibility are limited to single directions and have inconsistency in terms of the way they are calculated in different labs.

- The field of WBV is also lacking an important measure to quantify the discomfort of participants, especially when sitting with different postures.

Thesis Objectives:

1. Introduce effective tools to measure human response to whole-body vibration in a more precise and comprehensive manner

2. Investigate the effectiveness and limitations of the current seat-to-head transmissibility and compare that with the subjective measures

3. Introduce a new musculoskeletal-based predictive measure for the evaluation of discomfort in WBV with people in multiple postures

4. Develop a new seat-to-head transmissibility measure, called effective transmissibility, to investigate human response in complex multiple-axis whole-body vibration

CHAPTER 1: IMPROVED METHOD FOR ACCELEROMETERS USING MOTION CAPTURE[1]

1.1 Introduction

Accurate measurements of human response to whole-body vibration are essential to any conclusions about the health risks, discomfort, and the assessment of seat suspension systems in vibration environments. While accelerometers are traditionally considered the main measurement tools in whole-body vibration studies, their measurements become questionable when they are attached to inclined surfaces or when the motion has multiple directions. A correction methodology using motion capture data to aid traditional accelerometers was used in this work to quantify human response under single fore-aft, single-vertical, and multiple-axis whole-body vibration.

Traditionally, DC accelerometers have been the standard for collecting motion data in whole-body vibration (Griffin, 1990). DC accelerometers are very useful measuring tools; however, DC accelerometers pose two major difficulties: (i) components of gravity are present in the acceleration measurement, and (ii) they only can measure local acceleration. Accelerometers normally measure the local acceleration at a point in the direction of motion; therefore, an accelerometer should be attached to the surface such that its local axis is aligned with the direction of motion. Theoretically, six accelerometers should be used to describe the three-dimensional motion of each body segment. Furthermore, due to the nonlinear relationship between the linear and angular kinematics variables and the influence of the gravity-related terms and drift, nine

[1] Selected material presented at the 46th UK Conference on Human Responses to Vibration. *Rahmatalla, S.; DeShaw, J. A Hybrid System for Simultaneous Measurements of Vibration and Posture.* 46th UK Conference on Human Responses to Vibration, *Buxton, England 20-22 Sept 2011*.

accelerometers (Padgaonkar et al., 1975) are needed to resolve the complete kinematics. As a result, a very high number of sensors with connection wires are required for whole-body motion analysis, a process that becomes cumbersome and may affect the participant's normal movements.

To resolve these problems, a new hybrid system for capturing acceleration and motion data is introduced in this work. The new hybrid system developed utilizes motion capture data to calculate the orientation of the accelerometers relative to a global coordinate system. Once the global orientation is resolved the gravity components of each accelerometer axis can be accounted for and thus subtracted out of the accelerometer readings. With this arrangement, the accelerometer's local coordinate system can be related to the global coordinate systems, making it possible to investigate the relationship between the motions of any segments of the body without worrying about their location and orientation in the space. This is crucial to any multiple-axis WBV study. This system has the potential for usefulness in many labs and applications where accelerometers are used.

The objective of this work is to introduce a standardized measurement correction methodology in single and multiple WBV to minimize measurement errors when dealing with inclined surfaces or multi-directional motion. The proposed methodology has been validated in a simulation vibration environment and demonstrated in terms of the seat-to-head transmissibility.

1.2 Methodology

1.2.1 Gravity Components in DC Accelerometer Measurements

The gravity component (G) in the DC accelerometers can be used for calibration

purposes and when measuring inclination angles; however, it creates difficulties when the sensor is installed on inclined surfaces and when used for dynamic measurement of motions. For example, for situations when the accelerometer is attached to a flat, horizontal plane, the *G* component can be compensated for as it has no effect on the acceleration in the X-direction and can be subtracted from the vertical component of the acceleration if the motion is in the vertical direction. However, when the accelerometer is attached to inclined surfaces (Figure 1.1), as is the case with many locations on the human body, the *G* term will have components in $\mathbf{X_L}$ and $\mathbf{Y_L}$ and $\mathbf{Z_L}$ directions of the acceleration and will become change as the angle of the accelerometer changes with respect to gravity.

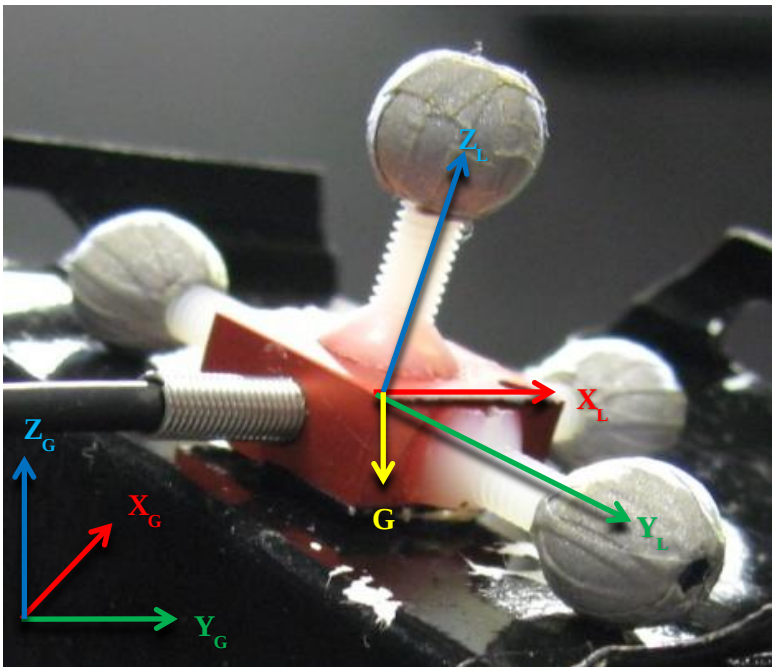

Figure 1.1 Example of an accelerometer where X_L, Y_L, and Z_L are the local axes of the accelerometer and where X_G, Y_G, and Z_G are global axes of the reference system. The acceleration of gravity (*G)* will be present in each component of the local accelerometer axes depending on the accelerometer orientation.

The need for multiple accelerometers to resolve the complete kinematics of a body is a limitation that can be overcome once the local coordinate system of the accelerometer is known. Depending on the application, one may wish to know the acceleration measurement in either local or global space; however, the use of DC accelerometers can present a problem if the measurement of gravity is not desired. Figure 1.2 shows a typical global and local coordinate system with the gravity vector (G) present.

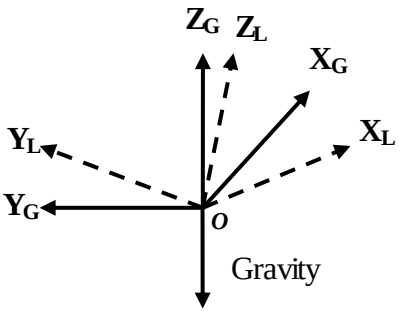

Figure 1.2 Local and global coordinate systems where the global system is represented by solid lines, the local system is represented by dashed lines, and the gravity vector (G) is oriented along the global $-Z_G$ axis.

The contribution from gravity can be determined by multiplying the transformation matrix $\mathbf{R}_{L/G}$ with the magnitude of gravity (-9.81 in the global Z direction). One way to eliminate the gravity components from the accelerometer's reading is to attach a local coordinate system to the accelerometer, which makes it possible to extract the real acceleration signal and isolate the gravity components, and to transform the acceleration signal in any desired direction.

1.2.2 Use of Motion Capture to Determine Accelerometer Orientation

Currently, marker-based motion capture systems have many applications in biomechanical studies (Gal et al., 1997; Boyer and Nigg, 2007; Chu and Caldwell, 2004;

Rahmatalla et al., 2008). With advanced technology in motion capture, it is possible to collect data with a sampling rate of more than 500 Hz and a high resolution reaching 0.01 mm. These systems have been shown to be accurate and repeatable. There are many advantages to using optical motion capture systems to collect motion data in WBV environments. First, the markers are low-weight passive sensors, meaning that they are merely reflective surfaces and can be attached easily to any area on the body of the participant. They are also immune to electromagnetic fields. Second, theoretically, only three markers are required to define the three-dimensional velocity and acceleration of each body segment; using more markers will increase accuracy, but there is a point at which the incremental improvement in accuracy is not meaningful. Still, as is the case with other sensors (i.e. accelerometers, EMG sensors, etc) markers can still be sensitive to skin movement (Cereatti et al., 2006; Lucchetti et al., 1998) and occlusions where the markers disappear from the camera scenes when an object comes between them. Most importantly, the finite differences acceleration based on marker displacement data becomes questionable at higher frequencies.

1.2.3 Hybrid Marker-Accelerometer System

The proposed system of this work is the hybrid marker-accelerometer system, which is composed of tri-axial DC accelerometers (Dytran 7523A1, Chatsworth, CA) fitted with four infrared reflective markers each (Figure 1.3). A 12-camera, V8i Vicon motion capture system (Vicon, Los Angeles, CA, USA) was used to collect data at 200 Hz. The motion capture data was synchronized with the accelerometer data at 200 Hz. The motion capture data was synchronized with the accelerometer data at 200 Hz. Static and dynamic trials in 3D vibration where captured and used in the analysis.

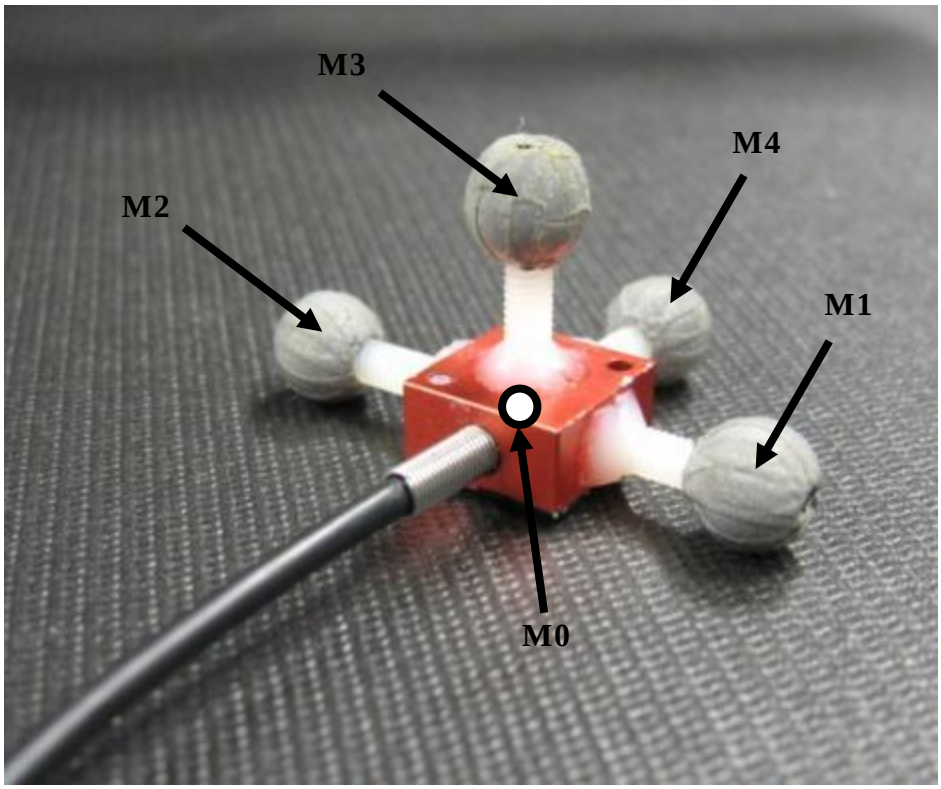

Figure 1.3 A tri-axial DC accelerometer with 4 retro-reflective motion capture markers (M1-M4) attached as a guide for its local coordinate system. M0 is the calculated center of the accelerometer.

The local coordinate system of the accelerometer is determined using the positions of markers M1, M2, and M3, with M4 as an extra additional marker to assist in defining the center of the coordinate system (M0) and to help in filling the markers in case of occlusion. Because the markers are placed orthogonally to one another the orientation vectors can be found by simply subtracting one point in space from another along the each of the three directional axes. A program written in MATLAB was utilized to compute the unit vectors to form rotation matrix with respect to global for each frame at 200 frames per second. The transformation matrix between the right-hand local coordinate system and a global system can be defined using the following transformation

matrix:

$$[R_{L/G}] = \begin{bmatrix} X_G \bullet X_L & Y_G \bullet X_L & Z_G \bullet X_L \\ X_G \bullet Y_L & Y_G \bullet Y_L & Z_G \bullet Y_L \\ X_G \bullet Z_L & Y_G \bullet Z_L & Z_G \bullet Z_L \end{bmatrix} \quad \text{(Eq. 1.1)}$$

where $\mathbf{X_G}$, $\mathbf{Y_G}$, and $\mathbf{Z_G}$ are the unit vectors (basis) of the global system, and $\mathbf{X_L}$, $\mathbf{Y_L}$, and $\mathbf{Z_L}$ are the unit vectors (basis) of the local system. Next, the contribution from gravity needs to be determined by multiplying the transformation matrix $\mathbf{R}_{L/G}$ with the magnitude of gravity (-9.81 in the global Z direction). The gravity contribution is then removed from the accelerometer measurement in the local coordinate system, as shown in equation 1.2. This calculation is performed at each time step of the sampling frequency, where A_{X_L}, A_{Y_L} and A_{Z_L} are the local raw-acceleration components and $\overline{A_{X_L}}$, $\overline{A_{Y_L}}$ and $\overline{A_{Z_L}}$ are now the local accelerometer measurements where the gravity is removed.

$$\begin{bmatrix} \overline{A_{X_L}} \\ \overline{A_{Y_L}} \\ \overline{A_{Z_L}} \end{bmatrix} = \begin{bmatrix} A_{X_L} \\ A_{Y_L} \\ A_{Z_L} \end{bmatrix} + \mathbf{R}_{L/G} * \begin{bmatrix} 0 \\ 0 \\ G \end{bmatrix} \quad \text{(Eq. 1.2)}$$

Now the accelerometer measures are corrected without the gravity component present; however, its measurement is still in its local coordinate system. Finally, if

desired, the local coordinate system can be transformed using the inverse of the transformation matrix $\mathbf{R}_{L/G}$ to transform to the global coordinate system as in equation 1.3:

$$\begin{bmatrix} \overline{A_{X_G}} \\ \overline{A_{Y_G}} \\ \overline{A_{Z_G}} \end{bmatrix} = \mathbf{R}_{L/G}^{-1} * \begin{bmatrix} \overline{A_{X_L}} \\ \overline{A_{Y_L}} \\ \overline{A_{Z_L}} \end{bmatrix} \quad \text{(Eq. 1.3)}$$

where $\overline{A_{X_G}}$, $\overline{A_{Y_G}}$ and $\overline{A_{Z_G}}$ compose the acceleration measurement in the global coordinate system with the gravity component removed.

1.3 Results

1.3.1 Validation of the Marker-Accelerometer System

The proposed hybrid system was first tested using an off-axis testing apparatus in a multiple vibration environment (Figure 1.4). A six-degree-of-freedom man-rated motion platform (Moog-EDU 624-1800 electrical system, Moog-FCS, Ann Arbor, MI, USA) was used to test the proposed hybrid system. This arrangement allows all three accelerometer axes to be off-alignment with respect to the global coordinate system (fore-aft, lateral, and vertical). The apparatus was attached rigidly to the shaking platform. For this dynamic vibration test, the shaker platform produced random vibration in the global x-axis (fore-aft direction) for 10 seconds between 0.5 and 12 Hz. Data were collected at 200 frames per second for all accelerometer measurements and synchronized with the motion capture data, which were also collected at 200 frames per second.

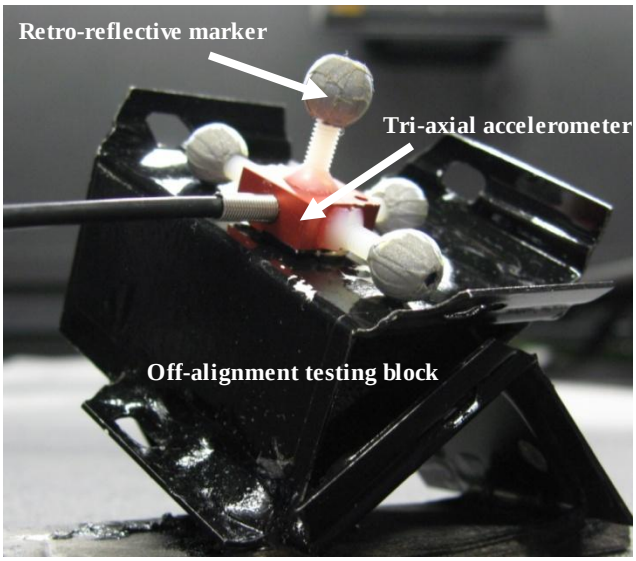

Figure 1.4 Testing block for dynamic vibration tests where all three accelerometer axes were rotated off-alignment from the global coordinate system. The testing block was rigidly attached to the motion shaker platform.

Figure 1.5a shows the raw local acceleration data of the dynamic vibration test where an acceleration signal is present in each axis. Each signal is not centered on zero since it is measuring the vibration acceleration magnitude with the gravity components present. Here it is hard to measure the true acceleration generated by the shaker; because the acceleration is local and arbitrary, one cannot tell the orientation or true acceleration (except for gravity) from this data. The signals are centered around 2.0, -3.5, and 8.5 m/s^2 for the channels X, Y, and Z, respectively. Figure 1.5b then shows the acceleration of the dynamic vibration test in the local coordinate system with the gravity component removed from the signal. Note that the signal is still present in all axes; however, the signal is centered on zero because the gravity component has been removed. Finally, Figure 1.5c shows the acceleration signal after being transformed to the global coordinate

system. The signal is now present in only the X-axis (fore-aft) and aligned with the global reference.

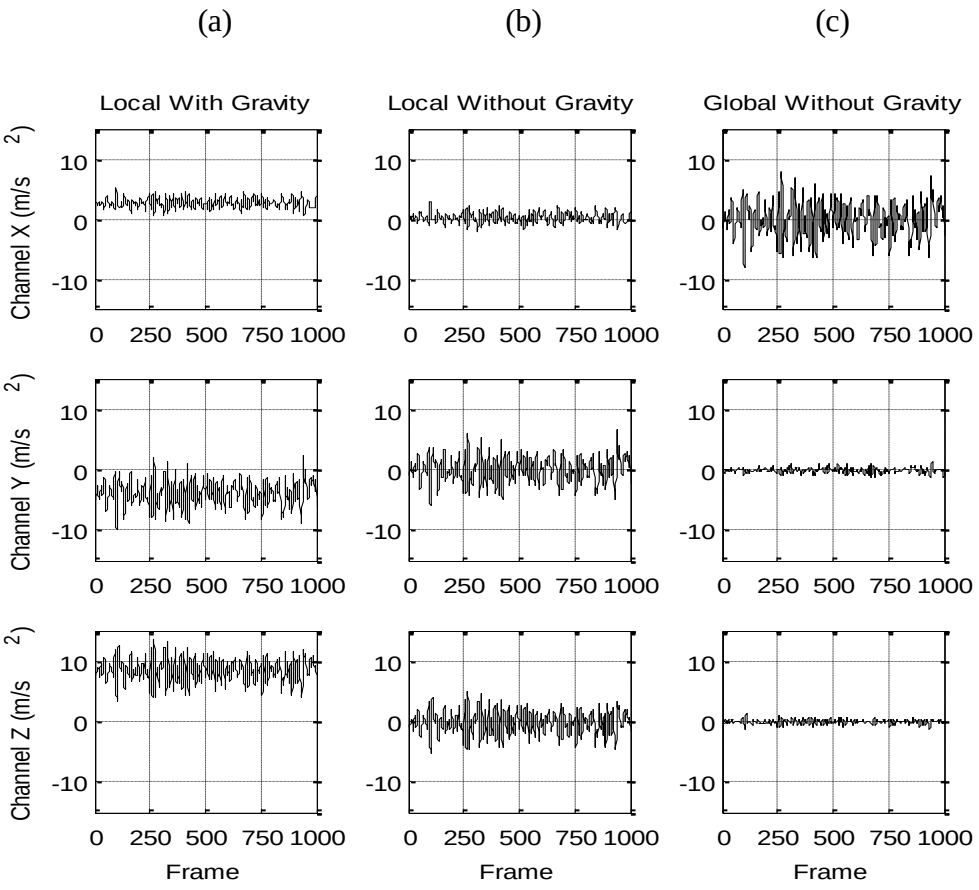

Figure 1.5 Acceleration measurement signals for channels X, Y, and Z during random fore-aft vibration (X- global direction) where (a) is the local acceleration with gravity present, (b) is the local acceleration with gravity removed from measurement, and (c) is the global acceleration with gravity removed from measurement.

1.3.2 Test-Participant Data in WBV

One participant was recruited and tested with the developed methodologies in seated WBV scenarios. Written informed consent, as approved by the University of Iowa Institutional Review Board, was obtained prior to testing. For the seated WBV condition,

the participant assumed an upright backrest-supported posture on an agriculture-based seat. The participant faced forward with his hands on his lap, as shown in Figure 1.6a, and was exposed to random fore-aft WBV and random 3D WBV. A tri-axial accelerometer with three markers attached for a guide was mounted to a head-mounted halo worn by the participant (Figure 1.6b).

(a) (b)

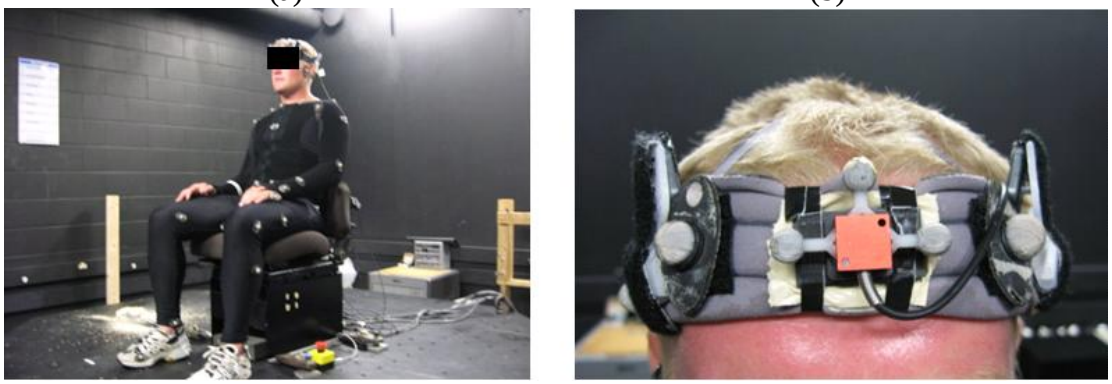

Figure 1.6 One participant seated on agriculture seat (a) where a head-mounted halo (b) was worn with an accelerometer and three markers attached.

The same marker/accelerometer hybrid system methodology was used to remove gravity from the signal, and then the individual motion components were extracted in the global coordinate system. The transmissibility for the individual motion components can be seen in Figure 1.7a for random fore-aft vibration. It can be seen that up to around 4 Hz the predominant motion response is in the fore-aft motion component. Additionally, between 3 and 6 Hz, a large motion component is seen in the vertical direction. The graph in Figure 1.7b shows the overall seat-to-head transmissibility where the resultant of the motion in all directions is used as the output.

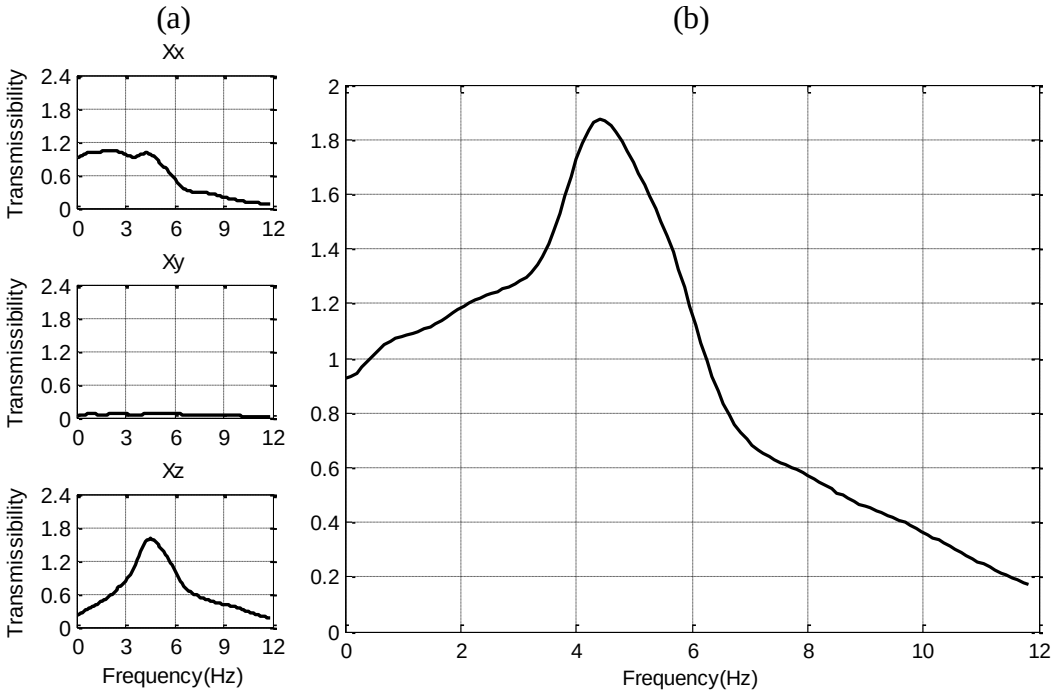

Figure 1.7 The seat-to-head-transmissibility components where uppercase X represents the input fore-aft motion and the lowercase x, y, and z represent the fore-aft, lateral, and vertical output motions, respectively. The figure on the left (a) represents the individual components while the figure on the right (b) represents the overall seat-to-head transmissibility where the resultant of the head motion is used as the output.

Figure 1.8 shows the nine different seat-to-head transmissibility components using the global coordinate system as the reference in 3D WBV. The fore-aft input to fore-aft output seat-to-head transmissibility gradually diminished with higher frequencies. The lateral input–lateral output seat-to-head transmissibility peaked at around 1 Hz where the vertical input–vertical output transmissibility peaked at around 4.5 Hz. The greatest peak in any direction had a magnitude of around 2.0 and occurred at 5 Hz, where the cross-coupled motion of the fore-aft input and vertical output was predominant. Other cross-coupled motions were seen but were not as distinguishable. The proposed method shows how the motion components can be extracted and used to

find individual transmissibility parts.

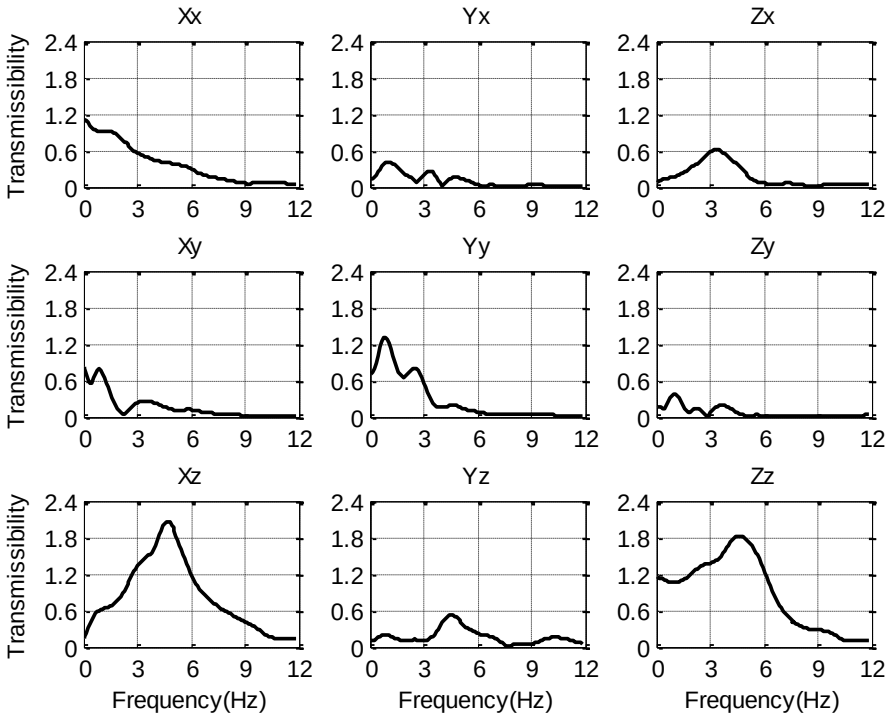

Figure 1.8 Seat-to-head-transmissibility components in 3D random vibration where uppercase letters designate the input motion components and lowercase letters represent the output motion components.

1.4 Discussion

In this work we have shown that once the local orientation of an accelerometer is known, then the gravity component can be removed and the individual components of motion can be decoupled. This indicates that if the orientation of the accelerometer is known in global space the need for multiple accelerometers on a rigid body segment is eliminated.

The proposed measurement techniques described in this paper allow researchers to analyze the motion in a way that is extremely difficult to do traditionally. For example,

no other studies were found that address correction in 3D vibration environments. The ability to monitor the 3D accelerometer orientation at a high sampling rate and accuracy makes the method presented in this paper extremely powerful. With this system, it becomes possible to investigate various biodynamical measures in any direction with a clear picture of the relationship between the direct and cross components of the motion.

Motion capture is a very reliable tool but has slight disadvantages. For example, the accuracy of removing the gravity is mainly dependent on how orthogonally the markers are placed to one another on the accelerometer. Second, markers are prone to occlusion, and that may affect the accuracy of their positions. Motion capture is reliable for measuring gross motion and acceleration in low-frequency vibration; however, with higher-frequency vibration, the acceleration data derived from marker-based positional data become unreliable due to resolution limitations and the need to use finite differences to calculate the acceleration. The proposed hybrid system, however, does not have these issues because it can measure accelerations from a tri-axial accelerometer and use the motion capture marker-based data only as a guide for position and orientation.

1.5 Conclusion

This work has introduced an acceleration measurement system for WBV studies in which a hybrid marker-accelerometer system overcomes current measurement difficulties, eliminates the need for multiple accelerometers, and can add accuracy when the vibration motion has multiple directions. The method presented has great potential for use in other labs, as it is easily reproducible and has the possibility to extend to multiple rigid body segments to monitor human motion. Being able to decouple the acceleration of motions in any reference direction will also make it more accurate for defining single-

directional transmissibility in any desired direction. The results also have demonstrated the flexibility in using the proposed systems by eliminating the gravity component from the accelerometer signals and by decoupling and transforming the acceleration components from the local system to the desired global system in multiple-axis whole-body vibration.

CHAPTER 2: COMPREHENSIVE MEASUREMENT IN WHOLE-BODY VIBRATION[2]

2.1 Introduction

Traditional measurements in whole-body vibration (WBV) studies using accelerometers present an effective way to quantify human response to WBV (Griffin, 1990). However, due to practical reasons, accelerometer readings are prone to misinterpretations, which may affect the quality of the resulting biodynamic response measurement and may result in inconsistency in the collected data across different labs. Many researchers in the field (Madakashira-Pranesh, 2011; Huang and Griffin, 2009; Matsumoto and Griffin, 1998; Smeathers, 1989) have found that the misalignment of the accelerometer due to the curvature of the human body and postural changes during the experiment can greatly alter the magnitude and frequency content measured. Correction schemes are normally applied to the accelerometer reading when it is attached to inclined surfaces (Madakashira-Pranesh, 2011; Huang and Griffin, 2009; Matsumoto and Griffin, 1998; Smeathers, 1989); however, these corrections are limited and would not be accurate with large postural changes or multidirectional motion.

Accelerometers normally measure the local acceleration at a point in the direction of motion; therefore, an accelerometer should be attached to the surface such that its local axis is aligned with the direction of motion. This process could be suitable for single-axial input motion where the output and input points move approximately in the same direction. However, the latter process will introduce errors if the input and output points

[2] Published in the Journal of Low Frequency Noise, Vibration and Active Control.
DeShaw, J.; Rahmatalla, S. Comprehensive measurement in whole-body vibration. *Journal of Low Frequency Noise, Vibration and Active Control*. **2012,** 31(2), 63-74.

have motion components in multiple directions (Hinz et al., 2010; Paddan and Griffin, 1988A; Paddan and Griffin, 1988B).

Recently, inertial systems have shown encouraging performance and wide applications with more systems capable of recording tri-axial linear accelerations, tri-axial angular velocities, and orientation in the global space. These sensors could be very beneficial to any multiple-axis WBV study where the sensor local coordinate system can be related to the global coordinate system, making it possible to remove the gravity effect (*G* component) in the sensor and to investigate the relationship between the motions of any segments of the body without concern regarding their location and orientation in the space. However, inertial systems could be sensitive to the electromagnetic fields and may drift like traditional accelerometers with time.

The objective of this work is to introduce a comprehensive measurement correction methodology in single- and multiple-axis WBV to minimize acceleration measurement errors when dealing with inclined surfaces, coupled motion, or multidirectional motion. The effectiveness of the proposed methodology was demonstrated in terms of the seat-to-head and seat-to-C7 transmissibility of twelve seated participants maintaining supported-back and unsupported-back upright posture during single-fore-aft, single-vertical, and multiple-axis WBV.

2.2 Methodology

2.2.1 Gravity Components in Accelerometer Measurements

The gravity component (G) in the DC accelerometers can be used for calibration purposes and when measuring inclination angles; however, it creates difficulties when the sensor is installed on inclined surfaces for dynamic measurement of motions. For

situations when the accelerometer is attached to a flat, horizontal plane (Figure 2.1a), the G component can be compensated for because it has no effect on the acceleration in the X-direction and can be subtracted from the vertical component of the acceleration if the motion is in the vertical direction. However, when the accelerometer is attached to inclined surfaces, as is the case with many locations on the human body, the G term will have components in both the XL and YL directions of the acceleration and will become more significant as the angle θ increases (Figure 2.1b). The problem becomes more involved if the accelerometer has two planes of inclinations; in this case, the acceleration from gravity will have components in the XL, YL, and ZL directions.

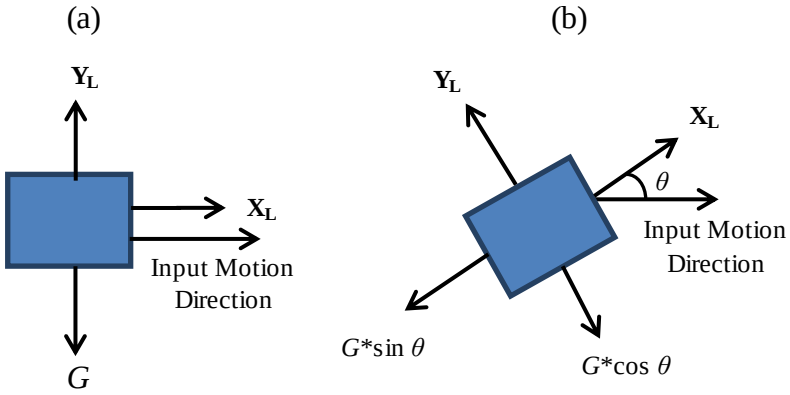

Figure 2.1. Orientation of accelerometer where X_L and Y_L are the local axes of the accelerometer where (a) the *G* component is easily known and (b) the *G* component depends on inclination angle θ.

The need for multiple accelerometers to resolve the complete kinematics of a body is a limitation that can be overcome once the local coordinate system of the accelerometer is known. Depending on the application, one may wish to know the acceleration measurement in either local or global space; however, the use of DC

accelerometers can present a problem if the measurement of gravity is not desired.

The inertial sensors have advantages over the traditional accelerometers due to their ability to provide additional information about the segment's kinematics. Each inertial sensor is comprised of 3D gyroscopes, 3D accelerometers, and 3D magnetometers, which give the sensor the ability to provide absolute orientation values, therefore making it possible to extract the real acceleration signal and isolate the gravity components. The inertial sensors used in this work, as one available inertial system, are MTx inertial trackers (Xsens Technologies, Enschede, Netherlands) in which the transformation matrix between the right-hand local coordinate system and a global system is defined as

$$\mathbf{R}_{L/G} = \begin{bmatrix} a^2+b^2-c^2-d^2 & 2bc-2ad & 2bd+2ac \\ 2bc+2ad & a^2-b^2+c^2-d^2 & 2cd-2ab \\ 2bd-2ac & 2cd+2ab & a^2-b^2-c^2+d^2 \end{bmatrix} \quad \text{(Eq. 2.1)}$$

where the unit quaternion $\mathbf{z} = a + b\mathbf{i} + c\mathbf{j} + d\mathbf{k}$ and $|\mathbf{z}| = 1$.

The contribution from gravity can be determined by multiplying the transformation matrix $\mathbf{R}_{L/G}$ with the magnitude of gravity (-9.81 in the global Z direction). The gravity contribution can then be removed from the inertial sensor's acceleration measurement in the local coordinate system, as shown in Equation 2.2. This calculation is performed at each time step of the sampling frequency, where A_{X_L}, A_{Y_L}, and A_{Z_L} are the local raw-acceleration components and $\overline{A_{X_L}}$, $\overline{A_{Y_L}}$, and $\overline{A_{Z_L}}$ are now the local accelerometer measurements where the gravity is removed.

$$\begin{bmatrix} \overline{A_{X_L}} \\ \overline{A_{Y_L}} \\ \overline{A_{Z_L}} \end{bmatrix} = \begin{bmatrix} A_{X_L} \\ A_{Y_L} \\ A_{Z_L} \end{bmatrix} + \mathbf{R}_{L/G} * \begin{bmatrix} 0 \\ 0 \\ G \end{bmatrix} \qquad \text{(Eq. 2.2)}$$

Although the accelerometer measures are corrected without the gravity component present, its measurement is in its local coordinate system. If desired, the local coordinate system can be transformed to the global coordinate system as in Equation 2.3:

$$\begin{bmatrix} \overline{A_{X_G}} \\ \overline{A_{Y_G}} \\ \overline{A_{Z_G}} \end{bmatrix} = \mathbf{R}_{L/G}^{-1} * \begin{bmatrix} \overline{A_{X_L}} \\ \overline{A_{Y_L}} \\ \overline{A_{Z_L}} \end{bmatrix} \qquad \text{(Eq. 2.3)}$$

where $\overline{A_{X_G}}$, $\overline{A_{Y_G}}$, and $\overline{A_{Z_G}}$ make up the acceleration measurement in the global coordinate system with the gravity component removed.

2.2.2 Participants and Experimentation

Twelve male participants participated in this study, with an average age of 23.1 ± 2.12 years, height of 184.15 ± 8.3 cm, and weight of 85 ± 14.58 kg. Participants reported no prior neck, shoulder, or head injuries nor any neurological conditions. Written informed consent, as approved by the University of Iowa Institutional Review Board, was obtained prior to testing. Participants were asked to remain in an upright-seated posture with and without backrest support for each 60-second vibration file. Files were run in the

fore-aft direction (X) at 1.8 m/s^2 RMS, vertical direction (Z) at 1.8 m/s^2 RMS, and in multi-axis directions (3D) at 1.8 m/s^2 RMS resultant acceleration. Each participant was fitted with inertial sensors adhered to skin overlaying the C7 and to a head-worn halo, similar to a study by Wang and Rakheja (2006A). An additional sensor was rigidly attached to the seat frame. Each inertial sensor had a mass of 30g and a contact surface area of 20 cm^2. Initial experimentations showed that the inertial sensor has a natural frequency around 25 Hz, which is outside the range of the frequency under consideration. Participants were asked to maintain a normal sitting posture with and without the use of a backrest. The footrest was adjusted so that each participant's thighs were horizontal. Participants were asked to avoid any involuntary movements.

2.3 Results

2.3.1 Validation of Inertial Sensors in Simulated Vibration Environment

A test was performed in 3D vibration to show the validity of using the current inertial sensors (Figure 2.2) in WBV studies. The sensor was first tested using an off-axes testing apparatus in a multiple vibration environment. This arrangement allowed all three accelerometer axes to be off-alignment with respect to the global coordinate system (fore-aft, lateral, and vertical). The apparatus was attached rigidly to the shaking platform. A six-degree-of-freedom man-rated motion platform (the Moog-FCS 624-1800 electrical system) was used for the test. For this dynamic vibration test, the shaker platform produced 3D random vibration for 15 seconds, and the data were recorded at 120 Hz. To verify the results, an additional traditional accelerometer tri-axial DC accelerometer, Dytran 7523A1, Chatsworth, CA) was rigidly fixed to the shaking platform, aligned with the global coordinate system, and used as a baseline between the two systems.

Figure 2.2 Testing block for dynamic vibration tests where all three sensor axes were rotated off-alignment from the global coordinate system. The testing block was rigidly attached to the motion shaker platform.

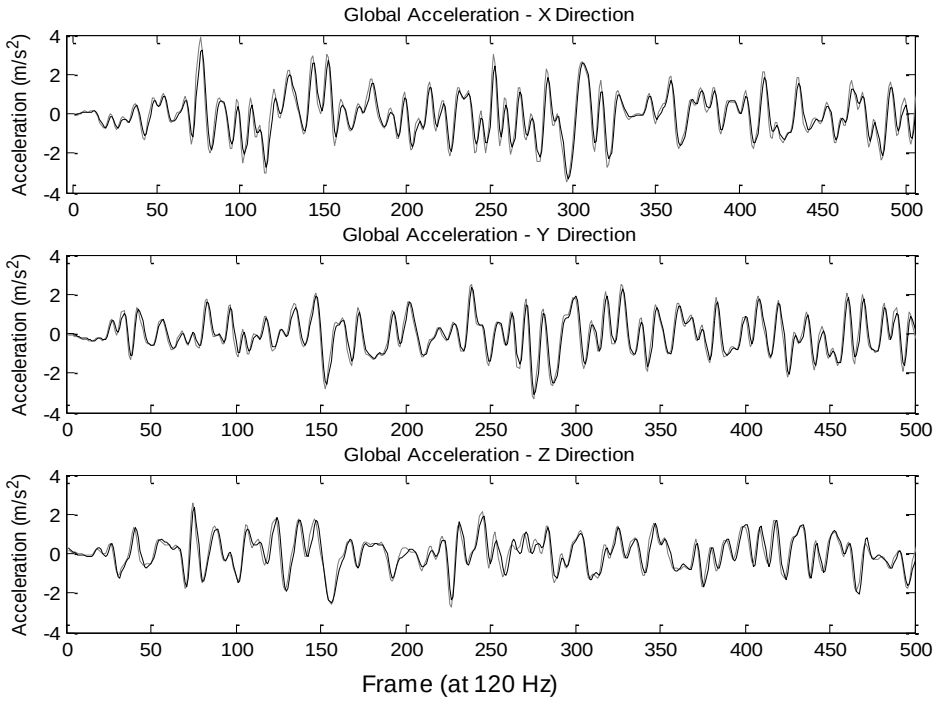

Figure 2.3 Comparison of inertial sensor accelerations (m/s^2) in 3D vibration on an off-axes testing block. The bold black line represents the acceleration signal of the accelerometer fixed to the shaking platform and aligned with the global coordinate system. The gray line represents the acceleration signal of the inertial sensor with the gravity component removed and the accelerations rotated to the global coordinate system.

The resulting acceleration components from the inertial sensor and traditional accelerometer test are depicted in Figure 2.3. It should be noted that the offset value of 9.81 was subtracted from the hard-mounted traditional accelerometer only in the Z direction. The output acceleration from the inertial sensor was transformed using the described methodology by first removing gravity (Equation 2.2) and then rotating to the global coordinate system (Equation 2.3). It can be seen that the inertial sensor signal follows very closely with the hard-mounted traditional accelerometer.

2.3.2 WBV Application

After the initial validation step, the proposed system is tested in a real WBV testing environment. In this work, the transmissibility was calculated by taking the cross-spectral density of the output acceleration at a point on the participant's body and the input acceleration at the rigid seat, divided by the auto-spectral density of the input acceleration. The input motion directions are denoted as uppercase letters, while the output motion directions are denoted by lowercase letters. For example, the transmissibility for fore-aft input vibration and output vertical vibration would be denoted as Xz.

2.3.2.1 Single Fore-Aft WBV

Inertial sensors were adhered to each participant's skin at the C7 level and to the front of a head-worn halo, as shown in Figure 2.4. The sensor on the head remained at relatively the same orientation as the global coordinate system; however, the sensor placed at the C7 location resulted in a moderate angle with respect to the vertical direction (Figure 2.5c). Madaksahira-Pranesh (2011) found this angle in a similar study to

be greater than 30 degrees, regardless of the sitting posture. Matsumoto and Griffin (1998) found an inclination angle of 20 to 35 degrees for the T1 vertebrae for a similar seated posture.

(a) (b) (c)

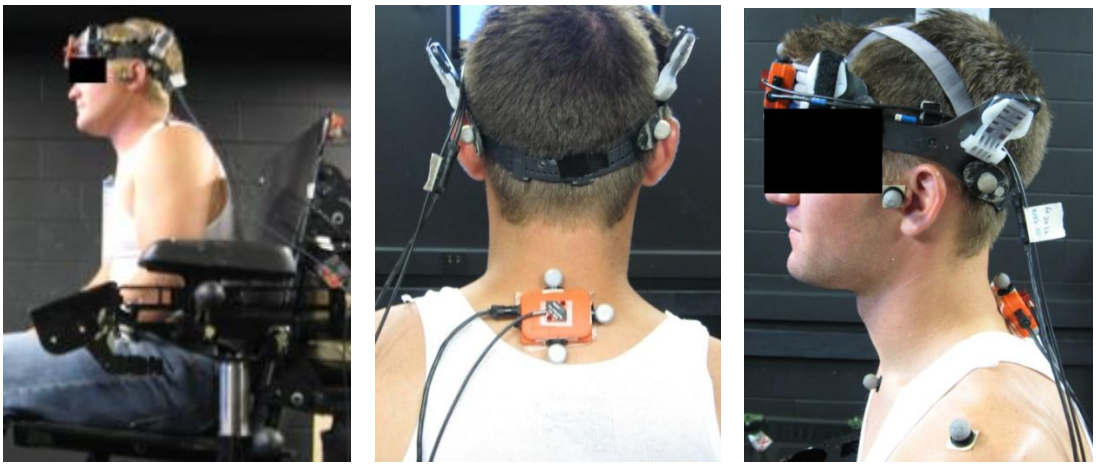

Figure 2.4 Seated posture and sensor setup for fore-aft and vertical WBV vibration test. (a) shows the unsupported backrest posture; (b) shows posterior view of C7 inertial sensor; and (c) shows the side view indicating the angle of tilt of the head and C7 inertial sensor.

Figure 2.5 compares the uncorrected (local) seat-to-head transmissibility to the corrected (global) seat-to-head transmissibility between the individual motion components for random fore-aft vibration during both backrest-supported (Figures 2.5a, 2.5b) and unsupported (Figures 2.5c, 2.5d) upright conditions. Because the orientation of the sensor is on the forehead and aligned very closely to the global coordinate system, only small differences can be seen between the corrected and uncorrected data.

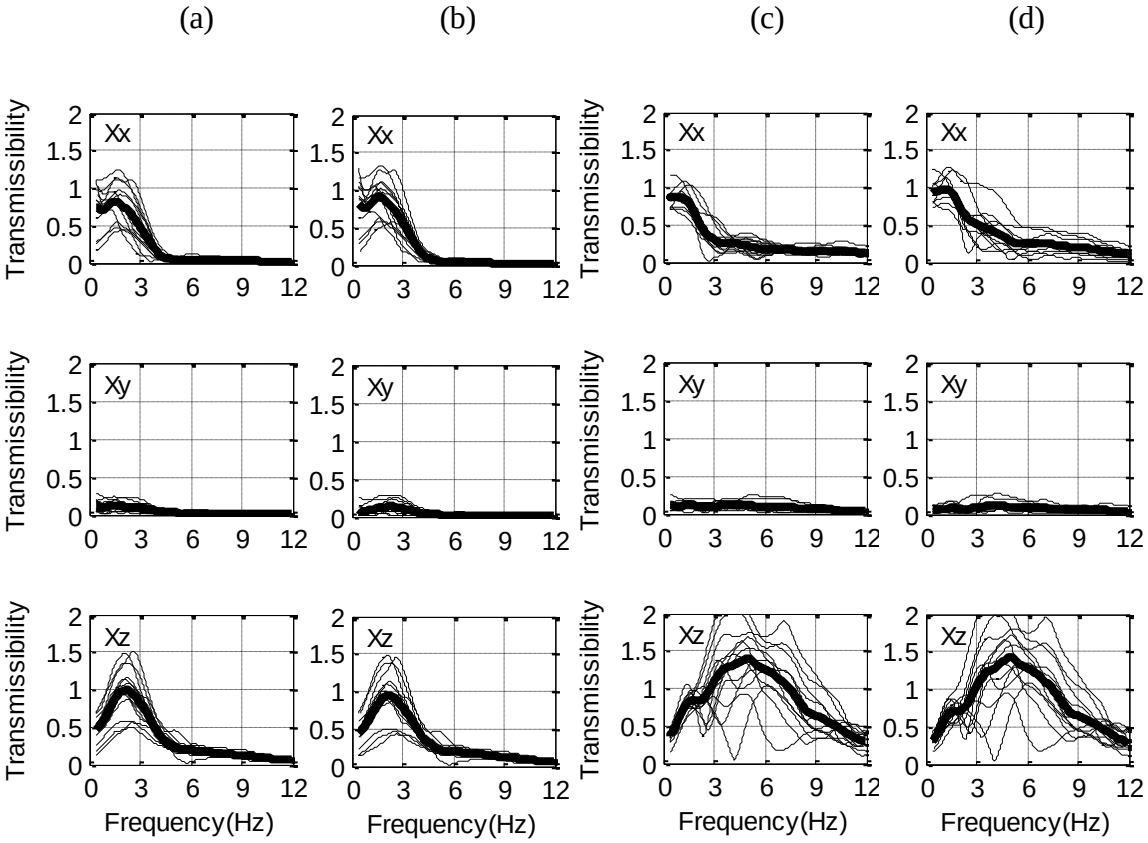

Figure 2.5 Seat-to-head transmissibility during fore-aft vibration. (a) uncorrected (local) data during unsupported upright seated posture; (b) corrected (global) data during unsupported-upright seated posture; (c) uncorrected (local) data during backrest-supported seated posture; (d) corrected (global) data during backrest-supported seated posture. Bold lines represent the mean data.

When the orientation of the sensor is greatly misaligned with the global coordinate system, considerable errors are present (as in measurement at the C7 location). Figure 6a shows the uncorrected (local) seat-to-C7 transmissibility components for random fore-aft vibration in an unsupported-upright posture. Here major motion components are seen in both the Xx and Xz transmissibilities. Figure 6b shows the corrected (global) seat-to-C7 transmissibility and demonstrates the considerable errors with the uncorrected (local) measurement. In the global system, the main transmissibility

component lies almost solely in the Xx directions. Similar behaviors exist for the supported-back condition as shown in Figure 6c and 6d. However, as expected, the transmissibility based on the global system has shown observable contribution in the Xz component (Figure 6d) due to the pitching motion of the head and neck.

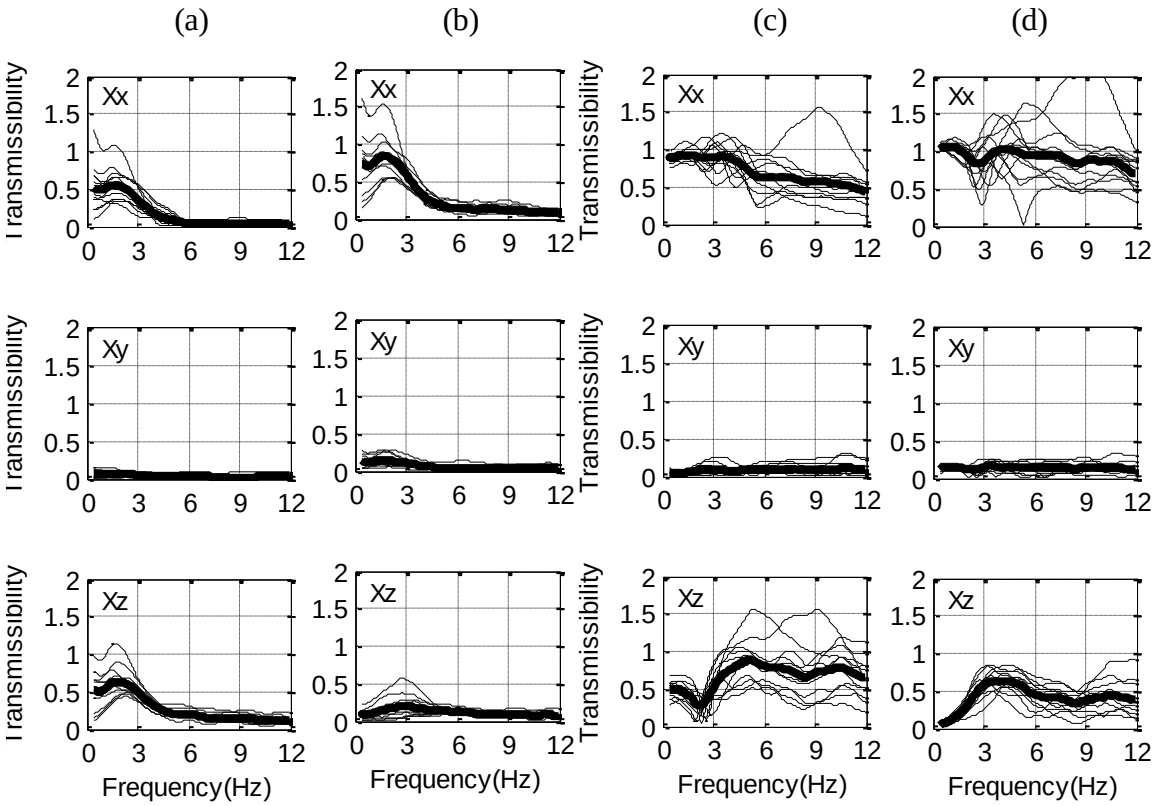

Figure 2.6 Seat-to-C7 transmissibility during fore-aft vibration. (a) uncorrected (local) data during unsupported-upright seated posture; (b) corrected (global) data during unsupported-upright seated posture; (c) uncorrected (local) data during backrest-supported seated posture; (d) corrected (global) data during backrest-supported seated posture. Bold lines represent the mean data.

It should be mentioned here that there are some discrepancies between the shapes of the seat-to-head transmissibility across different labs, especially in fore-aft WBV of

seated participants (Hinz et al., 2010; Paddan and Griffin, 1988B; Paddan and Griffin, 1998; Mandapuram et al., 2011). One explanation for this difference is the inclusion of the three-directional combined RMS acceleration of the output point instead of solely using the Xx component. For the unsupported backrest posture, Figure 2.7a shows considerable differences in the magnitude of the fore-aft seat-to-head transmissibility of the three-directional combined RMS acceleration from that of Figure 2.5b. The three-directional combined RMS acceleration for the backrest-supported posture (Figure 2.7b) demonstrates two peaks around 2 Hz and 5 Hz. The peak at 2 Hz is a result of the Xx component, while the peak at 5 Hz reflects the vertical resonance in the Xz component (Figure 2.5d).

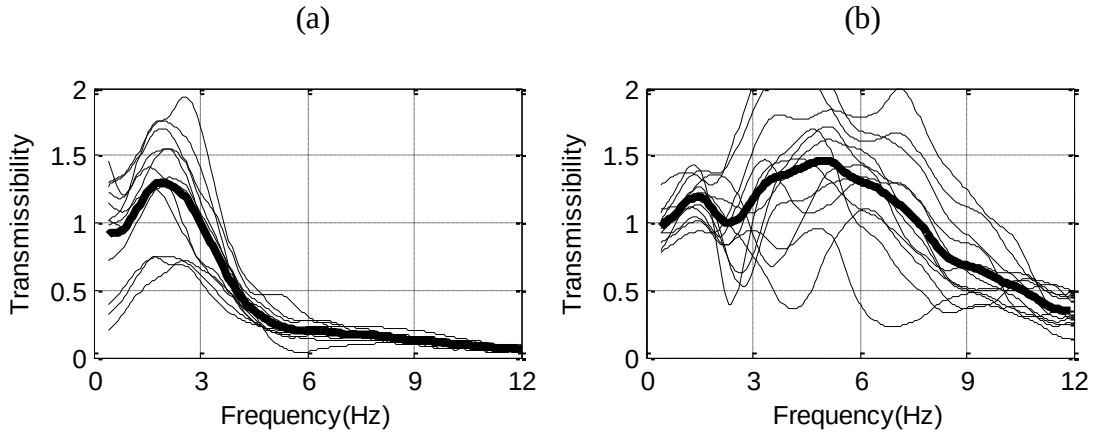

Figure 2.7 Combined (all output motions) seat-to-head transmissibility during fore-aft vibration. (a) unsupported-upright seated posture; (b) backrest seated posture. Bold lines represent the mean data.

2.3.2.2. Single Vertical WBV

The results for seat-to-C7 transmissibility for vertical vibration are presented in Figure 2.8, where major differences between the uncorrected (local) data (Figure 2.8a)

and the corrected (global) data (Figure 2.8b) are present. Transmissibilities with input/output motions of the same direction (Zz) should come close to 1.0 at frequencies near zero, whereas cross-coupled motions (Zx, Zy) should have transmissibilities close to zero at frequencies near zero.

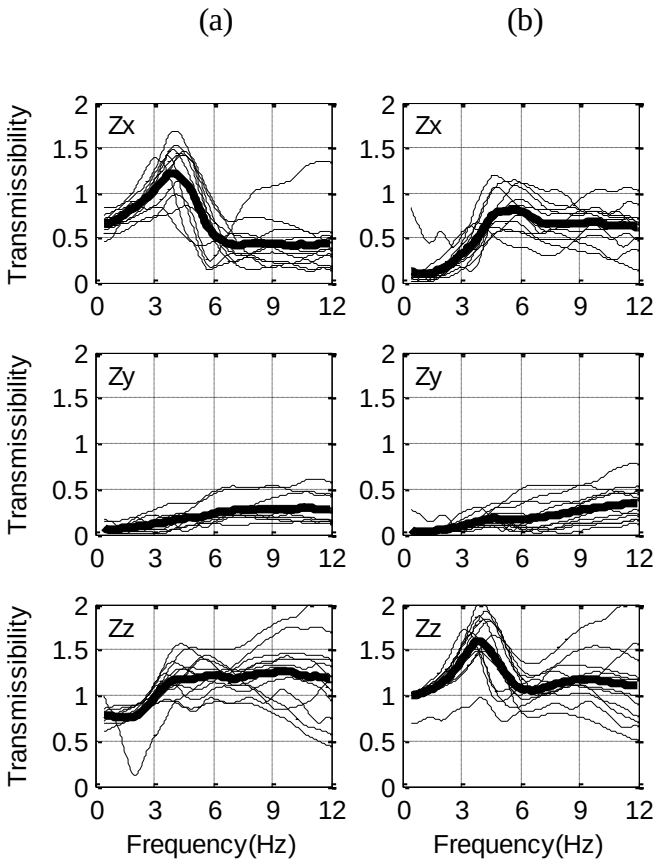

Figure 2.8 Seat-to-C7 transmissibility in vertical vibration for an unsupported upright posture. (a) uncorrected (local) data; (b) corrected (global) data. Bold lines represent the mean data.

2.3.3 Multiple-Axis WBV

While the conventional 2D correction method (Madakashira-Pranesh, 2011; Huang and Griffin, 2009; Matsumoto and Griffin, 1998; Smeathers, 1989) may work for

simple postures and motions, the method has difficulties correcting data in a realistic 3D WBV environment. Problems such as curvature of the human body and involuntary postural changes only increase the difficulty of acceleration measurements. Such difficulties can be overcome, however, by use of the proposed method.

Figure 2.9 shows the uncorrected (local) transmissibility for the transmission of vibration from the seat to the C7 location. As previously stated, uppercase letters indicate the vibration input direction, and lowercase letters indicate the vibration output. Figure 2.10 shows the corrected (global) transmissibility for the transmission of vibration from the seat to the C7 location. Major differences are seen between the two figures.

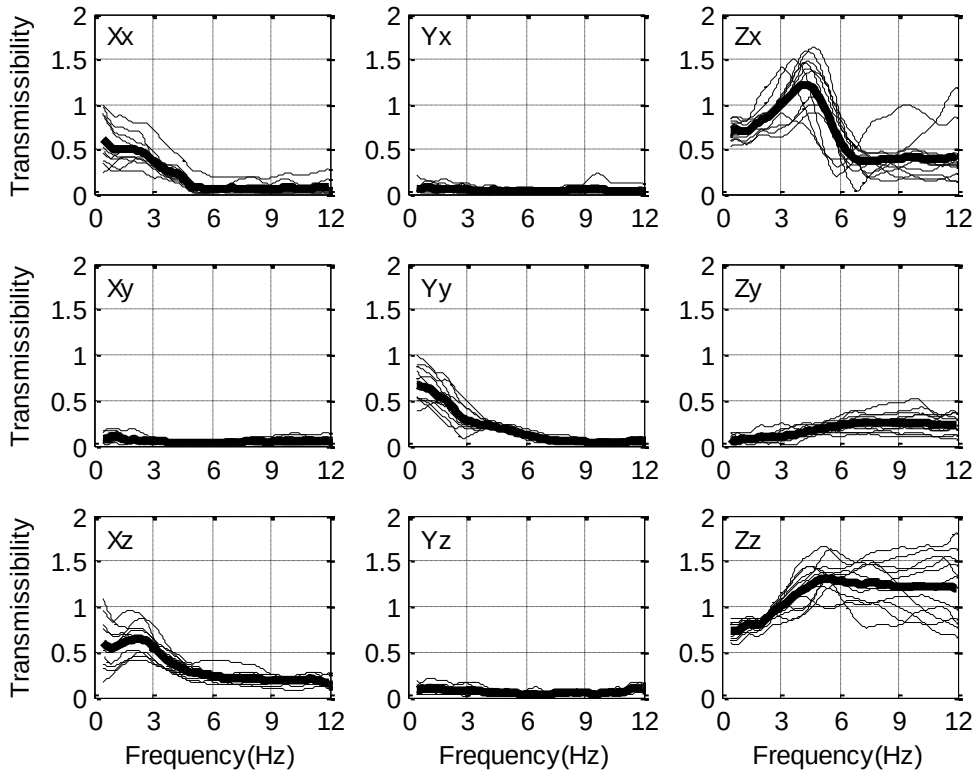

Figure 2.9 Seat-to-C7 transmissibility in 3D vibration for uncorrected (local) measurement. Bold lines represent the mean data.

As with vertical single-axis vibration, it can be seen that the data in Figure 2.9 are not correct because all input/output motions (Xx, Yy, Zz) with the same directions should come close to 1.0 at frequencies near zero. Additionally, all cross-coupled motions should be near zero at frequencies close to zero.

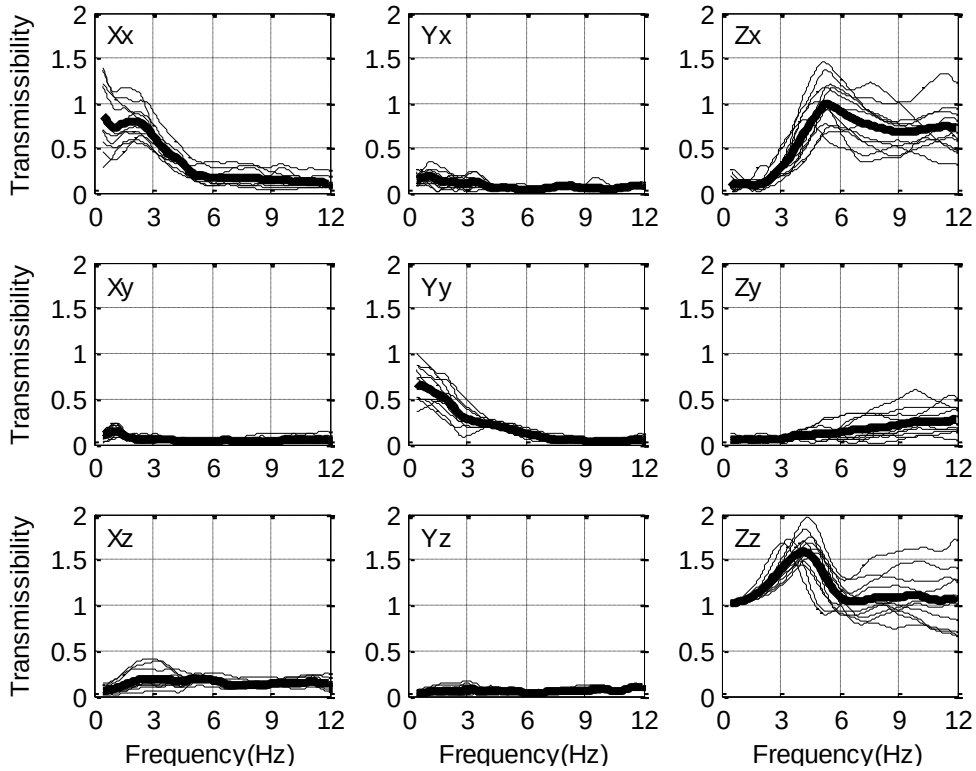

Figure 2.10 Seat-to-C7 transmissibility in 3D vibration for corrected (global) measurement. Bold lines represent the mean data.

2.4 Discussion

The ability of monitoring the kinematics of the segment's 3D orientation objectively makes the method presented in this work extremely useful, especially for standardization purposes and when sharing data across different labs. With this proposed

methodology, it becomes possible to investigate various biodynamic measures in any direction with a clear picture of the relationship between the direct and cross-components of the motion.

When the inclination angle changes during an experiment, the acceleration components change and no longer become valid. This can be seen when transmissibility values of cross-coupled motions are not near zero at frequencies close to zero. Additionally, transmissibility values between input/output motions (Xx, Yy, Zz) should be close to 1.0 as frequency nears zero. This trend seems to be extremely close for vertical input/output transmissibilities (Zz) but seems to be much more variable in the fore-aft (Xx) and lateral transmissibilities (Yy) (Hinz et al., 2010; Paddan and Griffin, 1988B; Paddan and Griffin, 1998; Mandapuram et al., 2011). This could be due to the posture conditions, the involuntary low-frequency motions of the head, and because the resonance transmissibility in these directions tends to be at low frequencies (below 2.0 Hz).

Researchers have also tried to correct the acceleration data due to problems with skin motion (Smeathers, 1989; Kitazaki and Griffin, 2011; Yoshimura et al., 2005; Mansfield and Griffin, 2000). During the setup of the current study, a large surface area (20 cm2) was used at the C7 testing area in an attempt to minimize skin motion. Additional correction for skin motion was not needed due to the natural frequency of the inertial sensor-skin system being higher than the frequency range being studied. This is similar to the findings of Kitazaki and Griffin (2011) for an accelerometer of approximately the same mass measured on the skin over the L3.

The inertial sensors have the benefits of less processing time and an all-in-one accelerometer, gyroscope, and magnetometer package for greater capability of collecting six-degree-of-freedom motion data. The current inertial sensors have the disadvantages, however, of being able to capture only up to 120 Hz, sensitive to electromagnetic fields, bulky, and will need to be refined and miniaturized before it can be adequately adapted for the use in actual WBV filed conditions.

2.5 Conclusion

This work presents a methodology for the correction of acceleration measurements in WBV when dealing with inclined surfaces or when the motion has multiple directions. The method presented an objective measurement that can be used across labs and for standardization purposes. Current correction methodologies may work well with uni-axial direction WBV testing, with some precautions; however, they will encounter considerable errors under multiple-axis WBV.

CHAPTER 3: PREDICTIVE DISCOMFORT OF NON-NEUTRAL HEAD-NECK POSTURES[3]

3.1 Introduction

It is well known that sitting postures play a significant role in the resulting level of discomfort and have long-term health consequences such as low back pain (Adams and Hutton, 1985; Griffin, 1990; Wilder and Pope, 1996; McGill, 1997; Chaffin et al., 1999; Mansfield, 2005A). In whole-body vibration (WBV) encountered in moving environments, the role of posture becomes more involved as people with non-neutral postures respond differently under vibration with diverse magnitudes and frequency content (Griffin, 1990; Mansfield, 2005A; Johanning et al., 2006; Waters et al., 2008; Olson et al., 2009; Smets et al., 2010). There are many occupations where people need to use non-neutral postures to monitor their equipment while both the person and the equipment are under vibration (Kittusamy and Buchholz, 2004; Rehn, Nilsson et al., 2005; Thuresson, et al., 2005; Eger et al., 2008; Newell and Mansfield, 2008). As a result, the relative motion between body segments sometimes reaches its upper or lower passive limits, causing in some instances a considerable degree of discomfort.

Researchers have realized the effect of posture on human response and risk evaluation in WBV (Kitazaki and Griffin, 1998; Paddan and Griffi, 1998; Hinz et al., 2002; Johanning et al., 2006; Okunribido et al., 2008; Wang et al., 2008; Baker and Mansfield, 2010). Nawayseh and Griffin (2005) investigated the dynamic responses at the seat and footrest of 18 participants sitting on a seat with and without a backrest and

[3] Published in Journal of Ergonomics.
Rahmatalla, S.; DeShaw, J. Predictive Discomfort of Non-Neutral Head-Neck Postures in Fore-Aft Whole-Body Vibration. *Ergonomics*. **2011,** 54, 263-272.

with varying foot heights. The participants used four different postures. They found that at frequencies below resonance, the backrest reduced vertical and fore-and-aft forces at the footrest. Additionally, they found that the forces on the seat and the footrest showed a nonlinear characteristic that varied between postures. Hinz et al. (2002) conducted experiments on 39 male participants sitting on suspension seats with and without backrests during vertical WBV. They concluded that backrest and posture conditions play an important role and should be included in risk assessment during WBV. Wang et al. (2006B) found a significant effect of sitting posture on the biodynamic response under vertical vibration after considering 36 different sitting postures and seat configurations. Their results showed important combined effects of inclined backrest and hand position on the absorbed power characteristics. Thus, although they are somewhat varied, most prior studies have demonstrated the importance of considering postures when investigating WBV.

Head-neck postures in WBV have received less attention compared to the considerable focus on the lower back area of the spine. Rehn et al. (2005) conducted a review on the occupational use of all-terrain vehicles (ATV). They showed that the non-neutral rotational positions of the neck are an ergonomic risk factor that occurs frequently and with short duration for professional ATV drivers. The prevalence of serious neck and lower back disorders among locomotive engineers was found to be nearly double that of the sedentary control group without such exposure (Johanning et al., 2006). Courtney and Cahn (1999) performed an ergonomic study to assess the workspace of the grab unloaders for bulk materials in ships. They found that all drivers complained of neck and back discomfort while spending 50% of their time looking down vertically. In a study of

14 Swedish helicopter pilots with neutral neck positions and neck flexing at 20 degrees, Thuresson et al. (2005) found that the neck position seemed to have significant influence on the induced load and muscle activities. Eger et al. (2008) found that simultaneous exposure to vibration and non-neutral postures such as neck rotation and truck rotation, flexion, and lateral postures could increase the load-haul-dump driver's risk of musculoskeletal injury in the mining industry.

Besides subjective measures (Kaneko et al., 2005; Hacaambwa and Giacomin, 2007), researchers are also interested in developing predictive measures to quantify discomfort in WBV (Ebe and Griffin, 2000). Among the prominent measures are the power absorbed (Mansfield et al., 2000; Wang et al., 2006A), the apparent mass (Mansfield and Maeda, 2007), driving point mechanical impedance (Holmlund et al., 2000; Mansfield, 2005B; Wang et al., 2008), and transmissibility (Paddan and Griffin, 1998; Paddan and Griffin, 2000; Wang et al., 2008). These measures have shown encouraging and consistent correlations with the subjective-reported discomfort measures; however, they showed sensitivity to the body postures and to the interaction of participants with the surrounding equipment (Wang et al., 2008). For example, recent studies (Mansfield and Maeda, 2005; Maeda et al., 2008) have shown the incapability of the apparent mass to capture the peak in the discomfort when the participants move while they vibrate, such as twisting their torsos or lifting their arms. In a relatively recent article, Wang et al. (2008) showed the inconsistency between the seat-to-head transmissibility and the apparent mass when the participants were using different postures.

In this work, a new musculoskeletal-based predictive measure is introduced for the evaluation of discomfort in WBV with people taking non-neutral neck postures. The hypothesis behind the proposed discomfort measure is that the head-neck discomfort is sensitive to the neck posture relative to the neck neutral position (Kee and Karwowski, 2001; Kee and Karwowski, 2003) and to the rate of change of the neck motion. The latter would generate considerable inertial stresses on the head-neck region and would make it very uncomfortable for the participants to recover their neutral head-neck positions. The proposed predictive discomfort was used and verified with four head-neck posture conditions.

3.2 Methods

3.2.1 Participants

Ten male participants were used in this study with an average age of 23.1 ± 2.12 years, height of 184.15 ±8.3 cm, and weight of 85 ± 14.58 kg. Participants reported no prior neck, shoulder, or head injuries, nor any neurological conditions. Written informed consent, as approved by the University of Iowa Institutional Review Board, was obtained prior to testing (Appendix B).

3.2.2 Experimental Procedure

Adjustable helmet-strap-mounted accelerometers (tri-axial crossbow accelerometers) and motion capture markers (Vicon motion capture system) were attached to the participants' head and neck areas. The participants were strapped to a rigid seat (Figure 3.1) mounted rigidly on a vibration motion platform (the Moog-FCS 628-1800 electrical motion system). The vibration platform was used to generate vibration rides in the x-direction (fore-and-aft) at discrete sinusoidal frequencies of 2 to 8

Hz with an increment of 1 Hz. All signals were run at constant magnitude of acceleration of 0.8 m/s^2 RMS and 1.15 m/s^2 RMS. Each discrete frequency ran in the x-direction for 15 seconds, followed by a 5-second stationary break. The authors found the 15 seconds duration was reliable for reporting discomfort (Miwa, 1968; Dickey et al., 2006) and for bringing the participants to their steady-state motion for the evaluation of seat-to-head transmissibility (Griffin et al., 1978; Smith, 2000).

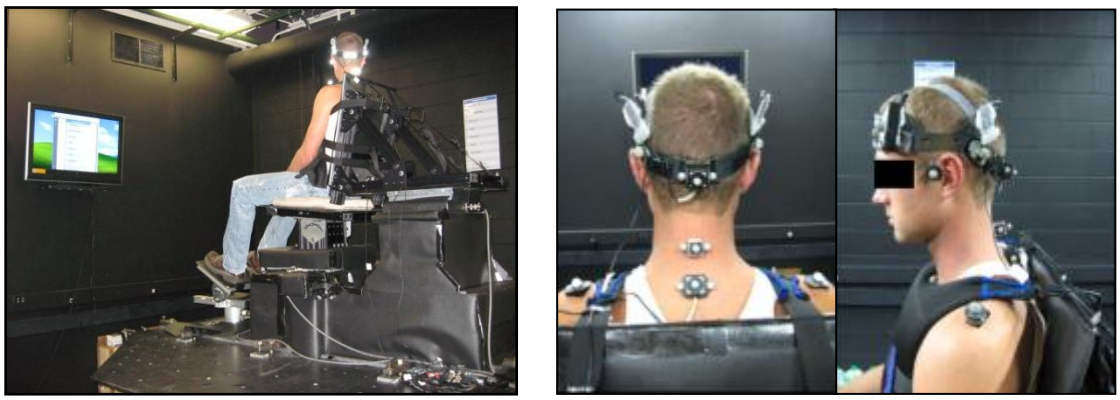

Figure 3.1 Experimental setup and marker locations on the participant. The picture on the left shows the participant, the seat, and the location of the discomfort scale-boards on the walls; the pictures on the right show the participant in a neutral posture with a close view of the markers on the participant.

Four head-neck posture combinations were investigated in this experiment, including: (1) head-up, (2) head-down, (3) head-to-side, and (4) normal. During the experiment, the participants were asked to ignore any other discomfort and rate only the discomfort due to the motion in their head-neck region. Four Borg CR-10 scale-boards were located at different locations to help each participant maintain his head-neck posture during the ride. The head-up scale-board was located on the ceiling of the room and was

angled toward the participant for clear view in the head-up posture. The head-down scale-board was located on the floor of the room and was also angled for appropriate viewing in the head-down posture. The scale-boards for the normal (neutral) posture and the head-to-side posture were orientated vertically and placed directly in front of and directly to the right of the participant, respectively.

During the 15-second ride, the participants were asked to maintain the desired posture for 5 seconds while they were vibrating at a certain frequency. The participants were asked to verbally rate their discomfort toward the end of the 5-second period. Once the rating had been given, the participants would change their posture to the normal posture (straight forward) and keep that position for the remaining 10 seconds of the same ride vibration. The participants then made a comparison discomfort rating between the 5-second non-neutral and 10-second neutral postures. The normal posture was used as the baseline, or control, for all experiments. During the last 5-second stationary break, the participant would reorient his head to the given posture and wait for the next vibration segment. Vibration sequences were randomized for each participant. In order to acquire correct timing and head-neck posture for data collection, the 10 participants were trained by giving responses to two random vibration sequences. For the head-up, head-down, and head-to-side postures, participants were instructed to rotate their heads to the maximum possible range of motion without excessively straining their necks. For example, for the head-to-side posture the average neck angle was around 55 degrees from neutral position; for the head-up posture the average angle was 17 degrees from neutral position, and for the head-down posture the average angle was 20 degrees from neutral position.

3.2.3 Motion Platform and Motion Setup

A six-degree-of-freedom, man-rated motion platform was used to generate the vibration motion for the experiment. The system has the capability to generate movements in the translational axes of over 0.39 meters and the rotational axes of more than 23 degrees, and an accurate frequency response of up to 20 Hz. Participants were strapped to a rigid seat mounted to the base of the Moog simulation platform. The seat pan was inclined at a 5-degree angle with the horizontal, and the seatback was inclined at a 14-degree angle with the vertical. The seat was covered with a soft thin rubber to increase general comfort while maintaining seat rigidity. For each participant, the seat height was adjusted appropriately to be as high as possible on the participant's back without obstructing the view of the C7 vertebra for the motion capture cameras. This height allowed the participant's shoulder blades to make complete contact with the backrest. Participants were strapped snugly to the seatback by use of a neoprene vest with three central straps and two shoulder straps, as shown in Figure 3.1 This was done in an effort to isolate the head-neck response from dampening effects of the middle and lower back. Quick-release buckles were included for safety, in case of an emergency.

3.2.4 Motion Capture Setup

3.2.4.1 Marker Protocol

A 12-camera Vicon motion capture system was used to acquire the motion of the head, neck, upper trunk, and seat. Data were acquired at 200 samples per second. Reflective markers were adhered to the participant's skin using medical-grade double-sided tape. A halo worn by the participants was fitted with four head markers, an accelerometer, and three markers on the accelerometer, which can clearly be seen in the

posterior view of Figure 3.1. Three markers fastened to a plastic structure were applied on the skin overlying the spinous process of C3. A second accelerometer was fitted with three markers and was applied on the skin overlying the spinous process of C7. Additionally, markers were placed on the shoulders, the clavicle, and the frame of the seat to measure the relative motion between the trunk and the seat. The motion capture reflective markers were attached superiorly and laterally to each eyebrow, the back of the head, one on each side, on the level of C1, and over the mastoid process. The markers mounted to the halo were used to define the head segment. The markers over the facial features were used as redundant markers and were not used in this work

3.2.4.2 Velocity and Acceleration

Once the marker position data were collected and appropriately low-pass filtered, they could be used to calculate the velocity and acceleration by differentiation of the continuous positional data. The filtering process was achieved by applying an eighth-order Butterworth filter in both directions to achieve zero lag. A cut-off frequency of 16 Hz was applied to all frequencies. The cutoff frequency was selected based on the power spectral density analysis of the neck accelerometer. A program in MATLAB was written to use a 5-point central difference method to approximate the differential of the position data to obtain realistic velocity data. The velocity data were then transformed by the same method to acceleration data. Caution should be taken when using this method, however, because the ends of the data are not accurate due to the differentiation.

3.2.5 Accelerometer Setup

Three DC Crossbow tri-axial accelerometers were used to collect acceleration data for the experiment. The acceleration data were collected at 200 samples per second.

One accelerometer was placed on the frame of the seat and aligned with the same axes as the shaker table so that a more direct comparison of motion could be made between the simulation ride vibration and the actual motion. The second accelerometer was located on the C7 vertebra. Three markers were attached to the body of each accelerometer to specify the location and the orientation in the local and global coordinate systems. The third accelerometer was mounted to the head by use of the halo apparatus worn by the participant. Excluding the head accelerometer, each accelerometer was adhered by medical-grade, double-sided tape; the head accelerometer was further secured by banded strips of duct tape. The accelerometers were used in this experiment specifically for comparison of the computed acceleration from the motion capture system and as a backup system in case the motion capture should be inadequate.

3.2.6 Subjective-Reported Discomfort

Participants reported their head-neck discomfort using the Borg CR-10 scale (Borg, 1982). The Borg CR-10 scale ranges from 0 to 10 as shown in Appendix A, with higher values indicating higher relative discomfort. For this experiment, participants were asked to ignore any other discomfort and rate only the discomfort occurring at their head-neck region. The Borg CR-10 scale was attached to four boards positioned at reasonable locations on the lab walls to help the participants maintain their head-neck posture during the experiment. During the experiments, each participant gave an additional response for the normal posture after an altered posture (head-down, head-to- side, or head-up). Each participant's normal posture discomfort responses from all frequencies under investigation were averaged for the normalization of their answers utilizing the normalization procedure used by Kee and Karwowski (2001). This ensured that while

some participants may have tendencies to give overall higher or lower responses, the general trends can be found. Once participant data were normalized, the 10 participants' discomfort responses were averaged for each discrete frequency and posture. This normalization procedure gave good correlation (R2=0.9955) with the normalization procedure used by Mansfield et al. (2000).

3.2.7 Randomization

A Latin-squares design (Williams, 1949) was used for randomization of the participants, postures, amplitudes, and frequencies. Latin-squares tables are used to reduce residual effects in studies with multiple treatments or doses. It was used here to randomize frequency duration effects. Each posture and amplitude combination was assigned a specific number, 1 through 8. Next, the Latin-squares pattern was applied to combine each posture and amplitude combination with each discrete frequency of 2 to 8 Hz so that every possible combination was tested. Each participant also started on the subsequent line of the Latin-squares table to further randomize any frequency or duration effects.

3.2.8 Biomechanical Measures

Seat-to-head transmissibility is considered as one popular biomechanical measure in WBV. It is defined as the complex ratio between the cross-spectral density of the input seat horizontal acceleration and the output head horizontal acceleration $S_{hs}(jw)$ divided by the auto-spectral density of the input horizontal seat acceleration $S_{ss}(jw)$ as seen in Equation 3.1. The transmissibility normally shows significant increase when resonance is occurring. For discrete sinusoidal vibration exposure, such as in this work, the transmissibility was computed in the time domain as the RMS of the output head-

acceleration divided by the RMS of the input seat-acceleration. The transmissibility calculation was performed using two approaches. In the first approach, the head acceleration in the fore-aft direction only was used as the output acceleration. In the second approach, the total magnitude RMS accelerations of the head in all directions (fore-aft, lateral, and vertical) were used as the output acceleration. For both approaches, the seat-acceleration in the fore-aft direction was used as the input component.

$$T_h(jw) = \frac{S_{hs}(jw)}{S_{ss}(jw)} \qquad \text{(Eq. 3.1)}$$

3.2.9 Predictive Discomfort

It is hypothesized in this work that the head-neck discomfort is associated with the range and severity of the angular motion of the head-neck segment relative to its neutral position. The neutral position is defined here as a comfortable position where the participant is looking forward normally. Four components that contributed to the segment discomfort *f(q)* are shown in Equation 3.2.

$$f(q) = \Delta q^{norm} + G \times QU + G \times QL + \Delta \ddot{q} \qquad \text{(Eq. 3.2)}$$

The first component, Δq^{norm} , is associated with the deviation of the segment from its neutral posture at the moment before the beginning of the vibration (Marler et al., 2005; Rahmatalla, et al., 2010) and seen in Equation 3.3. In Equation 3.3, q is the joint angle and q^N is the *neutral position* of the joint. For the neutral posture, for

example, $q = q^N$ and therefore Δq^{norm} becomes zero. q^U is the upper active limit of the range of motion of the joint, and q^L is the lower active limit of the range of motion of the joint.

$$\Delta q^{norm} = \frac{q - q^N}{q^U - q^L} \quad \text{(Eq. 3.3)}$$

The second term, $G \times QU$, is a penalty term associated with joint values that approach their upper passive limits (Equation 3.4), and the third term, $G \times QL$, is a penalty term associated with joint values that approach their lower passive limits (Equation 3.5). The two penalty terms vary between zero before the joint reaches the upper or lower 10% of its passive range, and $G=10^6$ when the joint reaches the upper or lower 10% of its passive range, which could happen under severe vibration conditions.

$$QU = \left(0.5 sin \left(\frac{5.0\ q^U - q}{q^U - q^L} + 1.571 \right) + 1 \right)^{100} \quad \text{(Eq. 3.4)}$$

$$QL = \left(0.5 sin \left(\frac{5.0\ q - q^L}{q^U - q^L} + 1.571 \right) + 1 \right)^{100} \quad \text{(Eq. 3.5)}$$

The fourth component of the segment discomfort in Equation 3.2 is linked to the severity of the motion during the vibration, demonstrated by the root mean square (RMS) value of the angular acceleration of the segment (Δq). The head-neck joint angle was

calculated between the torso segment at the T1-C7 level and the center of the head segment at C0 level in the (x-z) sagittal plane. All lateral movements were considered negligible.

3.3 Results

3.3.1 Participant-Reported Discomfort

Figure 3.2 shows the average normalized subjective ratings of 10 participants based on the Borg CR-10 scale in four different head-neck postures. In general, the normal head-neck posture showed a peak at 4 Hz and another peak at 6 Hz.

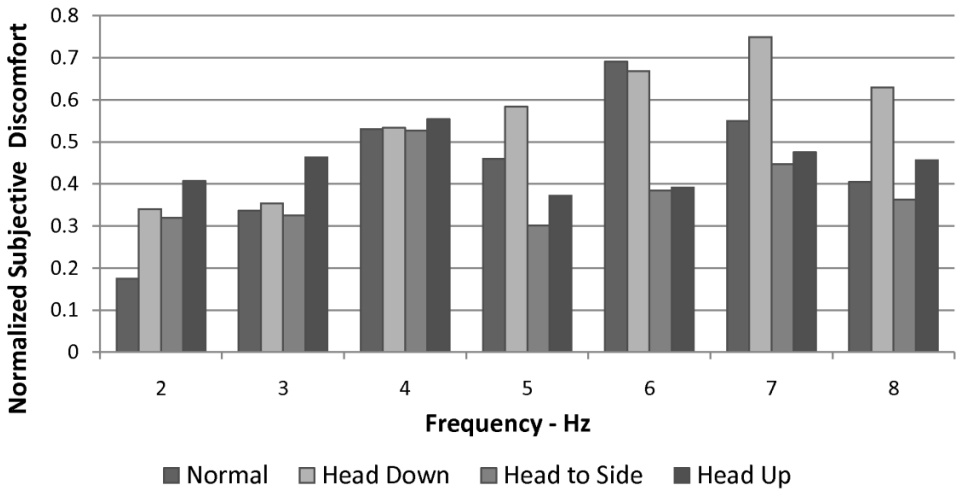

Figure 3.2 Normalized reported discomfort of all head-neck postures for 1.15 m/s2 RMS for fore-aft vibration input.

The head-up and head-to-side postures showed similar trends to that of the normal posture, with the first peak at 4 Hz, but showed a shift in the second peak to a higher frequency of 7 Hz. The head-down posture showed only one peak at 7 Hz. After the first peak (4 Hz), the head-up and the head-to-side postures showed lower discomfort levels

compared to the normal posture; however, the head-down posture was very sensitive to frequencies higher than 4 Hz and showed a higher discomfort value in that region. Figure 3 shows the difference in the discomfort values due to different vibration amplitudes of 0.8 and 1.15 m/s^2 RMS for the normal posture at 4 Hz and 6 Hz. As expected, the greater vibration amplitude yielded greater reported-subjective discomfort ratings.

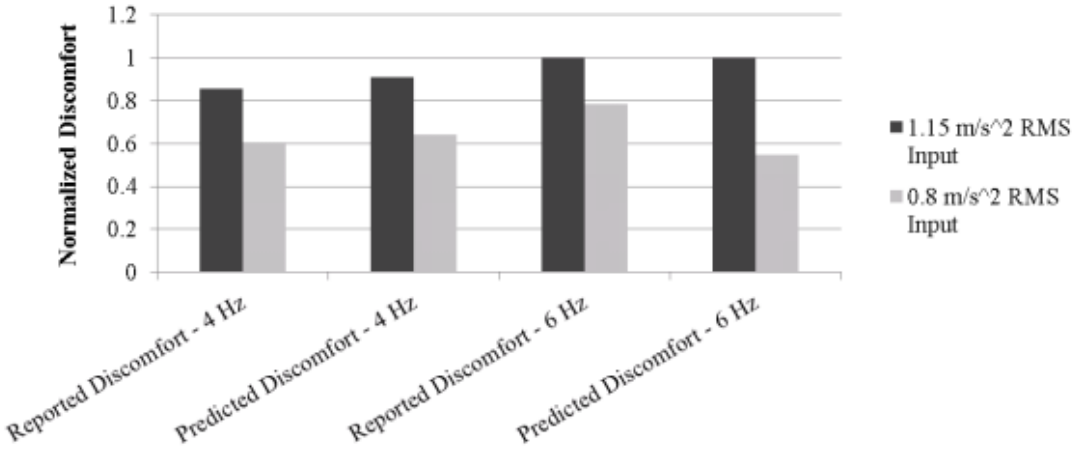

Figure 3.3 Predictive and reported discomfort for four participants taking normal posture.

3.3.2 Transmissibility

The seat-to-head transmissibility based on the ratio of the magnitude of the head acceleration in three directions to the magnitude of the seat acceleration in the fore-aft direction was used in the analysis. As shown in Figure 3.4, the normal head-neck, head-to-side, and head-up postures showed a peak around 6 Hz. The head-down posture showed a peak around 7 Hz. The latter showed a higher transmissibility at all frequencies. The head-up and head-to-side postures exhibited a similar trend to that of the normal posture, but were attenuated in the 4-7 Hz frequency range. The transmissibility values

for the normal, head-to-side, and head-up postures were less than 1 in the 2-3 Hz range, reached a peak of 1.3-1.6 at 6 Hz, and then settled around 1 after that.

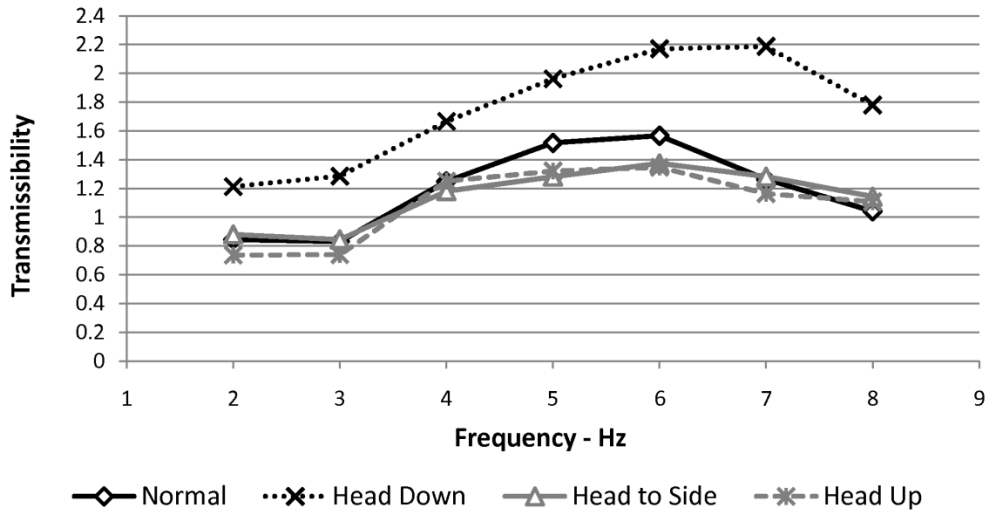

Figure 3.4 Transmissibility magnitudes for different head-neck postures for 1.15 m/s2 RMS ride in the fore-aft direction.

3.3.3 Objective Discomfort Function

For the trend comparison, the average raw data sets for the proposed predictive discomfort and subjective-reported discomfort were normalized by their maximum. Figure 3.5 depicts the latter two discomfort measures for the normal head-neck posture. It appears that the predictive discomfort has followed the trend of the reported discomfort by showing two peaks around 4 Hz and 6 Hz and a shallower valley around 5 Hz. The transmissibility (Figure 3.4) followed the trend of the reported discomfort but showed only one peak around 6 Hz. Similar characteristics were observed for the head-down posture in Figure 3.6, the head-to-side posture in Figure 3.7, and the head-up posture in Figure 3.8. The magnitude of the coefficient of determination (R^2) between the absolute

magnitude of the predictive discomfort and the absolute magnitude of the reported discomfort was 0.8772 for the normal posture, 0.883 for the head-down posture, 0.3213 for the head-to-side posture, and 0.3367 for the head-up posture.

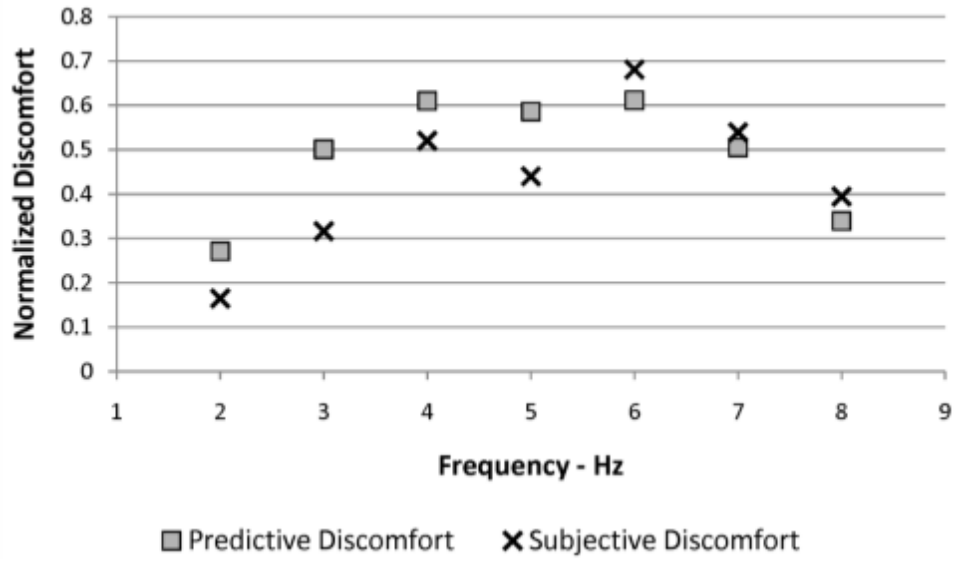

Figure 3.5 Normalized reported, transmissibility, and predictive discomfort for normal head-neck posture.

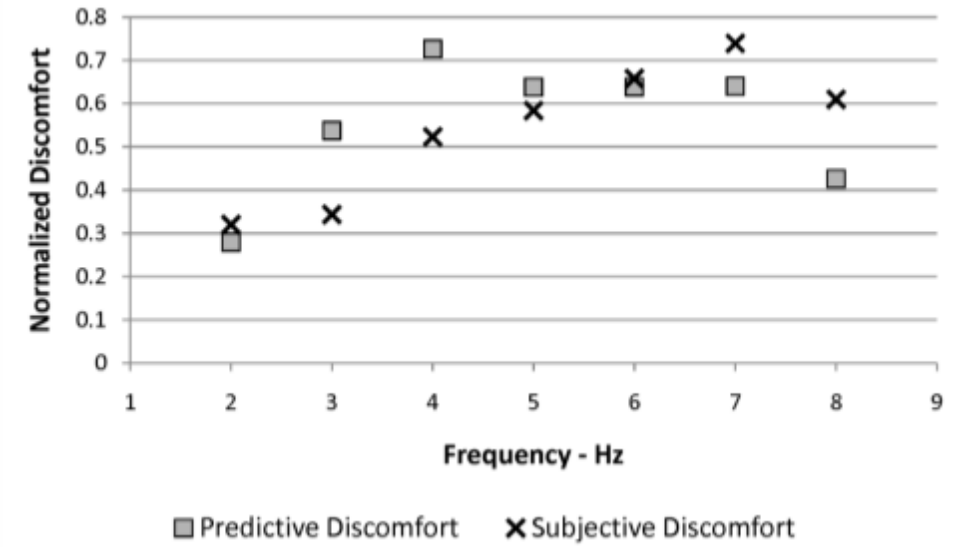

Figure 3.6 Normalized reported, transmissibility, and predictive discomfort for the head-down posture.

The R^2 between the absolute magnitude of the transmissibility and the absolute magnitude of the reported discomfort was 0.6595 for the normal posture, 0.8741 for the head-down posture, 0.229 for the head-to-side posture, and 0.005 for the head-up posture.

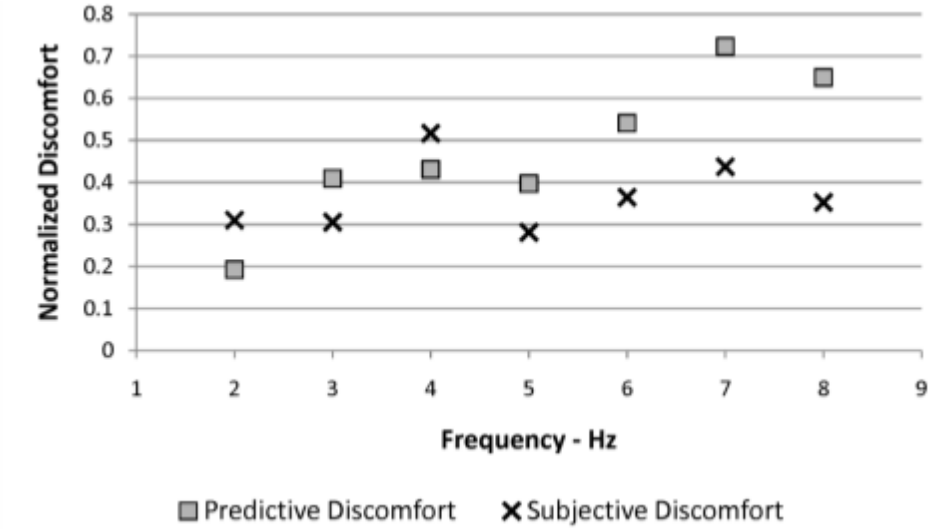

Figure 3.7 Normalized reported transmissibility, and predictive discomfort for head-to-side posture.

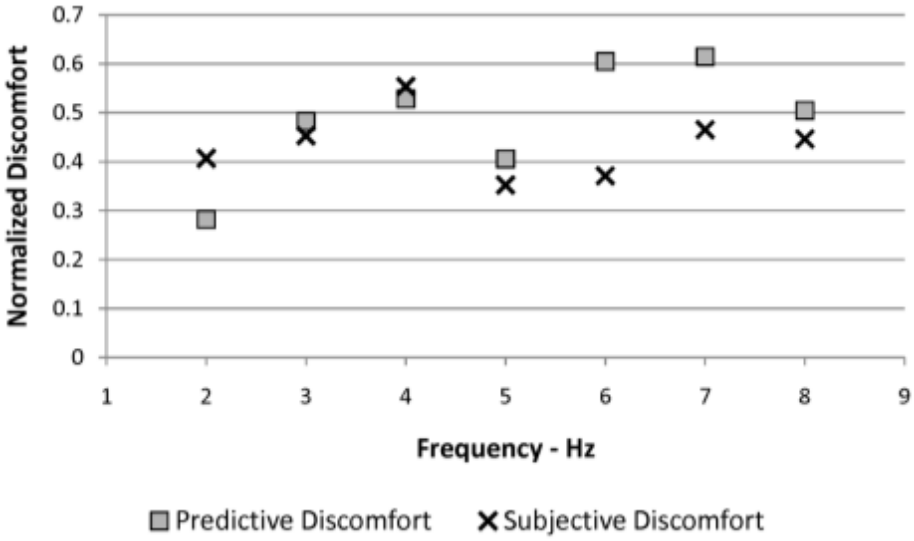

Figure 3.8 Normalized reported transmissibility, and predictive discomfort for head-up posture.

3.4 Discussion

The effect of head-neck posture on discomfort in WBV was investigated in this work using subjective-reported discomfort, predictive discomfort, and seat-to-head transmissibility. The study considered discrete vibration exposures in the fore-aft direction covering frequencies in the range of 2-8 Hz. The reason behind choosing this range of frequencies was based on a preliminary study where several participants were tested under fore-aft WBV with discrete-sinusoidal frequencies of 0.5, 1, 1.5, 2, 2.5, 3, 3.5, 4, 4.5, 5, 5.5, 6, 7, 8, 9, 10, 12, 14, and 16 Hz. The peaks in their reported discomfort were observed to be within the range of 2-8 Hz. The choice of this frequency range (2-8 Hz) was also based, to a certain degree, on the study conducted by Fard et al. (2003) in which the authors found that the head-neck complex behavior was quasilinear with one dominant resonance frequency between 0.8 and 1.6 Hz and another dominant frequency between 5 and 6 Hz. The slightly different peak locations between the study of Fard et al. (2003) and the current study could be related to the way the participants were strapped to the seat and the severity of tightness of the straps (Smith, 2000).

The results for the reported discomfort (Figure 3.2) showed that the head-neck posture has a significant effect on the reported discomfort level with $p<0.05$ for the neck-side posture at 2 Hz and 6 Hz, neck-down posture at 7 Hz, and neck-up posture at 5 Hz and 6 Hz. All postures, including the normal posture, reached a peak around 4 Hz. The second peak in the discomfort of the non-neutral postures shifted to a higher peak around 7 Hz instead of 6 Hz for the normal posture. This might be related to stiffer systems or larger motions. For the head-down posture, the magnitude of the reported discomfort was in general higher than that of normal posture. This could be associated with the difficulty

of generating more muscle moment in the head-down position to support the head-neck region, resulting in more uncontrolled, uncomfortable motions, or to the stiffening occurring in the head-neck complex in the fore-aft direction. The latter characteristic is consistent with the finding by Griffin and Lewis (1978), who showed stiff postures caused more head motion for frequencies above 4 Hz. The head-to-side and head-up postures showed less discomfort after the first peak at 4 Hz, but their magnitudes approach the normal posture around 7 Hz. In the latter postures, the participants may have more flexibility in using the major neck-back muscles to minimize the head-neck motion. This creates a stiffer system and may explain why there is a shift in the second peak in the head-to-side and head-up postures.

Figure 3.4 shows the peak transmissibility of the normal posture to be in the range of 5-6 Hz (Paddan and Griffin, 1998). The head-to-side and head-up postures exhibit similar trends to that of the normal posture. It is clear from Figure 3.4 that the head-down posture has the highest transmissibility for all frequencies, which is consistent with subjective-reported discomfort. This could be due to the difficulty of generating more muscle moment in the head-down posture.

The results showed that the coefficient of determination (R^2) between the absolute predictive discomfort and the absolute reported discomfort have strong correlation with magnitude above 0.85 for the normal and head-down postures. However, it showed weaker correlation for the head-to-side posture and head-up posture with R^2 of 0.3213 and 0.3367, respectively. The R^2 for the seat-to-head transmissibility and the absolute reported discomfort showed weaker correlation than that of the predictive discomfort for

the four postures with R^2 of 0.6595 for the normal posture, 0.8741 for the head-down posture, 0.229 for the head-to-side posture, and 0.00546 for the head-up posture.

In general, the proposed predictive discomfort has shown trends similar to those of the reported discomfort as shown in Figures 3.5-3.8. Figure 3.5 depicts the reported discomfort and the predictive discomfort for the neutral head-neck posture. The predictive discomfort followed the trend of the reported discomfort and showed peaks at 4 and 6 Hz. The transmissibility (Figure 3.4), on the other hand, generated one peak around 6 Hz. Figures 3.6-3.8 show characteristics of the non-neutral postures similar to those of Figure 3.5; however, in the head-to-side posture, the first peak in the predictive discomfort was shifted to 3 Hz instead of 4 Hz. This difference could be because the joint angle q in the current predictive discomfort equation only considered the effect of the fore-aft motion but did not take into account the effect of the lateral and vertical motions. The predicted discomfort was able to recognize the discomfort level in the head-down posture (Figure 3.6) in a manner similar to that of the subjective-reported discomfort. This trend suggests that workers in vibration environments should reduce any head-down postures to avoid unwanted head accelerations and discomfort. The latter is consistent with the finding of Alan and Alan (1999). While this can be true for short exposures, the authors believe that this needs to be further investigated in the future under longer vibration exposures (Griffin, 2007).

Increasing the amplitude of the vibrations from 0.8 m/s^2 to 1.15 m/s^2 has increased the discomfort level for both the reported-subjective and the predictive discomfort of the normal posture in a similar manner at frequencies of 4 and 6 Hz, as shown in Figure 3.3. The latter is a good indication of the relationship between

discomfort and the severity of the motion, which can be captured by the proposed predictive discomfort.

The predictive discomfort due to the initial starting posture, which comprises the first part of Equation 3.2, Δq^{norm} makes a significant contribution to the proposed predictive discomfort before the motion started and in the low-frequency range. For example, the predictive discomfort due to the initial starting posture will diminish for the case of neutral posture, but has a different magnitude for the remaining non-neutral postures. However, the results have shown that some of the non-neutral postures, such as the head-to-side and head-up postures (Figure 3.2), have shown lower reported-subjective discomfort than the normal posture at frequencies higher than 4 Hz. This is because of the effect of the fourth term in the predictive discomfort ($\Delta \ddot{q}$), which is related to the change of the angular acceleration and which will have a greater role at higher frequencies. It is also believed that the initial posture may make a greater contribution to the total reported-subjective discomfort with time due to the role of fatigue (Kittusamy and Buchholz, 2004).

The transmissibility, apparent mass, and energy input are all good measures to simulate how the input energy affects the operator's motion; still, these measures are too global to capture the characteristics of the discomfort due to local changes in posture. With different cab designs, the energy may enter the operator's body from different locations such as the foot-pedal, steering wheel, seat-back, and arm-rest (Newell and Mansfield, 2008), all of which could play significant roles in the discomfort magnitude. Many studies agree that there is an effect from posture and interaction with the equipment on the perception of vibration (Griffin et al., 1978; Jack and Eger, 2008; Rakheja et al.,

2010); however, there is no current objective measure that can capture or deal with these characteristics.

The current study showed the strength and relevance of the proposed predictive discomfort with the subjective-reported discomfort for different non-neutral head postures. The predictive discomfort was able to capture the trend, the shift in the peaks, and the valley in the subjective-reported discomfort for normal posture. It also closely followed the trend in the subjective-reported discomfort for different postures under investigation. Additionally, it showed better correlation with the subjective-reported discomfort than that of the seat-to-head transmissibility. The predictive discomfort was able to quantify the effect of the vibration magnitude on discomfort and demonstrate it in a manner similar to the subjective-reported discomfort. These characteristics show that the discomfort and perception of vibration in general are associated with the posture and acceleration. While the predictive discomfort has shown good performance in the fore-aft WBV, the encouraging results of this study will open the door for the proposed predictive discomfort for potential applications with more complex vibration environments, especially those involving multiple-axis WBV. With advances in computer modeling, the proposed predictive discomfort may provide efficient ways to develop reliable biodynamic models for design of equipment inside moving vehicles.

CHAPTER 4: PREDICTIVE DISCOMFORT AND SEAT-TO-HEAD TRANSMISSIBILITY[4]

4.1 Introduction

Seat-to-head transmissibility (STHT) is a widely used biomechanical measure in whole-body vibration (WBV) as an objective indicator for vehicle ride discomfort and to assess the effectiveness of vibration isolation systems in achieving low vibration amplification around resonance areas (Griffin, 1990). There is a general uncertainty in the calculation of the STHT in terms of its sensitivity to the location of the output point on the head. The STHT contains another uncertainty in the way people calculate it. In spite of the tremendous work that has been done on collecting data on the STHT, the discrepancies in the locations of the output point on the head and the manner in which the STHT is calculated and do not allow data to be compared easily across labs (Paddan and Griffin, 1998).

Many authors would agree that whole-body musculoskeletal-discomfort is correlated with the severity of the motion at the different joints and with body posture (Kee and Karwowski, 2001; Kee and Karwowski, 2003; Whitham and Griffin, 1978). Researchers have shown the neck and trunk segments being two of the major sources of discomfort and potential for long-term injury for seated people in WBV (Courtney and Cahn, 1999; Magnusson et al., 1996; Pope et al. 1998; Eger et al., 2008; Johanning et al., 2006; Rehn et al., 2005; Rehn et al., 2009). Therefore, the development of a new discomfort measure in the area of seated WBV should consider the effect of body posture

[4] Published in the Journal of Low Frequency Noise, Vibration and Active Control.
DeShaw, J.; Rahmatalla, S. Predictive discomfort and seat-to-head transmissibility in low-frequency fore-aft whole-body vibration. *Journal of Low Frequency Noise, Vibration and Active Control.* **2011,** 30(3), 185-196.

and should include the discomfort associated with the body joints, with the latter including the neck and trunk regions at the least.

In this work, a biomechanically based predictive discomfort measure presented by Rahmatalla and DeShaw (2011) is extended for the evaluation of discomfort for multiple joints with the focus on the neck and trunk joint discomfort during fore-aft discrete sinusoidal WBV. The predictive discomfort measure is less vulnerable to measurement locations and was compared with subjective reported discomfort and with the STHT considering two sitting postures.

4.2 Methods

4.2.1 Participants

Five healthy male participants with a mean age of 24 years (ranging from 19-29 years), a mean stature of 188 cm (ranging from 180-196 cm), and a mean body mass of 84.5 kg (ranging from 71-98 kg) were recruited. Written informed consent (Appendix B), as approved by the University of Iowa Institutional Review Board, was obtained prior to testing.

4.2.2 Experiments

Participants were seated in an uncushioned, rigid seat mounted to a vibration platform (Figure 4.1). Two sitting postures were considered, one with the participant sitting in a standard posture supported by the seat back, and the second in a forward unsupported upright posture. For both postures the participants' hands were kept in their laps. Vibrations of 15 second duration were generated using a six-degree-of-freedom man-rated vibration platform (Moog-FCS, Ann Arbor, MI, USA). Signals with constant unweighted RMS accelerations with a magnitude of 0.8 m/s^2 were tested. Discrete

sinusoidal frequencies of 0.5, 1, 1.5, 2, 2.5, 3, 3.5, 4, 4.5, 5, 5.5, 6, 7, 8, 9, 10, and 12 Hz were chosen and randomized.

4.2.3 Motion Capture Setup

Twelve 0.3 megapixel Vicon SV (Vicon, Los Angeles, CA, USA) cameras with a sampling rate of 200 frames per second were used in tracking the motion of the head and spine at the C7 (Rahmatalla et al., 2008). Reflective markers were adhered to the participant's skin using medical-grade double-sided tape (Figure 4.1).

Figure 4.1 Experimental setup and marker locations on a participant sitting with the supported-back position

A head-mounted halo was worn by the participants and fitted with four head markers. The head-mounted motion capture reflective markers were attached superiorly and laterally to each eyebrow and the back of the head, one on each side. The front of the

head was defined as the center of the two front head points and was near the center of the forehead, the back of the head was defined as the center of the two back head points and was near the intersection of the parietal and occipital bones, and the center of the head point was defined as the center of the front and back head points. Additionally, markers were placed on each side on the level of C1 over the mastoid process, the skin overlaying the C7 vertebra, the shoulders, the clavicle, the pelvis, and the frame of the seat to measure the relative motions between segments. Additional redundant makers were placed on each participant and were not used in this work.

4.2.4 Velocity and Acceleration

Once the marker position data were collected and appropriately low-pass filtered based on the power spectrum analysis of a companion seat-mounted accelerometer, the data were used to calculate the velocity and acceleration by differentiation of the continuous positional data using the finite difference method. The filtering process was achieved by applying an eighth-order Butterworth filter in both directions to achieve zero lag. A cut-off frequency of 14 Hz was applied to all time-position segments. A program in MATLAB was written to use a 5-point central difference method to approximate the differential of the position data to obtain realistic velocity data. The velocity data were then transformed by the same method to angular and linear acceleration data. After two seconds the participant was assumed to be at a steady state response and the root-mean-square values (RMS) of each acceleration signal were calculated.

4.2.5 Subjective Reported Discomfort

In each discrete frequency test, the participants reported their whole-body discomfort using the Borg CR-10 scale (Appendix A). The Borg CR-10 scale ranges from

0 to 10, with higher values indicating higher relative discomfort. The participants were exposed to 15 seconds of vibration at each frequency and experienced a 5-second resting period between tests. This duration is acceptable as found by Dickey et al. (2006). The participants rated their perceived discomfort during vibration by comparing it with their perception during the resting period. The reported discomfort was normalized by the method used by Hwang and Yoon (1981) and presented in Equation 4.1.

$$ND = \frac{RD - Min\ (RD\ of\ Subject)}{(Max - Min\ (RD\ of\ Subject)} \qquad \text{(Eq. 4.1)}$$

In Equation 4.1 *ND* is the normalized discomfort and *RD* is the reported discomfort.

The normalization of the subjective data ensured that while some participants may have tendencies to give overall higher or lower responses, general trends can be found. Once participant data were normalized by the above method, the participants' discomfort responses were averaged for each discrete frequency and posture.

4.2.6 Seat-to-head transmissibility

Seat-to-head transmissibility is a widely used biomechanical measure in WBV for the quantification of energy through the system (Demic and Lukic, 2009; Griffin, 1990; Jack and Eger, 2008; Wang et al., 2008; Wilder et al., 1982). It is defined as the complex ratio between the cross-spectral density of the input seat horizontal acceleration and the output head acceleration $S_{hs}(jw)$ divided by the auto-spectral density of the input horizontal seat acceleration $S_{ss}(jw)$ and is shown in Equation 4.2. The STHT normally shows significant increase when resonance is occurring. For discrete frequency rides,

such as those involved in this work, the STHT was computed in the time domain as the RMS of the output head-acceleration divided by the RMS of the input seat-acceleration.

$$T_h(jw) = \frac{S_{hs}(jw)}{S_{ss}(jw)} \qquad \text{(Eq. 4.2)}$$

With transmissibility, there is general uncertainty associated with the location of the output point on the head and with which motion components are to be used as the output accelerations. These discrepancies were evaluated and compared with the predictive discomfort measure presented in this work.

4.2.7 Predictive Discomfort

A single joint predictive discomfort considering the neck-joint was presented by Rahmatalla and DeShaw (2011) and was of the following form:

$$f(\boldsymbol{q}) = \Delta q_i^{norm} + G \times QU + G \times QL + \Delta \ddot{q}_i \qquad \text{(Eq. 4.3)}$$

where

$$\Delta q^{norm} = \frac{q - q^N}{q^U - q^L} \qquad \text{(Eq. 4.4)}$$

and q^U is the joint's upper limit, q^L is the joint's lower limit, q^N is the joint neutral position, $G \times QU$ is a penalty term associated with joint values that approach their upper

passive limits (Equation 4.5), and $G \times QL$ is a penalty term associated with joint values that approach their lower passive limits (Equation 4.6). Each penalty term varies between zero and G=10^6 (Marler et al., 2005; Rahmatalla et al., 2010).

$$QU = \left(0.5 sin \left(\frac{5.0 \ q^U - q}{q^U - q^L} + 1.571 \right) + 1 \right)^{100} \tag{4.5}$$

$$QL = \left(0.5 sin \left(\frac{5.0 \ q - q^L}{q^U - q^L} + 1.571 \right) + 1 \right)^{100} \tag{4.6}$$

The last term $\Delta q_i^{\cdot\cdot}$ represents the angular acceleration of the joint. This work generalizes Equation 4.3 to include the discomfort of multiple joints as shown in Equation 4.7.

$$f(\boldsymbol{q}) = \sum_{i=1}^{j} \omega_i \ \Delta q_i^{norm} + G \times QU + G \times QL \ + \sum_{i=1}^{j} \alpha_i \Delta q_i^{\cdot\cdot} \tag{4.7}$$

where j represents the number of joints under consideration, and ω_i and α_i are weights of the joint's discomfort reflecting the contribution from that joint to the whole-body discomfort. Due to their major role in discomfort in sitting positions, the neck and trunk joints are considered in this work as the two main sources of discomfort (Magnusson et

al., 1996). The magnitude weightings used for ω_i and α_i were based on equal weighting for the neck and trunk.

4.3 Results

For the unsupported-back condition, Figure 4.2 shows the mean subjective reported ratings based on the Borg CR-10 scale and the mean neck and mean trunk predicted discomfort. These values were then averaged and normalized according to their maximums. The mean subjective reported discomfort curve showed a peak around 2-3 Hz. The predicted neck discomfort curve followed a similar trend to that of the reported discomfort and showed a peak around 2.5 Hz. The predicted trunk discomfort showed similar characteristics but was higher than the predicted neck discomfort for all frequencies except for those between 3-4 Hz.

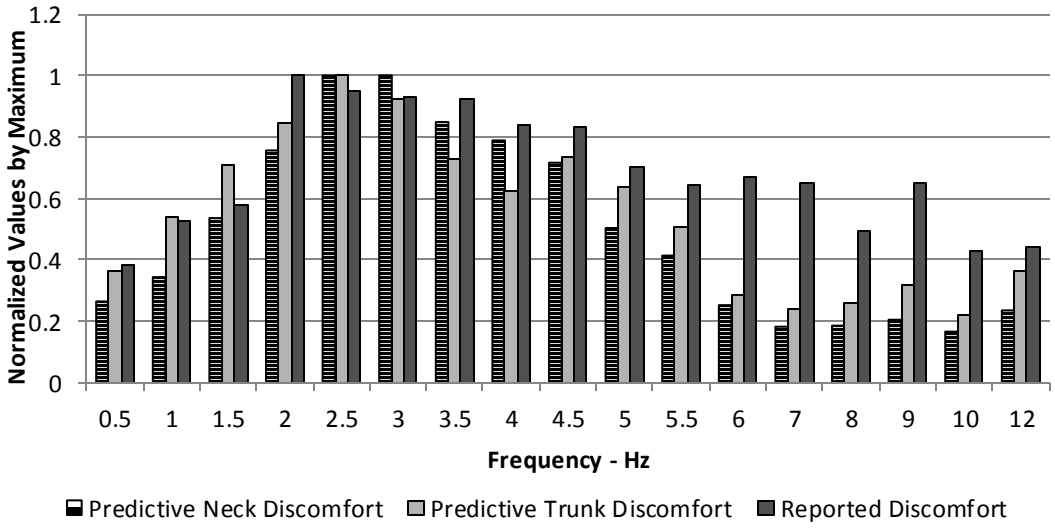

Figure 4.2 Comparison of predicted discomfort and reported discomfort for unsupported-backrest condition

For the supported back position, the peak in the reported subjective discomfort (Figure 4.3) shifted to 3.5-6 Hz and descended after that. The predicted neck discomfort

showed peaks around 3.5 Hz and descended after that. The predicted trunk discomfort showed peaks between 3.5-5 Hz in a trend similar to that of the predicted discomfort. For frequencies above 7 Hz, the neck discomfort was higher than the trunk discomfort.

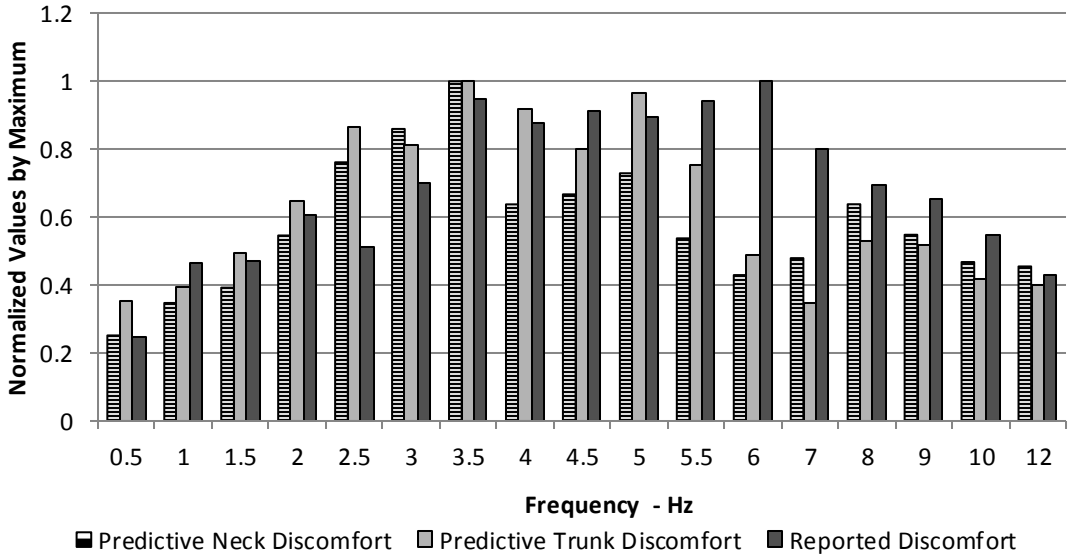

Figure 4.3 Comparison of predicted discomfort and reported discomfort for supported-backrest condition

The combined predicted discomfort calculated as a weighted sum of the neck and the trunk discomfort for the unsupported-back conditions is shown in Figure 4.4. As can be seen from the figure, the combined predictive discomfort curve more closely followed the subjective reported curve, with a dominant peak around 2.5 Hz. However, the combined discomfort showed lower values for frequencies above 6 Hz. For the supported-back position (Figure 4.5), the combined predicted discomfort showed a peak around 3-3.5 Hz and closely followed the subjective reported discomfort after that, except for the period between 6-7 Hz.

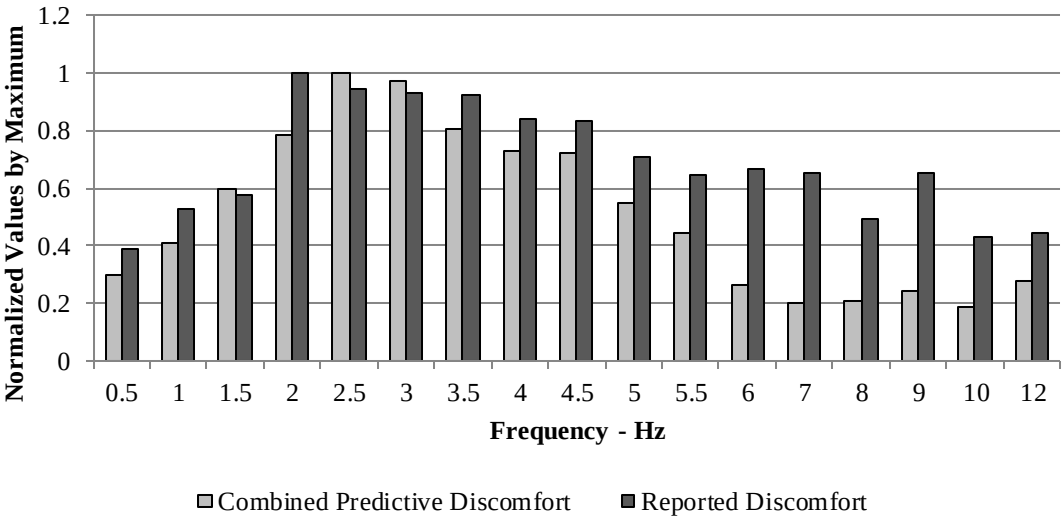

Figure 4.4 Combined Predictive Discomfort vs Subjective Reported Discomfort - Unsupported-Backrest Condition

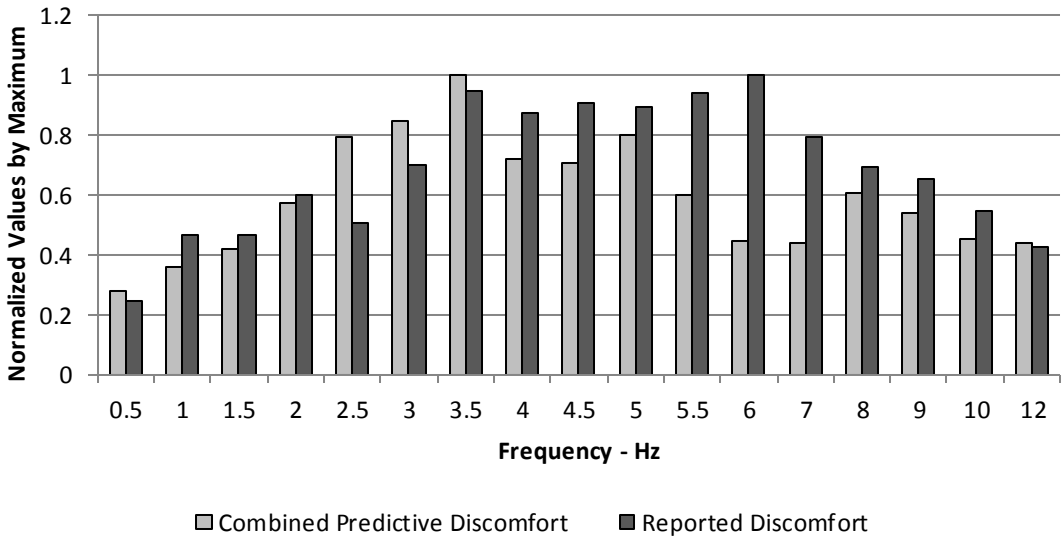

Figure 4.5 Combined predictive discomfort vs subjective reported discomfort - supported-backrest condition

In order to evaluate the true relationship between the predictive discomfort and the subjective discomfort, each was compared on an absolute scale with no normalization procedures. The coefficient of determination (R^2) found for each condition was evaluated

as shown in Figure 4.6. The coefficient of determination (R^2) was 0.739 for the unsupported-backrest condition and 0.323 for the supported-backrest condition.

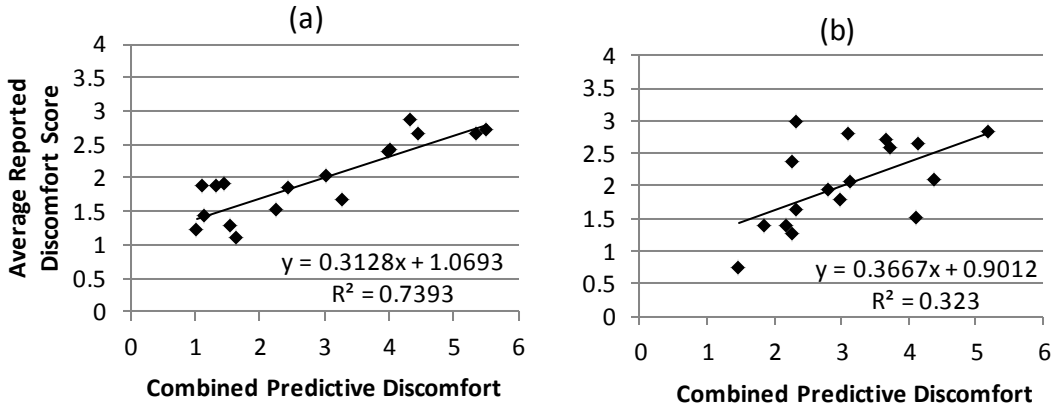

Figure 4.6 Average combined predictive discomfort vs average reported discomfort score for unsupported-backrest (a) and supported-backrest (b) conditions

Figure 4.7 shows the STHT for the unsupported-back condition T_{x-x} calculated based on the fore-aft component (x) of the seat and the fore-aft component (x) of a point on the head, and T_{x-xyz} calculated based on the fore-aft component of the seat (x) and the total components of a point on the head (xyz). Both T_{x-x} and T_{x-xyz} were investigated at three locations on the head in the sagittal plane and along the fore-aft direction, including a point at the center of the head, the front of the head, and the back of the head, as previously described. The points on the front of the head showed the highest magnitudes for both T_{x-xyz} and T_{x-x} . For the supported-back condition (Figure 4.7), the STHT showed obviously different characteristics between T_{x-x}, with T_{x-xyz} being higher for all points under investigation.

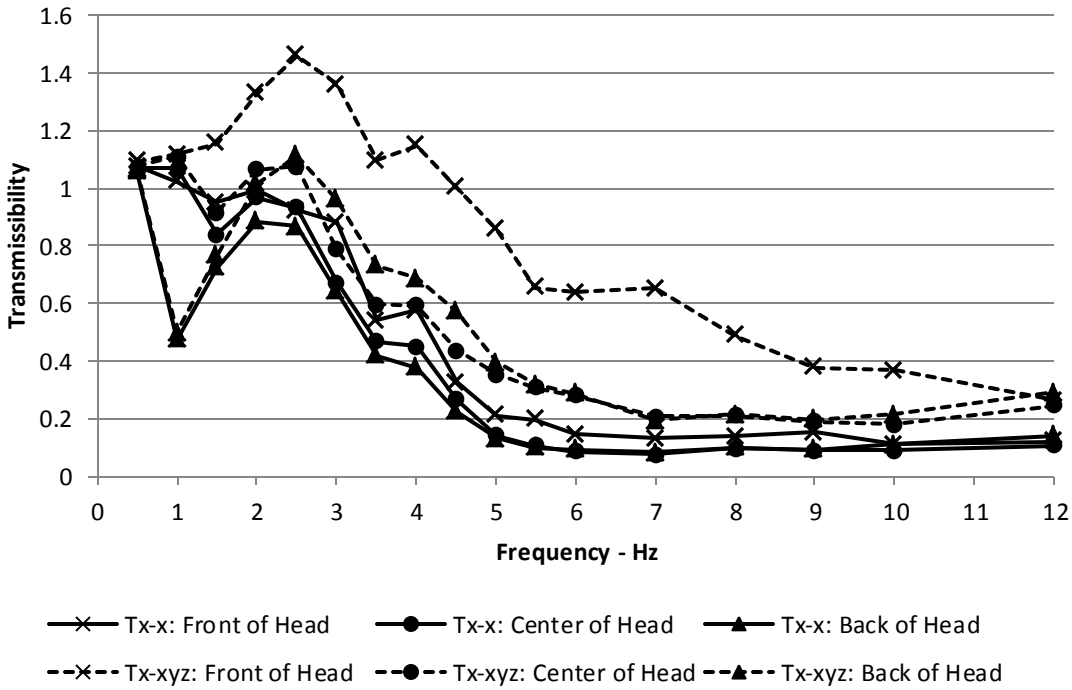

Figure 4.7 Seat-to-head transmissibility T_{x-x} and T_{x-xyz} based upon head point selection for unsupported-backrest condition

For both back-support conditions shown in Figure 4.7 and Figure 4.8, and regardless of the location of the points on the head or the calculation methods used to calculate STHT, the transmissibility showed higher magnitudes below 2 Hz than the subjective reported discomfort. After 2 Hz, the transmissibility for the unsupported-back condition showed good agreement with the subjective reported discomfort. The coefficient of determination between the transmissibility and the average subjective discomfort was not correlated for T_{x-x} and ranged from 0.090 to 0.434 for T_{x-xyz}, depending on the head point selection, with the front-of-the-head point having the best relationship. For the supported-back condition (Figure 4.8), the transmissibility T_{x-x} was not able to capture the peak characteristics of the subjective reported discomfort;

however, the transmissibility T_{x-xyz} showed more comparable trends with the subjective reported discomfort. While these general trends were somewhat better, the best correlation with the subjective reported discomfort came from the transmissibility T_{x-xyz} based upon the-front-of-the-head point with a coefficient of determination of only 0.196.

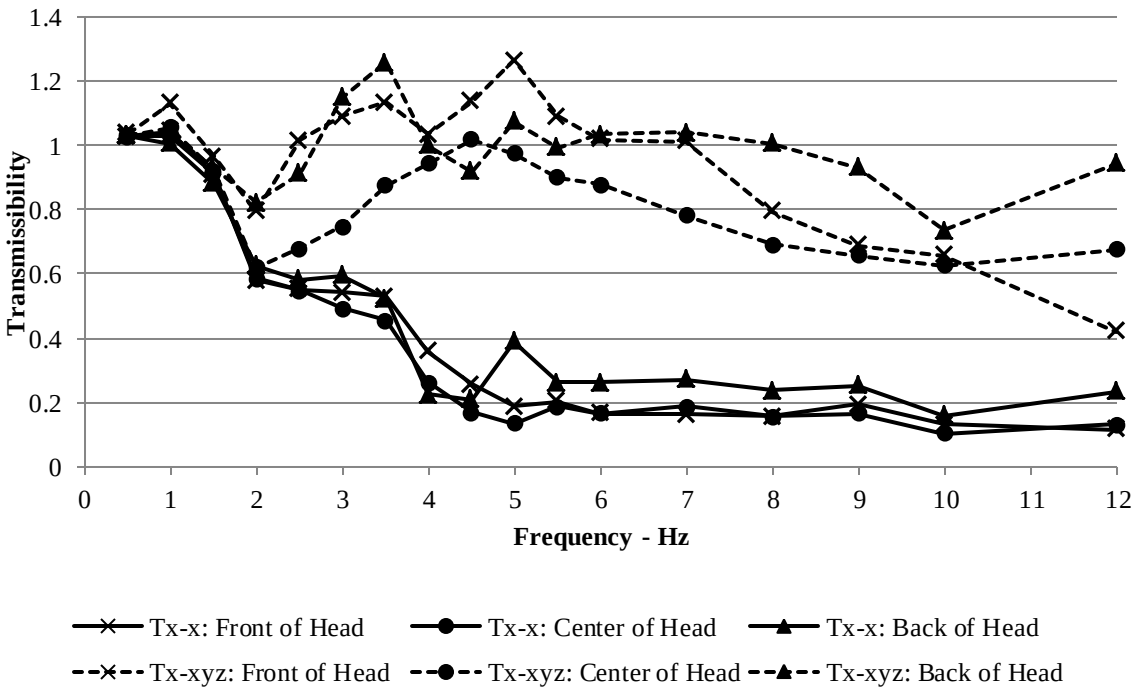

Figure 4.8 Seat-to-head transmissibility T_{x-x} and T_{x-xyz} based upon head point selection for supported-backrest condition

4.4 Discussion

The objective of this work was to develop a predictive discomfort in WBV that can deal with discomfort occurring at different joints and to show its invulnerability to the location of the measurement point on the head. The predictive discomfort measure has the benefit of overcoming the discrepancies in the STHT due to different practices in

various labs. The proposed predictive discomfort comprises four components. The first component captures the effect of posture on discomfort. This component has zero effect when the joint is in its neutral position, but will contribute to discomfort with non-neutral postures. A previous study (Rahmatalla and DeShaw, 2011) on the effect of non-neutral head-neck postures in fore-aft WBV showed the head-down posture, for example, had higher subjective and predictive discomfort than a neutral posture. In this work, the participants took postures close to their neutral positions, so the magnitude of the first component was zero. The second and third components generate peaks in discomfort when the joint reaches its physiological upper or lower limits. Again, in this work, the data have shown that the participants never reached their upper or lower joint limits, so the second and the third parts were equal to zero. The fourth part quantifies discomfort as a measure of the severity of the relative angular motion represented by the angular acceleration at the neck and trunk joints. The proposed predictive discomfort was tested and compared with the subjective reported discomfort and STHT under fore-aft WBV considering two sitting postures—supported-back and unsupported-back conditions. The study considered discrete ride files covering frequencies 0.5, 1, 1.5, 2, 2.5, 3, 3.5, 4, 4.5, 5, 5.5, 6, 7, 8, 9, 10, and 12 Hz.

As shown in Figure 4.2 and 4.3, the subjective reported discomfort for the unsupported- and supported-back conditions have shown similar characteristics to those reported in the literature (Maeda et al., 2008; Subashi et al., 2009), especially for the locations of the peak discomfort. The subjective reported discomfort has captured the effect of the seatback on discomfort, where the peak discomfort shifted from 2-3 Hz for the unsupported-back condition (Figure 4.2) to around 3.5-6 Hz for the supported-back

condition (Figure 4.3). The combined predictive discomfort for the neck and trunk regions showed peaks around 2.5 Hz for the unsupported-back condition (Figure 4.4) and then shifted to 3-3.5 Hz for the supported-back conditions (Figure 4.5), which follows the shift in the trend of the subjective reported discomfort when comparing the two postures.

The combined discomfort of the neck and trunk for the unsupported- and supported-back conditions (Figure 4.4 and Figure 4.5) showed good agreement with the subjective reported discomfort in terms of the location of the first peak and the general trend over the frequency range under consideration. The combined discomfort was also able to capture the shift in the first peak due to the back support in a way consistent with that of the subjective-reported discomfort. It should be mentioned here that the neck and trunk discomfort were equally weighted and combined based on the work of Genaidy and Karwowski (1993).

The STHT T_{x-x} and T_{x-xyz} calculated at different locations on the head showed similar general trends for the unsupported-back condition (Figure 4.7), however they showed much less correlation with the subjective reported discomfort as compared to the predictive discomfort. The coefficient of determination (R^2) for the STHT ranged from 0.090 to 0.434, depending on the head point selection with maximum correlation occurring at the front of the head where the horizontal and vertical component of the head-neck motion is the greatest. This could be due to largest distance between the point on the front of the head and the center of the rotation of the head-neck when compared to the other points at the center and the back of the head. If the back or center head points are used, this may have significant impact on clinical evaluation and biodynamic model development as the motion would be underestimated at these points. While the

transmissibility components did not correlate well with the subjective discomfort ratings, the predictive discomfort measure had an R^2 value of 0.739 for the unsupported-backrest condition. This could be attributed to the dependence of the predictive discomfort on the angular motion that is invulnerable to the location of the point on the head. Therefore, one suggestion to circumvent the difference of the location on the head in different studies is to use the angular component of the output motion instead of the transitional ones when calculating transmissibility and discomfort measures.

For the supported-backrest condition, the STHT T_{x-x} (Figure 4.8) did not follow the subjective reported discomfort; however, transmissibility T_{x-xyz} followed the general trends. While the general trend was followed, there was still much less correlation with the subjective reported discomfort than the predictive discomfort measure had with the subjective reported discomfort. The coefficient of determination (R^2) ranged from no correlation to 0.196 depending on the head point selection, whereas the predictive discomfort measure had an R^2 value of 0.323 for the supported-backrest condition. The transmissibility that accounted for three components of motion was better at relating to discomfort than the single component transmissibility. Also, as shown in the unsupported condition, the front head point seemed to be more sensitive to vibration and closer to the subjective discomfort ratings than the back and center head points. The low coefficient of determination for the transmissibility and the predictive discomfort with the subjective reported discomfort could be attributed to other physiological or psychological parameters that may be related to seating conditions but may not be strongly related to motion.

While applied to a single fore-aft direction, this work has demonstrated the

discrepancies in the results of the STHT, which depend on how the transmissibility is calculated and on the locations of the output point on the head (Griffin et al., 1979). While Paddan and Griffin (1992) investigated the effect of the locations of the point along the vertical direction of the head, this work showed that the STHT is also sensitive to the locations of the point of the head along the fore-aft direction, which could be due to the pitch motion of the head relative to the neck. Due to its dependency on the angular parameters, the proposed discomfort is expected to be less sensitive to the locations of the sensors, and therefore, more easily reproduced. The STHT demonstrated discrepancies when compared to the subjective reported discomfort. This is because STHT is sensitive to the locations of the output point on the head and to the number of head-motion components used in its calculation.

4.5 Conclusion

A predictive discomfort for the combined neck and trunk in fore-aft WBV is introduced in this work. The proposed discomfort quantifies whole-body musculoskeletal discomfort considering body posture, closeness of the joints to their limits, and severity of the angular acceleration at the joints. The proposed predictive discomfort captured the trend of the subjective reported discomfort and showed good potential to capture the effect of two seated postures: the unsupported- and supported-back conditions.

The major contributions of the proposed predictive discomfort, as the results showed, are: (i) it is dependent on the resulting angular motion of the segments, so it is less sensitive to the location of the sensors on the head and could be reproduced in different locations; and (ii) it can deal with postures and boundary conditions as presented in this work. Therefore, the proposed predictive discomfort has the potential to

be used and shared by different labs. With advances in computer modeling, the proposed predictive discomfort may provide efficient ways to assess discomfort in complicated environments and to develop reliable biodynamic models for design of equipment inside moving vehicles. The current study focused on the discomfort considering the weighted sum of the neck and trunk regions, but this could be expanded to add any number of segments of the body.

CHAPTER 5: PREDICTIVE DISCOMFORT IN SINGLE- AND MULTIPLE-AXIS WHOLE-BODY VIBRATION DURING DIFFERENT SEATED POSTURES[5]

5.1 Introduction

It is well known that sitting postures play a significant role in the resulting level of perceived discomfort and have long-term health consequences such as low-back pain (Adams and Hutton, 1985; Griffin, 1990; Magnusson et al., 1996; Wilder et al., 1996; McGill, 1997; Chaffin et al., 1999; Mansfield, 2005A, De Oliviera), with most recent studies highlighting the critical role of human postures on the biodynamic response of seated humans (Kittusamy and Buchholz, 2004; Mansfield and Maeda, 2005; Wang et al., 2006B; Rahmatalla and DeShaw, 2011; DeShaw and Rahmatalla 2011; Mandapuram et al., 2010). Many researchers have concluded that backrest and sitting-posture conditions play an important role in risk assessment during WBV (Hinz et al., 2002; Basri and Griffin, 2013; Wikstrom, 1993).

Many occupations require people to use non-neutral postures to monitor their equipment while both the person and the equipment are under vibration (Kittusamy and Buchholz, 2004; Rehn, Nilsson et al., 2005; Thuresson, et al., 2005; Eger et al., 2008; Newell and Mansfield, 2008; Smith, 2000, Wikstrom 1993). De Oliviera (2005) found that posture and cyclic compressive force due to vibration can lead to a high incidence of discomfort and back pain among helicopter pilots, while Smith (2000) showed that head-neck orientation was important to the vibration transmission to the heads and helmets of F-15 pilots. Rehn et al. (2005) indicated that all-terrain vehicle (ATV) drivers frequently use non-neutral rotational positions. They discovered that the non-neutral rotational

[5] In preparation for submission to a peer-reviewed journal.

positions of the neck are an ergonomic risk factor that occurs frequently and with short duration for professional ATV drivers. Eger et al. (2008) found that load-haul-dump operators drove with their necks rotated more than 40 degrees over 89% of the time, which is considered above the Swedish National Work Injury Insurance Criteria for neck rotation. They also found that simultaneous exposure to vibration and non-neutral postures such as neck rotation and truck rotation, flexion, and lateral postures could increase the driver's risk of musculoskeletal injury in the mining industry.

Besides purely subjective measures (Kaneko et al., 2005; Hacaambwa and Giacomin, 2007; Mansfield and Maeda, 2011) which often relate reported discomfort to current standards (ISO 2631-1, 1997; BS 6841, 1987)or to weighted RMS accelerations, researchers are also interested in developing predictive measures to quantify discomfort in WBV (Ebe and Griffin, 2000, Basri and Griffin, 2013). Ebe and Griffin (2000) stressed the importance of considering static seating postures as they developed a predictive discomfort model for WBV. Paddan and Mansfield, 2012, and Basri and Griffin 2013 address the issue with seated postures by using an inclined backrest where each study introduces new constants and weighting factors to be used in the current standards BS 6841 and ISO 2631-1.

Recent studies have evaluated human discomfort in single-axis WBV (Hacaambwa and Giacomin, 2007; Basri and Griffin, 2013; Paddan and Mansfield, 2012) but few have systematically studied discomfort 3D and 6D WBV(Mansfield and Maeda, 2011; Marjanen and Mansfield, 2010), especially between multiple postures. Mansfield and Maeda (2011) studied discomfort from single- and multiple-axis inputs; however, only a relaxed upright posture was used. They found that the root-sum-of-squares method

of summation of subjective ratings in individual axis was adequate for estimating the intensity of multiple-axis vibrations. Marjanen and Mansfield (2010) found that the ISO 2631-1 RMS method showed a reasonable correlation with discomfort (R^2 = 0.85; however, results varied greatly depending on the weighting factors and axes used in the calculation. While the results from these discomfort calculations may be appropriate in some circumstances using different weighting factors and coefficients, given a different posture or vibration scenario, the coefficients will likely need to be changed.

The current reference standard when determining discomfort or fatigue during whole-body vibration is the ISO 2631-1, Mechanical vibration and shock – evaluation of human exposure to whole-body vibration (International Organization for Standardization, 1997). This standard uses the input accelerations at the seat pan, seat backrest, and footrest to develop "frequency weighted accelerations," which then relate to fatigue and comfort limits. The standard can resolve single- and multiple-direction vibrations by taking the root-sum-square of the individual directions; however, the standard is limited when considering posture. Factors listed in the ISO 2631-1 involve the inclusion of a backrest and a footrest; any other postural effects are neglected. Many researchers in the field have criticized the ISO 2631-1 in real-life applications or cited inappropriate frequency- dependent weighting values or ease of use (Dickey et al., 2007; Kaneko et al., 2005), while others attributed to flaws in the standard to contact points or seatback orientation (Beard and Griffin, 2013; Basri and Griffin, 2012). Another limitation of the standards is that once the frequency weighted accelerations are calculated for a given vibration scenario, those accelerations must then be applied to another set of graphs to determine limits and guidelines for comfort and safety. Therefore, the novel contribution

of this work is to develop a straightforward model for human discomfort in whole-body vibration of all types and postures.

In this work, a biomechanically based predictive discomfort measure is modified from the discrete sinusoidal vibration conditions (DeShaw and Rahmatalla, 2011; Rahmatalla and DeShaw, 2011) to the prediction of discomfort for multiple seating postures and random vibration during single- and multi-axis WBV. The hypothesis behind the proposed discomfort measure is that the head-neck and trunk discomfort is sensitive to deviation from the neutral posture and to the rate of change in angular motion of the human joints. The current study seeks to systematically quantify differences in human discomfort from different seating postures and vibration scenarios using an all-encompassing predictive discomfort model. This model will then be compared to the current standard ISO 2631-1 and advantages and limitations of each will be discussed.

5.2 Methods

5.2.1 Participants

The discomfort and vibration response induced by whole-body vibration was measured in this work considering different vibration directions, postures, and vibration magnitudes. The participant group for this study consisted of twelve males with a mean age of 24.0 years (standard deviation of 2.7 years), mean height of 180.1 cm (standard deviation of 5.9 cm), and mean weight of 84.0 kg (standard deviation of 9.2 kg). The biodynamic response of the group was recorded for each participant under all combinations of posture and vibration type. All participants were generally healthy, reported no musculoskeletal conditions, and were approved by the University of Iowa

Institution Review Board prior to testing (Appendix B). Each participant was tested in a simulated vibration environment for a maximum duration of one hour.

5.2.2 Vibration Conditions

Vibrations were produced for this study using a six-degree-of-freedom man-rated motion simulator (Moog ECU-624-1800, Moog-FCS, Ann Arbor, MI, USA). The directions and magnitudes are shown in Table 5.1. The single-axis vibration conditions included random fore-aft, lateral, and vertical vibrations all from 0.5 to 12 Hz, each having an unweighted RMS acceleration magnitude of 1.8 m/s^2. The vibration files were created from white noise and band-pass, filtered to achieve the desired frequency range, and then transferred to the motion simulator at a sample rate of 512 Hz. Each vibration file lasted a total of 60 seconds.

Table 5.1 List of vibration conditions with the RMS linear accelerations and RMS angular accelerations for each translational direction and each rotational direction, respectively.

Vibration/ Direction	Translation Fore-Aft	Translation Lateral	Translation Vertical	Rotation Roll	Rotation Pitch	Rotation Yaw
Fore-Aft	1.8 m/s^2	-	-	-	-	-
Lateral	-	1.8 m/s^2	-	-	-	-
Vertical	-	-	1.8 m/s^2	-	-	-
3D-H	1.1 m/s^2	1.1 m/s^2	1.1 m/s^2	-	-	-
3D-L	0.6 m/s^2	0.6 m/s^2	0.6 m/s^2	--	-	-
6D-H	1.1 m/s^2	1.1 m/s^2	1.1 m/s^2	0.8 rad/s^2	0.8 rad/s^2	0.8 rad/s^2
6D-L	0.6 m/s^2	0.6 m/s^2	0.6 m/s^2	0.5 rad/s^2	0.5 rad/s^2	0.5 rad/s^2

Three-dimensional and six-dimensional random vibrations were also simulated from 0.5 to 12 Hz at two differing magnitudes each (Table 5.1). The 3D and 6D motion files were generated so that equal power occurred in each of the translational or rotation axes. Additionally, each vibration component was created with separate white noise so

that no resultant symmetry occurred in any two directions of the files. Each 3D and 6D vibration file lasted for a total of 60 seconds. A summary of the vibration conditions is presented in Table 5.1.

5.2.3 Postural Conditions

Figure 5.1 The four seating postures tested. (NB) for the no-backrest condition; (BS) for the backrest-supported condition; (B+A) for the backrest-supported and armrest-supported condition; and, finally, (B+A+R) for the backrest-supported, armrest-supported, and head-rotation condition.

Four seating postures were considered for this study: (NB) An upright seated posture with no backrest where the participants looked straight forward with their hands in their laps; (BS) a backrest-supported sitting posture where the participants looked

forward with their hands in their laps; (B+A) a backrest-supported sitting posture where participants' forearms rested on armrest supports and where the participants looked forward; and (B+A+R) a backrest-supported sitting posture where the participants used the armrest supports and rotated their heads to the side (Figure 5.1).

Table 5.2 List of vibration and posture combinations used during experiment where the conditions marked 'X' were used to find the constants for the model, the conditions marked with lowercase 'x' were used to in the model but not to find the constants, and the conditions marked 'TC' were used as test conditions to later validate the model.

Posture / Vibration Condition	No Backrest (NB)	Backrest Supported (BS)	Backrest and Armrest (B+A)	Backrest, Armrest, and Head Rotation (B+A+R)
Fore-Aft	X	X	X	x
Lateral	X	X	X	x
Vertical	X	X	X	x
3D-H	X	X	X	x
3D-L	X	X	X	x
6D-H	TC	TC	TC	TC
6D-L	TC	TC	TC	TC

During the B+A+R posture, the participants were asked to rotate their heads to the side as far as their range of motion would allow without physically straining their necks. In addition, the participants were asked to remain in the given posture for the full 60 seconds without making any additional movements that were not due to the vibration while they were having their biodynamic response recorded. Each participant experienced a completely randomized order of all posture and vibration conditions. A summary of all the combinations of vibration and posture is presented in Table 5.2. The single-axis vibrations and the 3D vibrations were used as a baseline to build the

predictive model, while the 6D vibrations were used to later validate the predictive model.

5.2.4 Discomfort Ratings

Each participant was asked to rate every test combination of vibration direction based on the Borg CR-10 scale. The Borg CR-10 scale (Appendix A) was used in this study to quantify discomfort induced from vibration and as a comparison between postures, vibration directions, and vibration magnitudes. The scale ranges from 0 to 10 and has anchoring keywords where higher values indicate higher exertion or discomfort. Because the reference value is zero at no vibration, the Borg CR-10 scale is an absolute scale and allows for the comparison between multiple postures and vibrational conditions. The participants were asked to rate the discomfort induced by the vibration on the Borg CR-10 scale for each type of input vibration (fore-aft, lateral, vertical, and 3D-H, 3D-L, 6D-H, 6D-L) and posture combination (NB, BS, B+A, B+A+R), as indicated in Table 5.2. The Borg CR-10 scale was viewed on a large flat-screen monitor directly in front of the participants for the NB, BS and B+A seating postures. For the B+A+R posture, a Borg CR-10 scale was physically mounted to the wall to the right of the participants. The participants were asked to wait for at least15 seconds before rating the discomfort. The order of testing for each input vibration and posture condition was randomized for each participant.

5.2.5 Measurement of Biodynamic Response

The biodynamic response for the participant group was measured using motion-tracking inertial sensor technology. Recently, inertial sensors have shown widespread applications as they are capable of recording tri-axial linear accelerations, tri-axial

angular velocities, and orientation in the global space. The sensors used in this work were MTx inertial trackers (Xsens Technologies, Enschede, Netherlands) and were recorded at 120 Hz. Each participant was fitted with inertial sensors adhered to skin overlaying the C7 and to a head-worn halo, similar to a study by Wang and Rakheja (2006A). This head-worn halo and sensor can be seen in Figure 5.1. An additional motion- tracking inertial sensor was rigidly attached to the seat frame. The sensor on the front of the head was used to measure the angular velocity in three rotational directions of the head-neck system, while the sensor on the C7 was used to measure the angular velocity in three rotational directions of the trunk. Each inertial sensor had a mass of 30 g, measured 38 mm by 53 mm by 21 mm and had a contact surface area of 20 cm^2. Many researchers tried to correct acceleration data due to problems with skin motion with some success (Kitazaki and Griffin, 1995; Yoshimura et al., 2005; Mansfield and Griffin, 2000). For this study, a large surface area (20 cm^2) was used at the C7 in an attempt to minimize skin motion. Additional correction for skin motion was not needed due to the natural frequency of the inertial sensor-skin system being higher than the frequency range being studied (around 25 Hz). This is similar to the findings of Kitazaki and Griffin (1995) for a similar mass accelerometer mounted on the skin.

5.2.6 Predictive Discomfort

The predictive discomfort model used in this work is a modification to previous works established during sinusoidal vibrations (DeShaw and Rahmatalla, 2011; Rahmatalla and DeShaw, 2011) where the subjective discomfort arose from the discomfort of static joint position, joint limits being reached, and the root-mean-square

angular acceleration during vibration. The general form of this concept is shown in Equation 5.1.

Frequency Dependent Discomfort = Static Joint Discomfort + Extreme Joint Limit Discomfort + Summation of Angular Acceleration (Eq. 5.1)

For a single joint, Equation 5.1 takes the form of Equation 5.2:

$$f(q) = \Delta q^{norm} + G \times QU + G \times QL + \Delta \ddot{q} \quad \text{(Eq. 5.2)}$$

Equation 5.2 evaluates the head-neck system during discrete sinusoidal vibration (Rahmatalla and DeShaw, 2011), where *f(q)* represents the head discomfort based upon frequency; Δq^{norm} represents the deviation of the head-neck segment from its neutral posture and is normalized from zero to one; *GxQU* and *GxQL* represent penalty terms for discomfort that arise when the joint is very near its extreme limits, indicating great discomfort; and $\Delta \ddot{q}$ represents the effect of the dynamic motion of the segment during the vibration and is demonstrated by the RMS value of the angular acceleration at the segment. Equation 5.2 was expanded by DeShaw and Rahmatalla (2011) to multiple joints in the body (specifically the head-neck segment and spine), where weighting factors ω_i and α_i were each 0.5. Thus, an equal weighting was attributed to each individual joint (Equation 5.3). While only two joints (j=2) were presented in the study, this form could be expanded to any number of joints in the body.

$$f(\boldsymbol{q}) = \sum_{i=1}^{j} \omega_i \ \Delta q_i^{norm} + G \times QU + G \times QL \ + \sum_{i=1}^{j} \alpha_i \Delta q_i^{\cdot\cdot} \qquad \text{(Eq. 5.3)}$$

The current work presents a new general form in which perceived discomfort can be predicted during random whole-body vibration in single-, three-, and six-directional input seat vibrations. While the root-mean-square angular acceleration term in Equation 5.3 contributed very well to the discomfort magnitude during sinusoidal vibration conditions, the RMS angular velocity appears to be more effective than the angular acceleration during random vibration. In this work, the predictive model of Equation 5.3 is modified with an angular velocity term instead of an acceleration term as presented in Equation 5.4.

$$f(q) = \sum_{i=1}^{j} \omega_i (\Delta q_i^{norm} + G\text{x}QU + G\text{x}QL) + \sum_{i=1}^{j} \propto_i (\Delta \dot{q}_i) \qquad \text{(Eq. 5.4)}$$

While the goal of the previous works (Rahmatalla and DeShaw, 2011; DeShaw and Rahmatalla, 2011) was to locate the peak area of discomfort in the frequency spectrum, the goal of this work is to develop a model that predicts the overall discomfort experienced by each participant during random whole-body vibration.

5.2.7 Predictive Discomfort in Terms of Borg CR-10

In order to extend the benefit of Equation 5.4 and use it for comparison with subjective reported discomfort, each term in Equation 5.4 is transformed to an equivalent

Borg CR-10 value. Relating all terms to a Borg CR-10 equivalent value will allow for the direct comparison between posture and vibration conditions to that of an actual reference scale of accompanying anchor words (Appendix A) that describe the actual subjective feeling of the participants. Additionally, because extreme joint limits were not reached in this study, the terms *GxQU* and *GxQL* were not active and will be removed from the subsequent equations. The resulting predictive equation in terms of Borg CR-10 can be presented as Equation 5.5.

$$f(q)^{Borg} = \sum_{i=1}^{j} \omega_i \left(\Delta q_i^{Borg}\right) + \sum_{i=1}^{j} \alpha_i \left(\Delta \dot{q}_i^{Borg}\right) \quad \text{(Eq. 5.5)}$$

In Equation 5.5, the predictive function represents the overall discomfort arising from all frequencies during the random vibration, and j represents the total number of joints under consideration. Due to their major role in discomfort in sitting positions, the head-neck and trunk joints are considered in this work as the two main sources of discomfort. In this work, the magnitude weightings used for ω_i and α_i were based on equal weighting for the head-neck and trunk (Genaidy and Karwowski, 1993; DeShaw and Rahmatalla, 2011).

The next term, Δq_i^{Borg}, represents the equivalent Borg CR-10 score for the contribution of each joint due to static discomfort. This is calculated by the percent deviation from the joint-neutral position to the joint maximum range of motion multiplied by the maximum static discomfort experienced from the Borg CR-10 scale. At the end of each study, each participant rated the static discomfort due to the rotation at the head during a period of no vibration. For this study, the median response of discomfort for the

head-neck joint was 0.5 and the spine was zero on the Borg CR-10 scale. The final term, $\Delta q^{\bullet}{}_{i}^{Borg}$, represents the equivalent Borg CR-10 score due to the angular velocity motion at the head and at the C7. To calculate $\Delta q^{\bullet}{}_{i}^{Borg}$ in terms of Borg CR-10 scores, the RMS angular velocities for the head-neck and the spine at the C7 were plotted beside the average group discomfort values, as shown, respectively, in Figures 5.2a and 5.2b, for the single-axis and 3D vibration conditions (see Table 5.2).

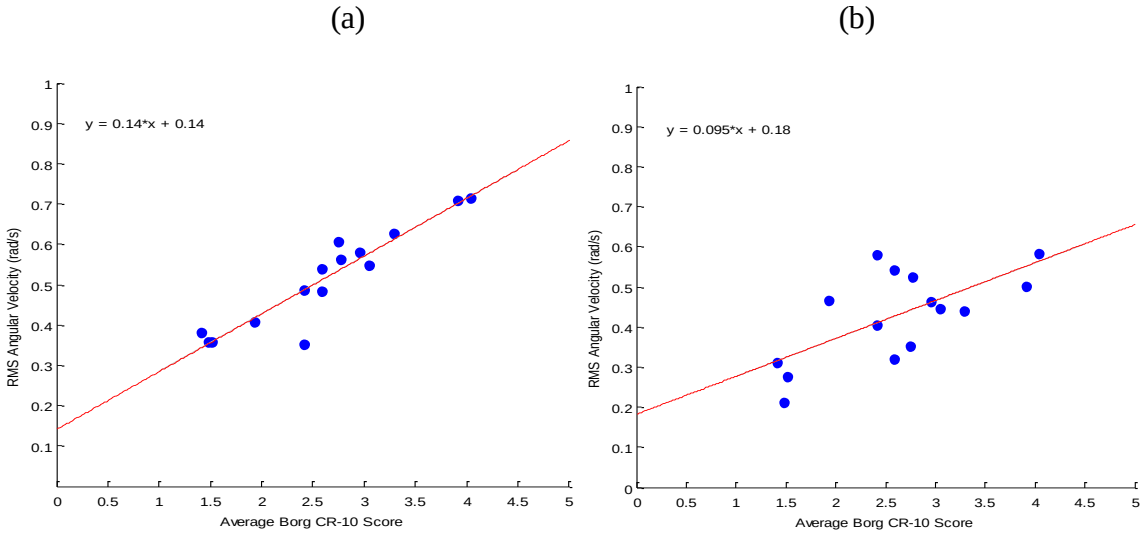

Figure 5.2 Equivalent Borg CR-10 plots for the (a) head-neck and (b) spine. The average Borg CR-10 score of 12 participants is compared to RMS average of all angular velocity components of the head during single-axis and 3D vibration. Each point represents one posture during one vibration condition. The least-squares relationship line is also shown with an equation of $y = 0.14x - 0.14$ for the head-neck (R^2=0.931), and $y = 0.095x + 0.18$ for the spine (R^2=0.672).

Each point in Figures 5.2a and 5.2b represents one posture during one vibration condition. The mathematical relationship between the angular velocity and the equivalent Borg CR-10 discomfort was determined by using the least-squares-method for the best fit

on the initial test conditions. The initial test conditions used to find the equivalent Borg CR-10 values were the vibrations in the X, Y, Z, and 3D directions (see Table 5.2). In cases where the input vibration caused more than one major rotational component in the angular velocity of the head-neck system or trunk system, the resultant angular velocity in three-directions was used.

The final form of the predictive discomfort equation with all components in terms of Borg CR-10 units becomes

$$f(q)^{Borg} = 0.5\left(\Delta q_{Head}^{Borg}\right) + 0.5(7.1428 * \Delta\dot{q}_{Head} - 1.0) + 0.5\left(\Delta q_{Spine}^{Borg}\right) + 0.5\left(10.5263 * \Delta\dot{q}_{Spine} - 1.895\right) \quad \text{(Eq. 5.6)}$$

where $f(q)^{Borg}$ represents the overall predictive discomfort in Borg CR-10 units due to the static posture and vibration response from angular joint components q.

5.2.8 ISO 2631-1 Frequency Weighted Accelerations

The current reference standard when determining comfort or fatigue during whole-body vibration is the ISO 2631-1, Mechanical vibration and shock – evaluation of human exposure to whole-body vibration (ISO 2621-1, 1997). This standard uses the input accelerations at the seat pan, seat backrest, and footrest to develop "frequency weighted accelerations," which then relate to fatigue and comfort limits. The frequency weightings can then be further combined using root-mean-square for multiple-axis vibrations and further combined using weighting factors depending on the contact point involved (Marjanen and Mansfield, 2010).

In this study, the frequency weighted acceleration values were calculated to the specifics of ISO-2631-1using methodology similar to Marjanen and Mansfield (2010). The seven vibration conditions listed in Table 5.1 were used in each frequency calculation. Consideration was also taken for the contact point (footrest, seat pan, and backrest) for each of the four postures; however, the only postural distinction in the ISO-2631-1 is between a no-backrest (NB) and a backrest-supported posture (BS). Therefore, the 28 posture and vibration conditions (see Table 5.2) resulted in only 14 unique frequency weighted accelerations values and while the other 14 combinations that included armrest and rotated postures yielded the same result as the simply supported backrest posture.

5.3 Results

Figure 5.3 shows the predictive discomfort for 12 participants during each posture and for single-axis and 3D vibrations. Because the predictive model was transferred to have all equivalent Borg CR-10 units, both axes on the figure have a Borg CR-10 score. A high correlation is seen between all the test conditions with an $R^2 = 0.9273$. A slope near 1.0 indicates that the predicted model is of the same scale as the discomfort rating of the participants and greatly due to the Borg CR-10 equivalent factors shown in Figure 5.2. Each round point on Figure 5.3 represents a posture during every vibration condition of fore-aft, lateral, vertical, 3D-L and 3D-H that was used to find the factors relating RMS angular velocity to discomfort. The predictive model was then tested using new 6D-L and 6D-H vibration conditions. The diamond points represents each of the four postures in 6D vibration and also fits in very well with the original data set.

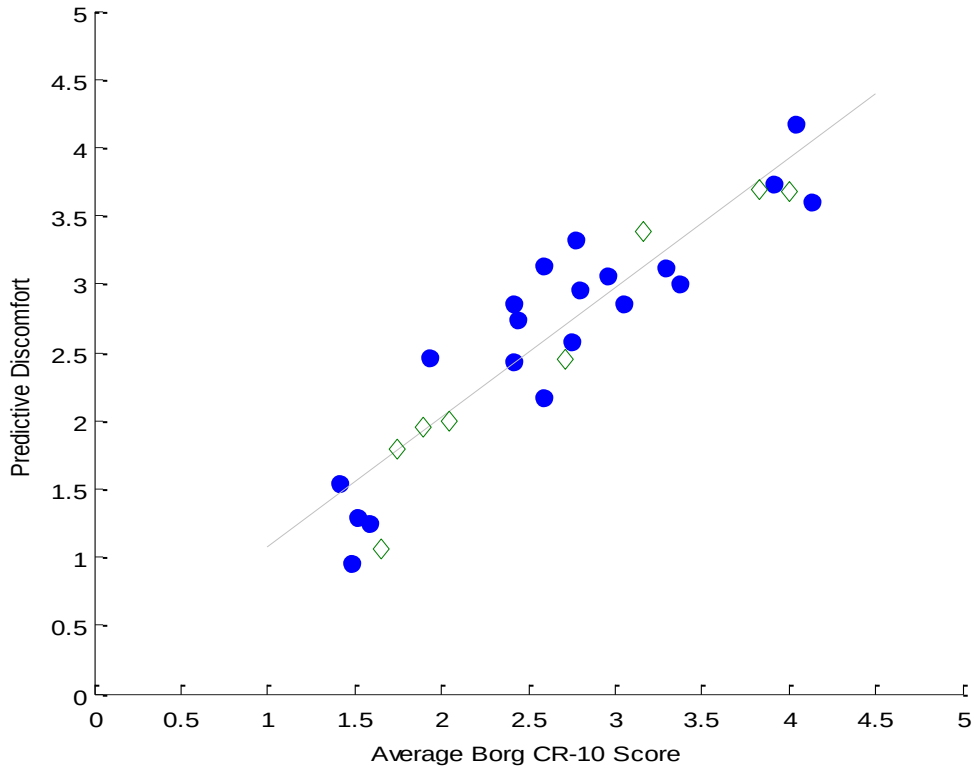

Figure 5.3 Average predictive discomfort compared to the Borg CR-10 score of 12 participants during 28 posture and vibration conditions. The round points represent every posture during each vibration condition of fore-aft, lateral, vertical, 3D-L and 3D-H. The diamond points represent every posture during 6D-L and 6D-H vibration conditions. The regression line is also shown with a slope near 1.0 and R2 = 0.9273.

Figure 5.4 compares the predicted discomfort to that of the 12 participants' reported discomfort in 6D vibration. While some small discrepancies occur, the rank order between predicted and actual discomfort is consistent across all conditions. The greatest discomfort is seen in the backrest and armrest condition during higher magnitude 6D vibration, followed by the backrest, armrest, and rotation posture. The no-backrest posture was more comfortable during both the high and low 6D vibration magnitudes.

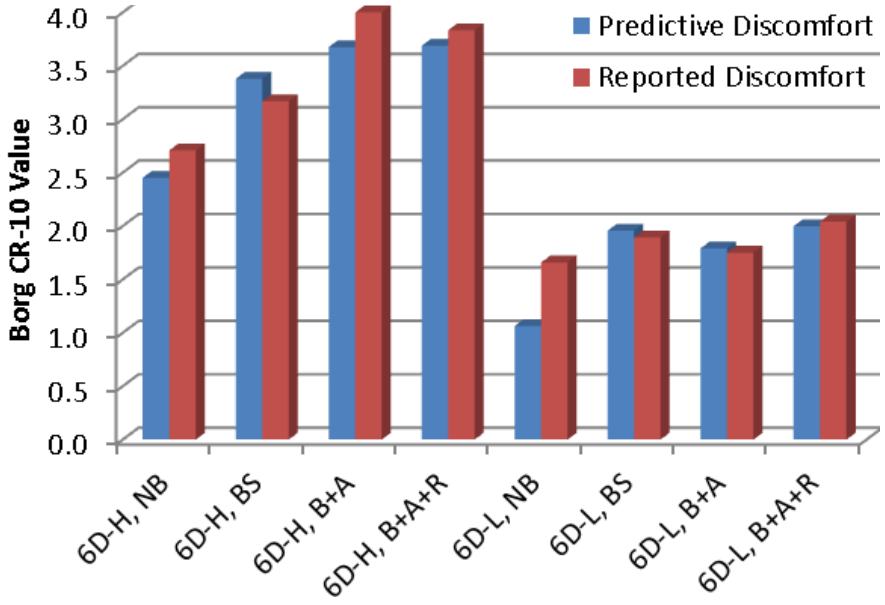

Figure 5.4 Average predictive discomfort compared to the Borg CR-10 score of 12 participants in four postures during high and low magnitude 6D vibrations.

The frequency-weighted accelerations according to the ISO 2631-1 were also calculated for each posture and vibration combination. Figure 5.5 shows the results of these calculations compared to the reported discomfort ratings from the 12 participants. Across a large spectrum of vibration conditions the frequency weighted accelerations from ISO 2631-1 correlated fairly well with the reported discomfort with $R^2 = 0.8951$. While the intercept of the regression line is near zero, the slope is around 0.3, indicating a scaling factor is present between the Borg CR-10 scale and the ISO frequency weighted acceleration.

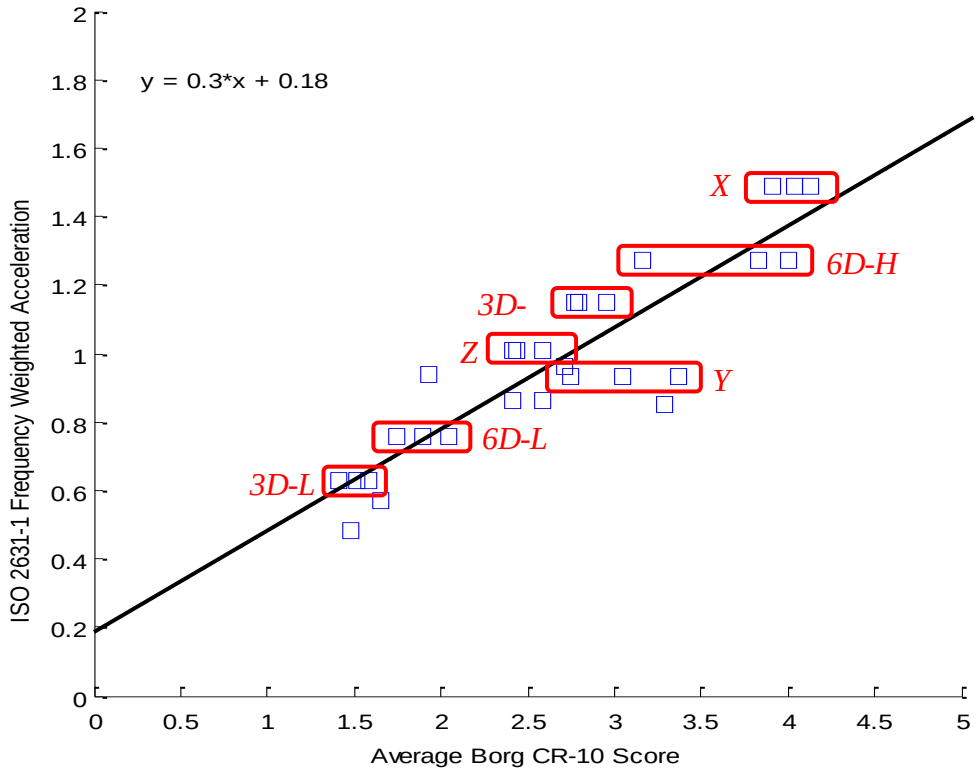

Figure 5.5 ISO 2631-1 frequency weighted accelerations plotted against the average discomfort rating for 12 participants during four postures and seven vibration scenarios. The block of each three postures the ISO standard does not distinguish between are shown in the red boxes, with the vibration type listed. A regression line is also shown with an $R^2 = 0.8951$.

While the correlation is high, Figure 5.5 shows that the ISO 2631-1 does not account for posture, only for backrest and footrest contact. This can be seen in Figure 5.5 where three postures yield the same frequency weighted accelerations and are highlighted by red boxes. In this study, where 28 vibration and posture conditions were used, only 14 unique frequency weightings are generated due to three postures being repeated by the standard (BS, B+A, B+A+R). For example, in 6D-L vibration, the current standards estimate a frequency weighted acceleration of around 0.75 m/s^2 for each of the BS, B+A, and B+A+R postures due to the input accelerations at the seat and footrest being the same

and disregarding posture. These repeated values are highlighted by the red boxes in Figure 5.5.

5.4 Discussion

Many occupations require people to use non-neutral postures to monitor their equipment while both the person and the equipment are under vibration. Therefore, there is a great need for a straightforward predictive discomfort model that can address the issues of posture and vibration content. In this work, a biomechanically based predictive discomfort measure is modified from the discrete frequency forms to the evaluation of discomfort for multiple seating postures and random vibration during single- and multi-axis WBV.

The inability to capture discomfort levels from alternative postures is a severe limitation of the current standards. Wikstrom (1993) exemplifies this by showing a large reduction in acceptable exposure time during rotated seated postures compared to the ISO guidelines. As was seen in Figure 5.5, the frequency-weighted acceleration from ISO 2631-1 shows a reasonable correlation with discomfort overall; however, it can only distinguish between vibration input conditions (at the feet, seat pan, and seat back). Current researchers are expanding upon these flaws (Basri and Griffin, 2013) by adjusting weightings for backrest angle and input conditions. Even as these weighting factors continue to improve, there will always be limitations to posture conditions that can be better addressed by using a biomechanically based model, such as the one in the current work.

Because reported discomfort amongst participants is highly variable, the mean of the ratings was used for this study, comparable to Marjanen and Mansfield (2010). A

limitation of the predictive model is that a sufficient number of participants must be tested to reduce the inter-participant variability. Because human perceptions and feelings are unique, it would be nearly impossible to predict discomfort on a per-person basis. However, the power of this predictive model is that once a reasonable set of participants are evaluated, that data can be extended to a larger population. A limitation of the predictive model is that it requires validation in multiple vibration scenarios including changes in frequency content and magnitude.

The fact that the predictive model is presented in equivalent Borg CR-10 units is extremely useful for evaluating discomfort in real-world scenarios. Many of the standards and models exist to provide only general limits for exposure durations and are limited by how to describe the actual instantaneous perceptions due to WBV. In this study, relating all terms to a Borg CR-10 equivalent value allows for the direct comparison between posture and vibration conditions to that of an actual reference scale of accompanying anchor words indicating actual perceptions of discomfort.

CHAPTER 6: EFFECTIVE SEAT-TO-HEAD TRANSMISSIBILITY IN WHOLE-BODY VIBRATION: EFFECTS OF POSTURE AND ARM POSITION[6]

6.1 Introduction

Transmissibility is a widely used measure for quantifying the transferred vibration in mechanical and biomechanical systems (Inman, 2006; Griffin, 1990). One major usage of transmissibility in mechanical systems is to assess the effectiveness of vibration isolation systems in achieving low vibration amplification around resonance areas. Within this context, the frequency-dependent transmissibility matrix for multiple-input/multiple-output (Preumont et al., 2006) is normally composed as the ratio between the input and output signals.

The transmissibility concept is a popular tool in assessing seat dynamics. Novel seats with effective vertical vibration suppression have been designed using the transmissibility as a guide for seat quality (Griffin, 1990; Niekerk et al., 2003; Westhuizen et al., 2006). Still, seats that show good performance in the vertical direction may behave poorly under multiple-axis seat motion. This could be due to the effect of ignoring the coupling between the transmissibility in the main directions: fore-aft, lateral, and vertical and those resulting from the cross-axis motions (Smith et al., 2008). Only a few papers have been published to assess seat vibration under multiple-axis inputs and single-output (Smith et al., 2008; Qiu and Giffin, 2004). In general, weighted and unweighted root mean square (RMS) accelerations were normally used to define the

[6] Published in the Journal of Sound and Vibration.
Rahmatalla, S.; DeShaw, J. Effective seat-to-head transmissibility in whole-body vibration: Effects of posture and arm position. *Journal of Sound and Vibration*. **2011,** 330(25), 6277-6286.

effective transmissibility amplitude. Mainly researchers used these weighted accelerations with standards to find limits for comfort or exposure assessment.

In biomechanical systems, researchers in the area of human response to whole-body vibration (WBV) would agree, in general terms, on the potential of the seat-to-head transmissibility (STHT) in capturing the perception of vibration of seated people for single-input/single-output motions (Griffin, 1990; Qiu and Griffin, 2003; Demic and Lukic, 2009; Paddan and Griffin, 1998; ISO 2631-1). This traditionally results in a single graph, which has been used widely as a measure of seat effectiveness and as an indication of the amount of vibration transferred through the body (Demic and Lukic, 2009; Wang et al., 2008). However, for real-life scenarios the input motion normally comprise single- or multiple-axis components; likewise, the output motion on the body would normally have multiple-axis components. In such cases, the STHT matrix contains a full matrix with many out-of-diagonal cross-axis elements (Preumont et al., 2006; Smith et al., 2008; Qui and Griffin, 2004); therefore, it becomes very hard to infer the most effective information from it.

While STHT in WBV has shown encouraging and consistent correlations with the subjective-reported discomfort measures (Paddan and Griffin, 1998; Paddan and Griffin, 2000), it showed sensitivity to body postures and to the interaction of participants with the surrounding equipment (Griffin, 1990; Wang et al., 2008). Researchers have realized the importance of postures and their effect on transmissibility in WBV (Paddan and Griffin, 1998; Nawayseh and Griffin, 2005, Kitazaki and Griffin, 1998; Hinz et al., 2002; Okunribido et al., 2008; Wang et al, 2006B; Baker and Mansfield, 2010). Although their findings varied to some degrees, most prior studies have demonstrated the importance of

considering postures and arm positions when investigating WBV. Also, the current standards (ISO 2631-1, 1997) are limited to posture conditions.

Limited work has been done on STHT in WBV considering multiple-input and multiple-output scenarios; however, the effect of cross-axis motions was not the main issue in these articles (Paddan and Griffin, 1998; Wang et al., 2008). To the authors' knowledge, there is no reported work on calculating effective STHT of multiple-axis seat-input to multiple-axis head-output motions. In this work, the concept of the effective seat-to-head transmissibility (ESTHT) is introduced, in which the single-input/multiple-output and multiple-input/multiple-output transmissibility matrix is transformed into a single graph, similar to those for single-input and single-output. The singular value decomposition and maximum distortion energy theory were used to achieve that goal. The ESTHT for discrete fore-aft single-input/multiple-output, random vertical single-input/multiple-output, and random multiple-input/multiple-output vibrations were investigated considering two sitting postures and two arm positions.

6.2 Methods

6.2.1 Singular Value Decomposition

The singular value decomposition (SVD) is a very effective scheme to extract the principal components of a rectangular matrix with their principal directions. This is done by decoupling the matrix and converting it to a diagonal form. The SVD is similar to the eigenvalue decomposition of rectangular matrices (Heath, 1997). For a matrix like **H** with m x n elements, the SVD has the following form:

$$\mathbf{H} = \mathbf{U}\Sigma\mathbf{V}^{T} \qquad \text{(Eq. 6.1)}$$

where **U** is an *m* x *m* orthogonal matrix, **V** is an *n* x *n* orthogonal matrix, and **Σ** is an *m* x *n* diagonal matrix with

$$\mathbf{\Sigma} = \begin{cases} 0 & \text{for } i \neq j \\ \Sigma_i \geq 0 & \text{for } i = j \end{cases}$$

where The diagonal terms are called the singular value of **H** and are ordered such that

$$\Sigma_i \geq \Sigma_{i+1}$$

and where the columns of **U** and **V** are the corresponding singular vectors.

6.2.2 Effective Transmissibility

In general terms, transmissibility represents the energy through the system (Demic and Lukic, 2009; Wang et al., 2008). While this energy can enter the system via many directions, the transmissibility matrix is a full matrix (Newland, 1984). The diagonal components of this matrix represent the transmissibility between the direct axes (fore-aft, lateral, and vertical). The out-of-diagonal elements of the matrix represent the coupling terms between the axes.

The dynamic response of the human body can be designated as internal stress (Hinz and Seidel, 1987), therefore, the transmissibility or the energy through the body can be considered as a stress-like quantity. In this work, we propose using the maximum distortion energy theory (Hibbeler, 2008) as one way to compute an effective number that

represents the effective transmissibility of the principal components of the transmissibility matrix.

$$H_{\text{eff}} = \sqrt{H_{11}^2 + H_{22}^2 + H_{33}^2 - H_{11}H_{22} - H_{22}H_{33} - H_{11}H_{33}} \qquad \text{(Eq. 6.2)}$$

6.2.3 Effective Seat-to-Head Transmissibility

6.2.3.1 Single-Input and Single-Output

Usually, the STHT is defined as the complex ratio between the cross-spectral density of the input seat acceleration and the output head acceleration $\mathbf{S}_{hs}(j\omega)$ divided by the auto-spectral density of the input seat acceleration $\mathbf{S}_{ss}(j\omega)$ (Equation 6.3).

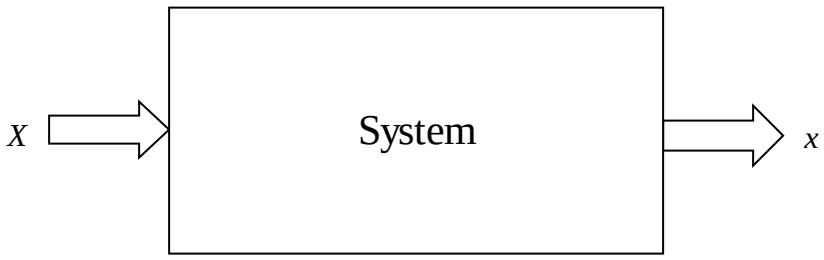

Figure 6.1 Single-direction input and single-direction output system.

For single-input and single-output motions (Figure 6.1), the STHT can be represented as the ratio between the cross-spectral density of the input and the output divided by the auto-spectral density of the input:

$$H_{Xx}(\omega) = S_{XX}{}^{-1}(\omega) S_{Xx}(\omega) \qquad \text{(Eq. 6.3)}$$

where S_{Xx} represents the cross-spectral density between the input motion (X) and the output motion (x), and S_{XX} represents the auto-spectral density of the input motion (X).

6.2.3.2 Multiple-Input and Multiple-Output

The system in Figure 6.2 has an input file with three components in the three Cartesian directions represented by uppercase letters: fore-aft (X), lateral (Y), and vertical (Z), and the output has three directions of motion represented by lowercase letters fore-aft (x), lateral (y), and vertical (z). The transmissibility matrix for this case can be expressed as:

$$\begin{bmatrix} H_{Xx} & H_{Xy} & H_{Xz} \\ H_{Yx} & H_{Yy} & H_{Yz} \\ H_{Zx} & H_{Zy} & H_{Zz} \end{bmatrix} = \begin{bmatrix} S_{XX} & S_{XY} & S_{XZ} \\ S_{YX} & S_{YY} & S_{YZ} \\ S_{ZX} & S_{ZY} & S_{ZZ} \end{bmatrix}^{-1} \begin{bmatrix} S_{Xx} & S_{Xy} & S_{Xz} \\ S_{Yx} & S_{Yy} & S_{Yz} \\ S_{Zx} & S_{Zy} & S_{Zz} \end{bmatrix} \qquad \text{(Eq. 6.4)}$$

The resulting transmissibility matrix is complex, with each component having real and imaginary parts (ω was omitted from Equation 6.4 for simplification). Therefore, it becomes difficult to deal with the transmissibility in this form for practical applications. However, the principal diagonal components of the transmissibility matrix can be computed using the singular value decomposition at each ω using Equation 6.1. The form to transform the 3 x 3 transmissibility matrix using SVD is shown where:

$$\text{SVD}\left\{\begin{bmatrix} H_{Xx}(\omega) & H_{Xy}(\omega) & H_{Xz}(\omega) \\ H_{Yx}(\omega) & H_{Yy}(\omega) & H_{Yz}(\omega) \\ H_{Zx}(\omega) & H_{Zy}(\omega) & H_{Zz}(\omega) \end{bmatrix}\right\} = \mathbf{U}\boldsymbol{\Sigma}\mathbf{V}^{\mathrm{T}}$$

in which

$$\boldsymbol{\Sigma} = \begin{bmatrix} H_{11}(\omega) & 0 & 0 \\ 0 & H_{22}(\omega) & 0 \\ 0 & 0 & H_{33}(\omega) \end{bmatrix}$$

where $H_{11}(\omega)$, $H_{22}(\omega)$, and $H_{33}(\omega)$ represent three principal components in the orthogonal space. At each frequency, the principal diagonal components can be transformed to a single number using the maximum distortion energy theory (Equation 6.2).

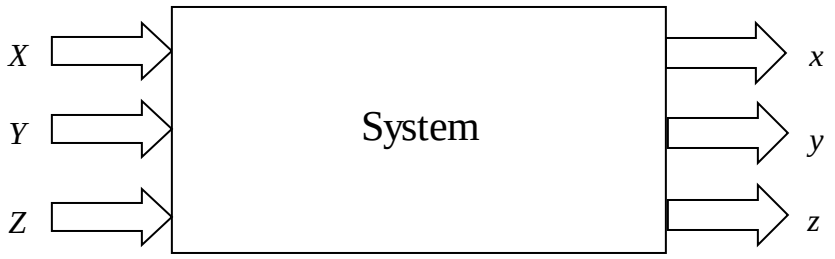

Figure 6.2 Multiple-direction input and multiple-direction output system.

The proposed approach can be easily extended to any number of inputs and outputs to compute a single effective number at each frequency. This number has the

potential to be used for evaluating a participant's perception to vibration in multiple-input and multiple-output WBV.

6.2.3.3 Single-Input/Multiple-Output

A single fore-aft direction input and three directional outputs system is shown in Figure 6.3. The transmissibility matrix of the system has non-zero components in only one of its rows. The matrix in this form has a rank of one and therefore has only one principal component. As a result, the effective transmissibility can be computed directly using the singular value decomposition.

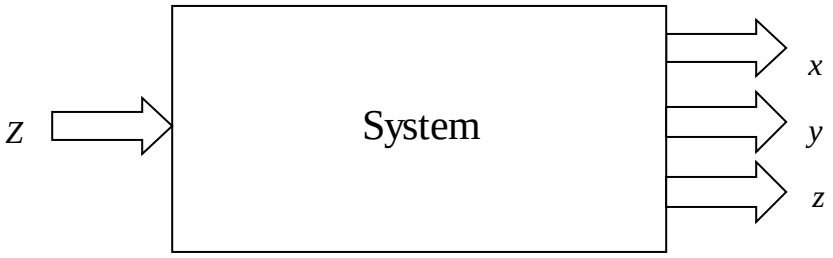

Figure 6.3 Single-direction input and multiple-direction output system.

6.3 Experiments

6.3.1 Discrete Vibration: Fore-Aft

Five healthy male participants with a mean age of 24 years (ranging from 19-29 years), a mean stature of 188 cm (ranging from 180-196 cm), and a mean body mass of 84.5 kg (ranging from 71–98 kg) were recruited. Written informed consent (Appendix B), as approved by the University of Iowa Institutional Review Board, was obtained prior to testing. Participants were seated in an uncushioned, rigid seat mounted to a vibration

platform. Two sitting postures were considered, one with the participant sitting in a standard posture supported by the seat back, and the second in a forward upright unsupported-back posture. For both sitting postures, the participants were sitting with their arms on their laps and their feet on a foot pedal (Figure 6.4).

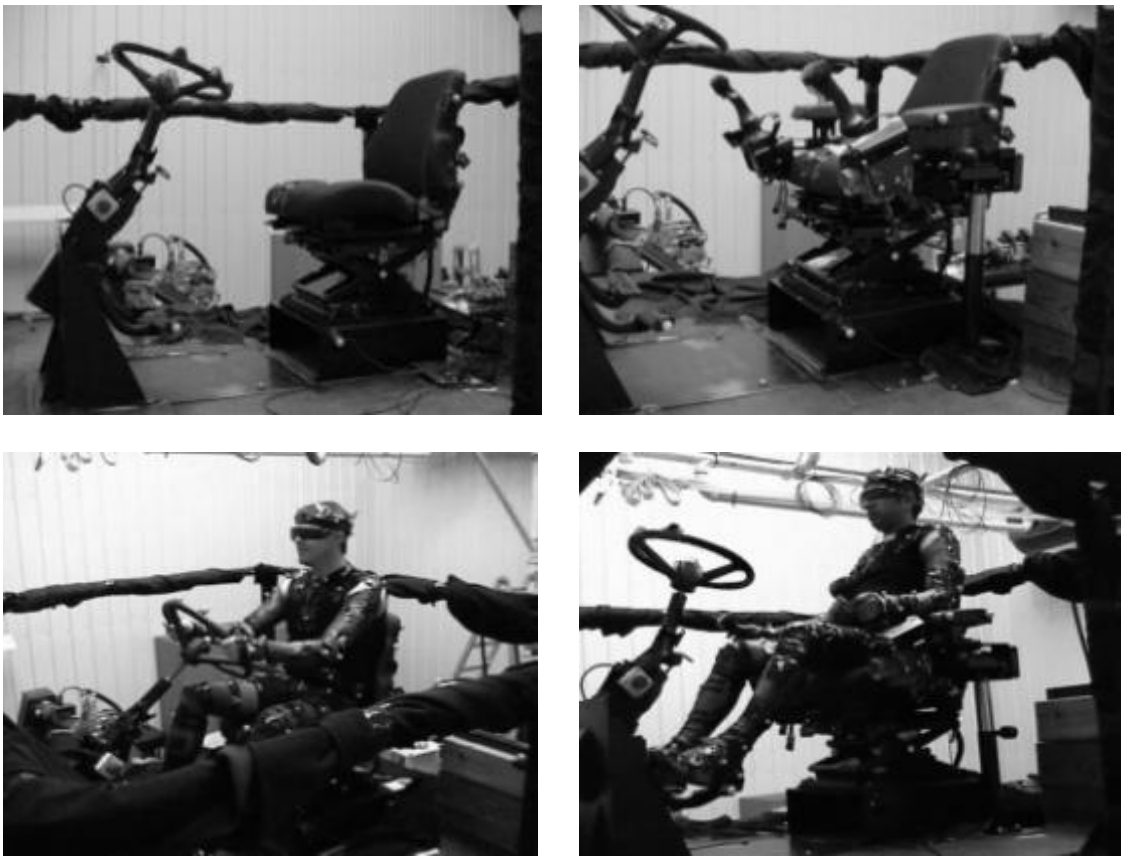

Figure 6.4 Seating configurations during the experiment. Steering wheel (SW) (upper left), armrest (AR) (upper right), operator using steering wheel (SW) (lower left), and operator using armrest (AR) (lower right)

Vibration was generated using a six-degree-of-freedom man-rated vibration platform (Moog-FCS, Ann Arbor, MI, USA). Signals with a constant unweighted RMS

acceleration magnitude of 0.8 m/s^2 were tested. Discrete frequencies of 0.5, 1, 1.5, 2, 2.5, 3, 3.5, 4, 4.5, 5, 5.5, 6, 7, 8, 9, 10, 12, 14, and 16 Hz were chosen and randomized.

6.3.2 Random Vibration: Vertical and Multiple-Axis

Another five healthy participants were tested with a mean age of 33.5 years (ranging from 22-45 years), a mean stature of 176.5 cm (ranging from 165-188 cm), and a mean body mass of 77.5 kg (ranging from 64-91 kg). Tests consisted of vertical single-axis and three translational (*X*, *Y*, and *Z*) multiple-axis whole-body vibration using ride files 60 seconds in length recorded from a heavy construction machine, the Caterpillar D10 dozer. Written informed consent, as approved by the University of Iowa Institutional Review Board, was obtained prior to testing. A six-degree-of-freedom Servotest (Sears Seating Facility, Davenport, IA, USA) hydraulic motion platform was used in the testing and seen in Figure 6.4. Two arm positions were considered in this study, including one posture where the participants grasped the steering wheel (SW) and one posture where participants used a floor-mounted armrest (AR). In both cases, the feet were supported by the foot support as shown in Figure 6.4.

6.4 Results

6.4.1 Discrete Vibration: Fore-Aft

Figure 6.5 depicts the discrete fore-aft ESTHT for the supported (gray-line) and unsupported (dark-line) back conditions. For the unsupported back condition, the ESTHT showed a distinctive peak around 1 Hz, 2-2.5 Hz, and a slight peak at 12 Hz. For the supported back, the ESTHT showed a peak around 1 Hz followed by a second dominant peak around 4.5 Hz, and a small peak around 12 Hz. The supported back condition showed higher transmissibility after 3 Hz.

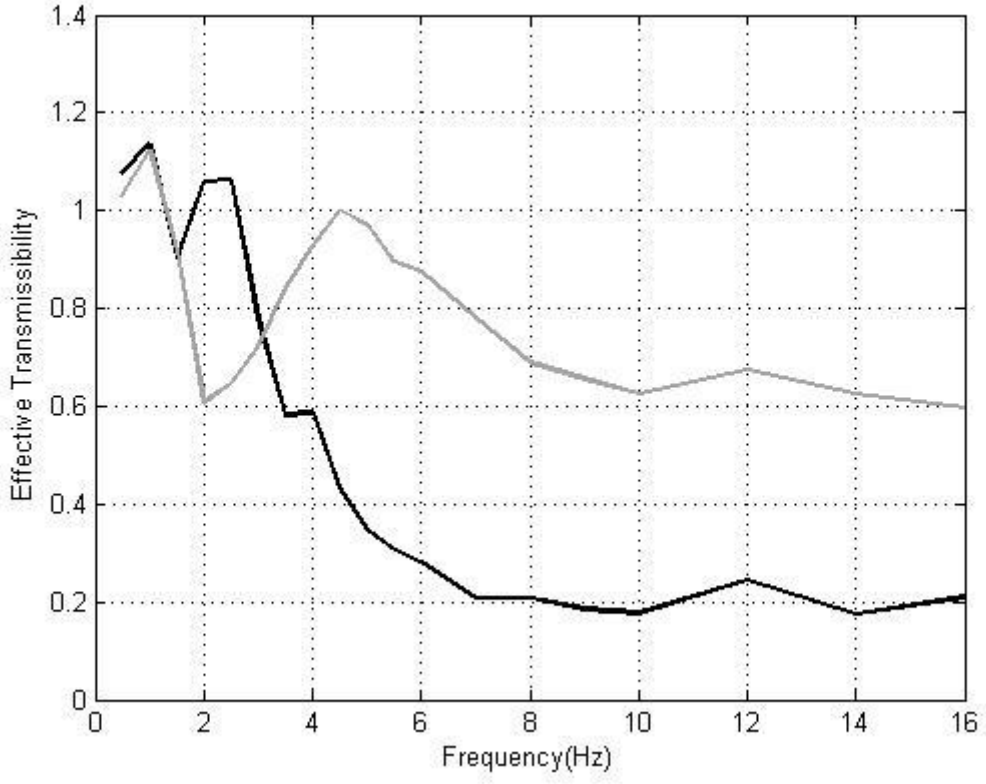

Figure 6.5 Effective seat-to-head transmissibility (ESTHT) for discrete single-input and multiple-output fore-aft (Xx) direction, for supported (gray-line) and unsupported (dark-line) backrest conditions.

6.4.2 Random Vibration: Single-Vertical

The STHT matrix for the vertical single-input and multiple-output has three components. Figure 6.6 shows the characteristics of each component for the AR (Figure 6.6a) and SW (Figure 6.6b) conditions. For both conditions, the median of the (*Zx*) and (*Zy*) showed relatively smaller contributions across the frequencies under investigation when compared to the median of the (*Zz*) component. The median for the *Zz* component of the AR condition (Figure 6a) showed a peak around 4-5 Hz, while the median of the *Zz* component of the SW condition (Figure 6.6b) showed a peak around 3-3.5 Hz. Due to

anomalies in the data of one participant during the SW condition, data of only four participants were used in the construction of Figure 6.6b.

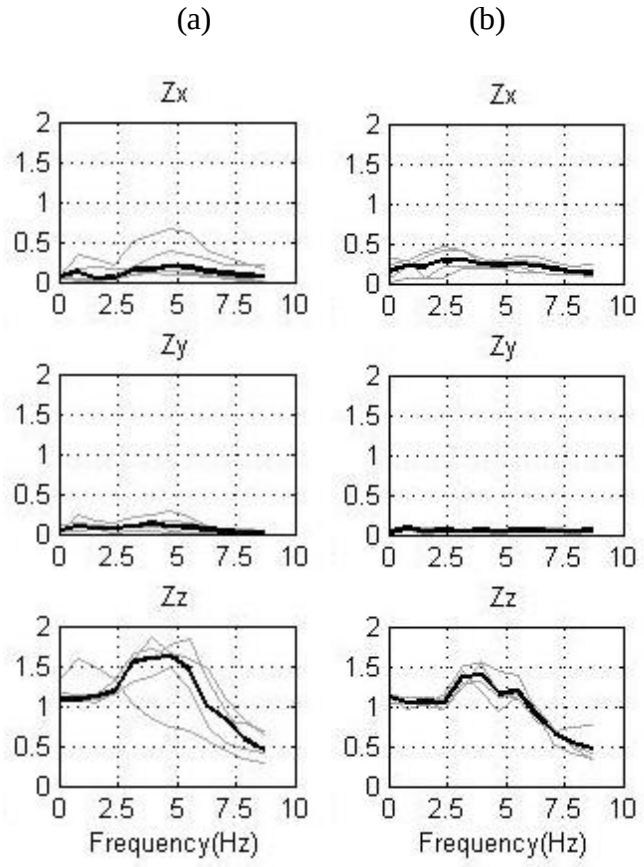

Figure 6.6 Individuals (gray-line) and median (dark-line) seat-to-head transmissibility (STHT) for random single input (vertical direction Z) and multiple-output (fore-aft x, lateral y, and vertical z directions). The armrest (AR) condition is shown in (a), and the steering wheel condition (SW) is shown in (b)

The mean of the ESTHT for the AR (dark-line) and SW (gray-line) conditions (Figure 6.7) have shown similar characteristics with peaks around 4 Hz. The AR condition showed a relatively higher magnitude than the SW condition for the frequency range up to 4.5 Hz.

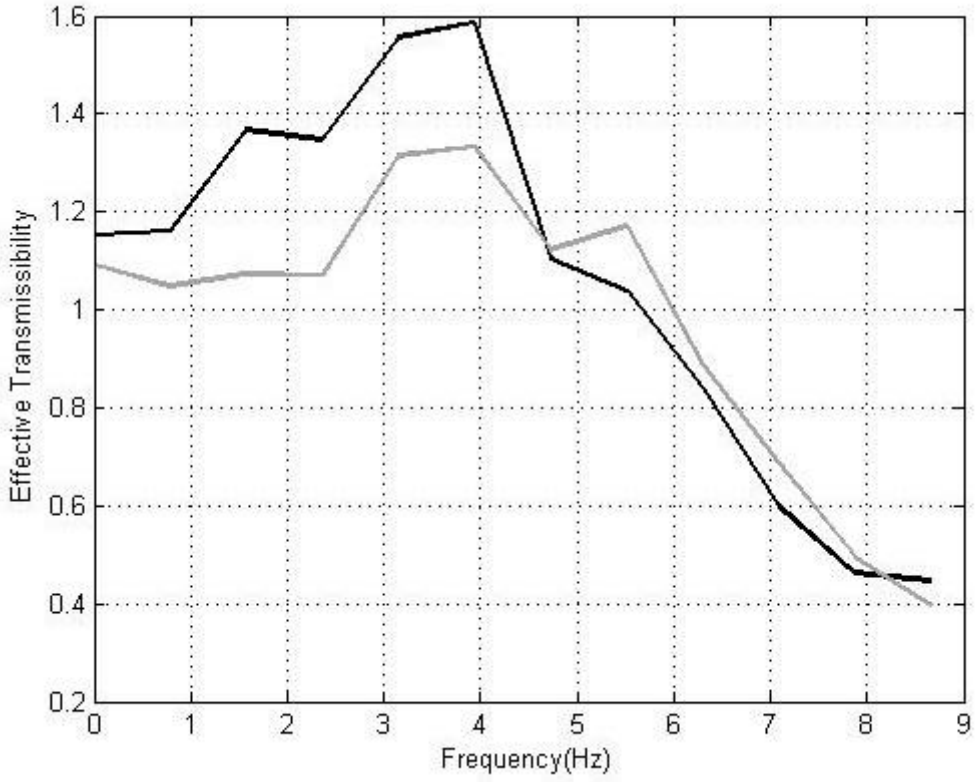

Figure 6.7 Mean effective seat-to-head transmissibility (ESTHT) of five participants (dark-line) for armrest (AR) condition, and of four participants (gray-line) for SW condition during vertical-random single-input and multiple-output directions.

6.4.3 Random Vibration: Multiple-Axis

For the random multiple-input and multiple-output, the STHT matrix has nine components. Figure 6.8 shows the components for the AR condition with their medians. As can be seen from Figure 6.8, the diagonal components have the major contribution, while the remaining out-of-diagonal components have smaller roles, except for the *Xz* component which has a comparable magnitude to those of the diagonal components with a peak around 4.5 Hz. Meanwhile, the *Zz* component showed the highest magnitude among the nine components with a prominent peak around 3.5 Hz.

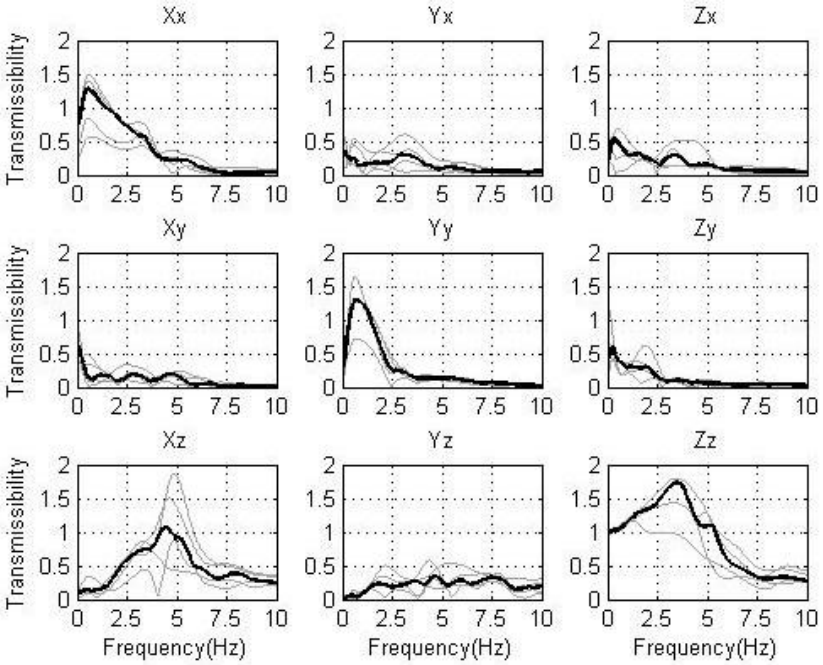

Figure 6.8 Individuals (gray-line) and median (dark-line) seat-to-head transmissibility (STHT) of five participants for armrest condition (AR) during random multiple-input and multiple-output directions.

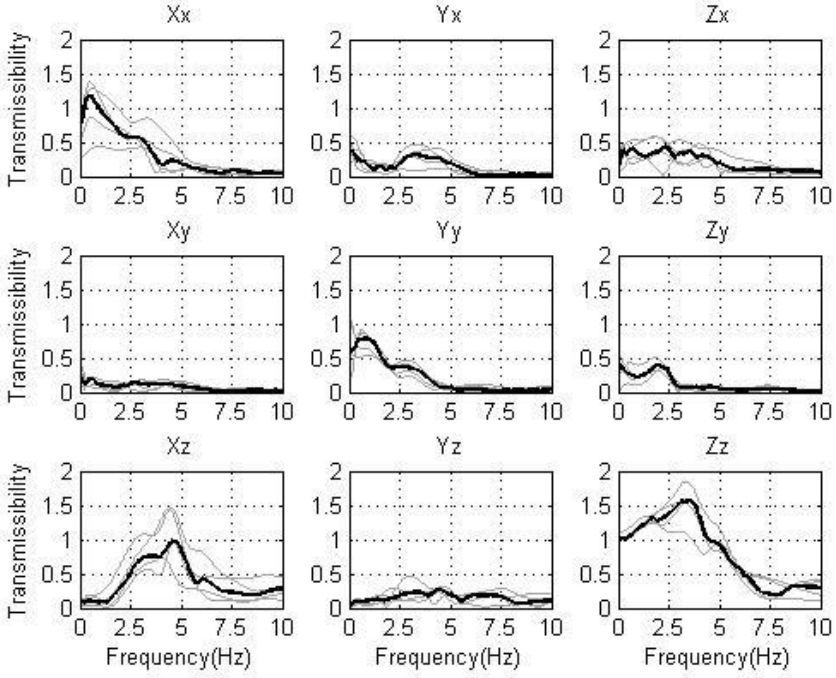

Figure 6.9 Individuals (gray-line) and median (dark-line) seat-to-head transmissibility (STHT) of five participants for steering wheel condition (SW) during random multiple-input and multiple-output directions.

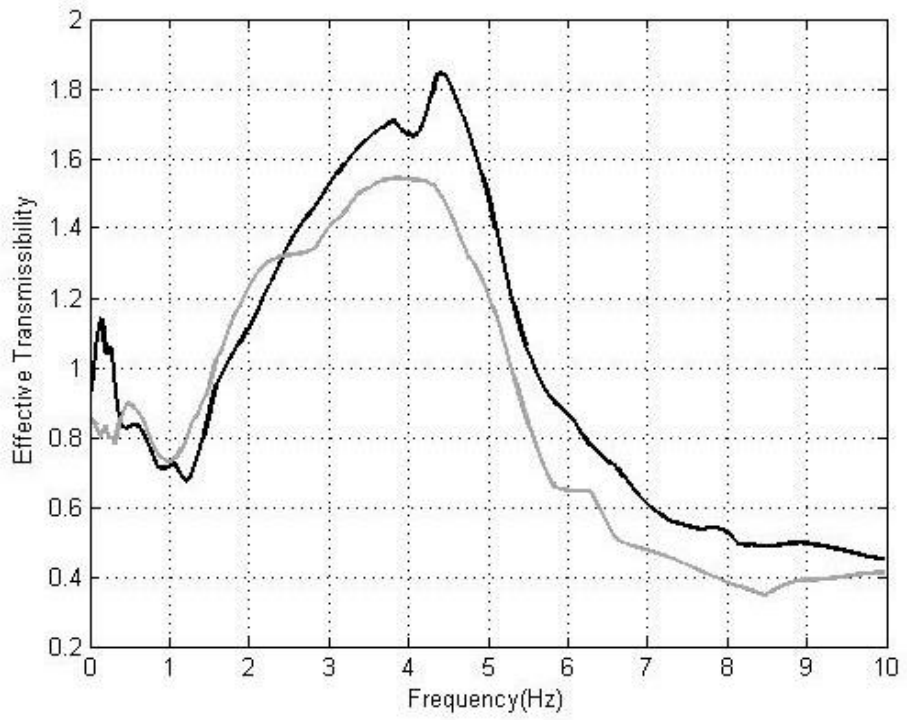

Figure 6.10 Mean effective seat-to-head transmissibility (ESTHT) of five participants (dark-line) for armrest (AR) condition and of five participants (gray-line) for SW condition during random multiple-input and multiple-output directions.

Similar characteristics were observed for the median of the SW condition components as shown in Figure 6.9, with the *Yy* and *Zz* components having smaller magnitude than those of the AR condition of Figure 6.8. Figure 6.10 shows the mean ESTHT for the AR (dark-line) and SW (gray-line) conditions. As can be seen from the figure that the AR condition has a peak around 4.5 Hz, while the SW condition has a lower peak around 4 Hz.

6.5 Discussion

The concept of ESTHT is introduced in this work, which represents an objective way to transform the multiple-input and multiple-output transmissibility matrix to a single graph similar to those of single-input and single-output. The results for the discrete

rides in the fore-aft direction with single-input and multiple-output showed that the proposed method was very effective in capturing the locations of the resonance areas for the supported and unsupported back conditions. As shown in Figure 6.5, the peak in the ESTHT graph for the discrete fore-aft direction shifted from 4.5 Hz for the supported posture to around 2.5 Hz for the unsupported posture. These results are consistent with the literature (Griffin, 1990; Rahmatalla and DeShaw 2011) and the reported subjective discomfort (Subashi et al., 2009; Rahmatalla et al., 2010).

For the random single-input and multiple-output vertical vibration, the mean ESTHT for the AR and SW conditions showed similar characteristics; however, the AR condition demonstrated a relatively higher magnitude up to 4.5 Hz as shown in Figure6.7. While little information is available on the effective use of armrests during WBV (Newell and Mansfield, 2008), and how that is comparable to the steering wheel condition, the difference between the mean ESTHT for the AR and SW conditions could be attributed to the position of the arms. As in both conditions, the arms generated additional support to the trunk. However, the SW condition may allow more flexibility in using the arms and possibly more interaction/coupling between the shoulder and neck muscles and therefore is expected to generate less head motion. Figure 6.6 may show to a certain degree some of that characteristics where the *Zy* and the *Zz* components for the AR condition showed relatively higher magnitudes than those of the SW condition.

For the multiple-input and multiple-output random vibration, the components of the AR conditions have in general terms similar characteristics to those of the SW conditions, with the diagonal components in both conditions playing major roles. However, the diagonal components for the AR conditions (Figure 6.8) were in general

higher than those for the SW condition (Figure 6.9) indicating that the participants were showing more head motion in the AR condition. These results are to some extent consistent with the observation for the single-input and multiple-output vertical vibration scenario, but clearly more obvious. The difference between the two conditions around resonance could be attributed to the higher nodding motion of the head during the AR condition due to the fore-aft motions that affect the *Xx* and *Xz* components.

The nine transmissibility components in figures 6.8 and 6.9 gave useful insights into what is happening in all directions and how the input motion affects each component of the output motion as can be seen in Equation 6.4. As can be seen (Figures 6.8 and 6.9) that it is very hard to infer an objective description from the nine graphs regarding the overall resulting motion. This could be more problematical if the input and the output motions have each six degrees of freedom for example. However, the mean ESTHT for the AR and SW conditions (Figure 6.10) were able to objectively capture these differences to some extent in one graph with a clear differentiation between the two arms positions under investigation.

While the results of this work showed similar characteristics to those in the literature (Mandapuram et al., 2010; Hinz et al., 2010) in terms of the general trends, still there could be some differences due to the nature of the current experiments and measurements. For example, in this work the operator's environment was designed to be as possibly realistic and similar to real life scenarios; where Caterpillar seats with their armrest, steering wheel, back-support, and foot supports were used with vibration files from the field. Another reason could be attributed to the position-based measurements of this work where some differences may occur due to the finite differences calculation.

This study is timely as advances in seat's design, especially as the addition of the armrest the controls attached to it, has imposed constraints on the motion of the trunk which can lead to low back pain (Wilder et al., 1996) but also can generated noticeable increase in the head motion (Rahmatalla et al., 2010). Therefore, the introduction of an objective quantification represented by the ESTHT for such type of motions would be very beneficial to the fields of seat/equipment design and human biomechanics in WBV.

6.6 Conclusion

It can be inferred from the results that the proposed ESTHT concept presents an objective tool to assess relatively complicated input/output motions and gain insights into the effect of posture and the surrounding equipment on the biodynamic response of the operators. While the results for the single-input and multiple-output for the fore-aft and vertical vibrations have similar characteristics to those in the literature (Rahmatalla et al., 2010; Mandapuram et al., 2010; Hinz et al., 2010), the results for the multiple-input and multiple-output vibration need further investigations with more participants and seating conditions to be used effectively as guides for designing vehicle seating and arm supports in WBV.

CHAPTER 7: EFFECTIVE SEAT-TO-HEAD TRANSMISSIBILITY DURING MULTIPLE POSTURES AND MULTIPLE AXIS VIBRATIONS INCLUDING 6-DEGREE-OF-FREEDOM VIBRATIONS[7]

7.1 Introduction

In the area of human response to whole-body vibration (WBV), researchers would agree on the potential of the seat-to-head transmissibility (STHT) in capturing the perception of vibration of seated people for single-input/single-output motions (Griffin, 1990; Qiu and Griffin, 2003; Demic and Lukic, 2009; Paddan and Griffin, 1998). Although these studies have laid the groundwork for WBV research, they are limited because real-life vibration environments involve multiple-axis inputs and outputs. In such cases, each input and output combination, whether translational or rotational, will have a separate transmissibility. For three-axis translational input and output motions, the STHT matrix contains a full 3 x 3 matrix with many out-of-diagonal cross-axis elements (Preumont et al., 2006; Smith et al., 2008; Qui and Griffin, 2004). Additionally, if rotational inputs and outputs are considered, a full matrix of 6 x 6 transmissibility components can be represented. Because each vibrational output axis is dependent on other axes, it becomes difficult to infer the most effective information from any single transmissibility component.

In addition to limitations in vibration axes, many studies have showed sensitivity to body postures and to the contact point with the seat, backrest, and steering wheel (Griffin, 1990; Wang et al., 2008). The seat-to-head transmissibility in WBV has shown encouraging and consistent correlations with the subjective-reported discomfort measures

[7] In preparation for submission to a peer-reviewed journal.

(Paddan and Griffin, 1998; Paddan and Griffin, 2000); however, in general, researchers have realized the importance of postures and their effect on transmissibility in WBV (Paddan and Griffin, 1998; Nawayseh and Griffin, 2005, Kitazaki and Griffin, 1998; Hinz et al., 2002; Okunribido et al., 2008; Wang et al, 2006B; Baker and Mansfield, 2010). Although their findings varied to some degree, most studies have demonstrated the importance of considering postures and vibration axes when investigating WBV.

Because seat-to-head transmissibility is a widely used measure for quantifying the transferred vibration in mechanical and biomechanical systems (Inman, 2006; Griffin, 1990; Hinz et al., 2010), one major usage of transmissibility in is to assess the effectiveness of isolation systems in seat design. The location of the greatest amplitude of vibration transferred through the body is traditionally shown as a single graph dependent on frequency content, which has been used extensively as a measure of seat effectiveness (Demic and Lukic, 2009; Wang et al., 2008). Novel seats with effective vertical vibration suppression have been designed using the transmissibility as a guide for seat quality (Griffin, 1990; Niekerk et al., 2003; Westhuizen et al., 2006). Seats that show good performance in the vertical direction may behave poorly under multiple-axis seat motion. These single axis representations are problematic, however, because in real-life scenarios, the input vibration has multiple-axis inputs. Additionally, the output motion at the head or any other part of the body normally has a response in more than one axis.

Limited work has been done on STHT in WBV considering multiple-input and multiple-output scenarios; however, the overall effects from cross-axis motions were not the focus of these articles (Paddan and Griffin, 1998; Wang et al., 2008; Hinz et al., 2010). A few papers have been published to assess seat vibration under multiple-axis

inputs and single-axis outputs (Smith et al., 2008; Qiu and Giffin, 2004) or single-axis inputs and multiple-axis outputs. In general, weighted root-mean-square (RMS) accelerations were used to define the effective transmissibility amplitude based on the International Standard ISO 2631-1 (1997) or the British Standard BS 6841 (1987).

In this work, the concept of the effective seat-to-head transmissibility (ESTHT) is developed for complicated postures during single-axis, 3D, and 6D vibration based on previous methodologies (Rahmatalla and DeShaw, 2011) in which the single-input/multiple-output and multiple-input/multiple-output transmissibility matrix is transformed into a single graph, similar to those for single-input and single-output graphs.

7.2 Methods

7.2.1 Singular Value Decomposition

The singular value decomposition (SVD) is an effective scheme to extract the principal components of a rectangular matrix with their principal directions. This is done by decoupling the matrix and converting it to a diagonal form. The SVD is similar to the eigenvalue decomposition of rectangular matrices (Heath, 1997). For a matrix like **H** with m x n elements, the SVD has the following form:

$$\mathbf{H} = \mathbf{U}\Sigma\mathbf{V}^{T} \qquad \text{(Eq. 7.1)}$$

where **U** is an m x m orthogonal matrix, **V** is an n x n orthogonal matrix, and $\mathbf{\Sigma}$ is an m x n diagonal matrix with

$$\mathbf{\Sigma} = \begin{cases} 0 & \text{for } i \neq j \\ \Sigma_i \geq 0 & \text{for } i = j \end{cases}$$

The diagonal terms are called the singular value of **H** and are usually ordered such that

$$\Sigma_i \geq \Sigma_{i+1}$$

where the columns of **U** and **V** are the corresponding singular vectors.

7.2.2 Effective Transmissibility

In general terms, transmissibility represents the energy transmitted through the system (Demic and Lukic, 2009; Wang et al., 2008). When this energy enters and exits the system from all directions, the transmissibility is a full *m* x *m* matrix (Newland, 1984). The diagonal components of this matrix represent the transmissibility between the direct axes (fore-aft to fore-aft, lateral to lateral, and vertical to vertical) and the out-of-diagonal elements of the matrix represent the coupling interaction between the axes (fore-aft input motion causing vertical output motion for example).

The idea of an overall energy through the body can be related to that of an internal stress (Hinz and Seidel, 1987; Rahmatalla and DeShaw, 2011), therefore, the transmissibility through the body can be considered a stress-like quantity. For this study, we use the maximum distortion energy theory (Hibbeler, 2008) to compute a resultant number that represents the effective transmissibility (H_{eff}) of the principal components of the full transmissibility matrix (Equation 7.2).

$$H_{\text{eff}} = \sqrt{H_{11}^2 + H_{22}^2 + H_{33}^2 - H_{11}H_{22} - H_{22}H_{33} - H_{11}H_{33}} \qquad \text{(Eq. 7.2)}$$

7.2.3 Effective Seat-to-Head Transmissibility

Seat-to-head transmissibility is defined as the complex ratio between the cross-spectral density of the input seat acceleration and the output head acceleration $\mathbf{S}_{hs}(j\omega)$ divided by the auto-spectral density of the input seat acceleration $\mathbf{S}_{ss}(j\omega)$

$$H_{Xx}(\omega) = S_{XX}{}^{-1}(\omega) S_{Xx}(\omega) \qquad \text{(Eq. 7.3)}$$

where S_{Xx} represents the cross-spectral density between the input motion (X) and the output motion (x), and S_{XX} represents the auto-spectral density of the input motion (X).

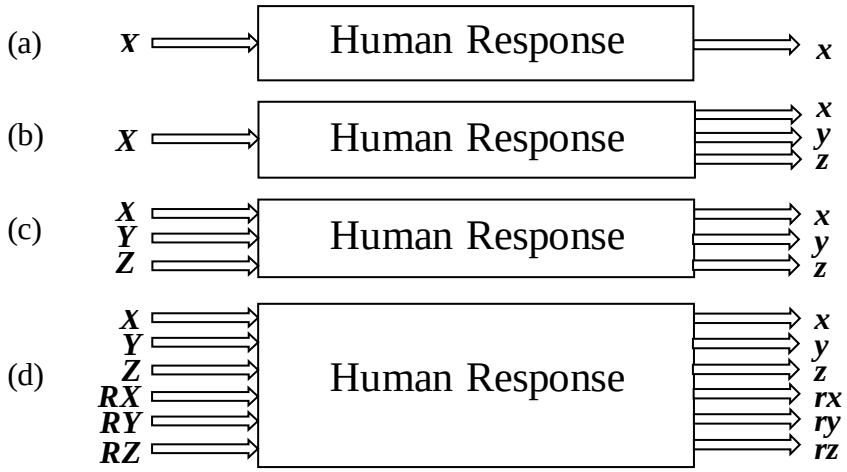

Figure 7.1 Four different systems studied in whole-body vibration. (a) single-input/single-output, (b) single-input/multiple output, (c) 3D multiple-input/multiple output and (d) 6D multiple-input/multiple output. Uppercase letters indicate input vibration, and lowercase letters indicate output vibrations.

For single-input and single-output motions (Figure 7.1a), the STHT can be represented as the ratio between the cross-spectral density of the input and the output

divided by the auto-spectral density of the input. This is the simplest vibrational analysis usually conducted by researchers in the field as the measurement can be done with only single-axis accelerometers. If only one input direction is considered but multiple output directions are considered then the system changes to that of Figure 7.1b. An example of this type of system is single-axis vibration input (i.e. vertical) and the three-dimensional acceleration data of the head as the output. In this case, the transmissibility matrix of the system has non-zero components in only one of its rows. The matrix in this form has a rank of one and therefore has only one principal component. As a result, the effective transmissibility can be computed directly using the singular value decomposition.

When each of component three-directional input and three-directional output systems are considered, the system takes on the form of Figure 7.1c. The system in Figure 7.1c has an input with three components in the three Cartesian directions represented by uppercase letters: fore-aft (*X*), lateral (*Y*), and vertical (*Z*), and the output has three directions of motion represented by lowercase letters fore-aft (*x*), lateral (*y*), and vertical (*z*). The transmissibility matrix for this case can be expressed as Equation 7.4:

$$\begin{bmatrix} H_{Xx} & H_{Xy} & H_{Xz} \\ H_{Yx} & H_{Yy} & H_{Yz} \\ H_{Zx} & H_{Zy} & H_{Zz} \end{bmatrix} = \begin{bmatrix} S_{XX} & S_{XY} & S_{XZ} \\ S_{YX} & S_{YY} & S_{YZ} \\ S_{ZX} & S_{ZY} & S_{ZZ} \end{bmatrix}^{-1} \begin{bmatrix} S_{Xx} & S_{Xy} & S_{Xz} \\ S_{Yx} & S_{Yy} & S_{Yz} \\ S_{Zx} & S_{Zy} & S_{Zz} \end{bmatrix} \quad \text{(Eq. 7.4)}$$

Equation 7.4 can also be expanded in the same way for 6D vibration using three translational and rotational inputs and three translational and rotational outputs as in the system shown in Figure 7.1d. The resulting full 6 x 6 transmissibility matrix is shown in Equation 7.5.

$$\begin{bmatrix} H_{Xx} & H_{Xy} & H_{Xz} & H_{Xrx} & H_{Xry} & H_{Xrz} \\ H_{Yx} & H_{Yy} & H_{Yz} & H_{Yrx} & H_{Yry} & H_{Yrz} \\ H_{Zx} & H_{Zy} & H_{Zz} & H_{Zrx} & H_{Zry} & H_{Zrz} \\ H_{RXx} & H_{RXy} & H_{RXz} & H_{RXrx} & H_{RXry} & H_{RXrz} \\ H_{RYx} & H_{RYy} & H_{RYz} & H_{RYrx} & H_{RYry} & H_{RYrz} \\ H_{RZx} & H_{RZy} & H_{RZz} & H_{RZrx} & H_{RZyr} & H_{RZrz} \end{bmatrix} = \quad \text{(Eq. 7.5)}$$

$$\begin{bmatrix} S_{XX} & S_{XY} & S_{XZ} & S_{XRX} & S_{XRY} & S_{XRZ} \\ S_{YX} & S_{YY} & S_{YZ} & S_{YRX} & S_{YRY} & S_{YRZ} \\ S_{ZX} & S_{ZY} & S_{ZZ} & S_{ZRX} & S_{ZRY} & S_{ZRZ} \\ S_{RXX} & S_{RXY} & S_{RXZ} & S_{RXRX} & S_{RXRY} & S_{RXRZ} \\ S_{RYX} & S_{RYY} & S_{RYZ} & S_{RYRX} & S_{RYRY} & S_{RYRZ} \\ S_{RZX} & S_{RZY} & S_{RZZ} & S_{RZRX} & S_{RZRY} & S_{RZRZ} \end{bmatrix}^{-1} \begin{bmatrix} S_{Xx} & S_{Xy} & S_{Xz} & S_{Xrx} & S_{Xry} & S_{Xrz} \\ S_{Yx} & S_{Yy} & S_{Yz} & S_{Yrx} & S_{Yry} & S_{Yrz} \\ S_{Zx} & S_{Zy} & S_{Zz} & S_{Zrx} & S_{Zry} & S_{Zrz} \\ S_{RXx} & S_{RXy} & S_{RXz} & S_{RXrx} & S_{RXry} & S_{RXrz} \\ S_{RYx} & S_{RYy} & S_{RYz} & S_{RYrx} & S_{RYry} & S_{RYrz} \\ S_{RZx} & S_{RZy} & S_{RZz} & S_{RZrx} & S_{RZry} & S_{RZrz} \end{bmatrix}$$

$$\left[\begin{array}{ccc:ccc} H_{Xx} & H_{Xy} & H_{Xz} & H_{Xrx} & H_{Xry} & H_{Xrz} \\ H_{Yx} & H_{Yy} & H_{Yz} & H_{Yrx} & H_{Yry} & H_{Yrz} \\ H_{Zx} & H_{Zy} & H_{Zz} & H_{Zrx} & H_{Zry} & H_{Zrz} \\ \hdashline H_{RXx} & H_{RXy} & H_{RXz} & H_{RXrx} & H_{RXry} & H_{RXrz} \\ H_{RYx} & H_{RYy} & H_{RYz} & H_{RYrx} & H_{RYry} & H_{RYrz} \\ H_{RZx} & H_{RZy} & H_{RZz} & H_{RZrx} & H_{RZyr} & H_{RZrz} \end{array}\right]$$

Figure 7.2 The transmissibility components when considering 6D-input and 6D-output motions. The upper-left quadrant represents the translational-input to translational-output, the quadrant upper-right represents the rotational-input to translational-output, the lower-left quadrant represents the translational-input to rotational-output, and the lower-right quadrant represents the rotational-input to rotational-output.

Figure 7.2 shows the same 6 x 6 transmissibility matrix portioned into quadrants of like units. The upper-left quadrant represents the translational-input to translational-output, the quadrant upper-right represents the rotational-input to translational-output, the lower-left quadrant represents the translational-input to rotational-output, and the lower-right quadrant represents the rotational-input to rotational-output. The resulting

transmissibility matrices are complex, with each component having real and imaginary parts (ω was omitted from Equation 7.4 and 7.5 for simplification). Therefore, it becomes difficult to deal with the transmissibility in this form for practical applications. However, the principal diagonal components of each 3 x 3 transmissibility matrix can be computed using the singular value decomposition (SVD) at each ω using Equation 7.1.

For 6D input/output transmissibilities, the single value decomposition is taken for each quadrant of translational and rotation transmissibilities. More specifically, the SVD is taken by partitioning the large 6 x 6 full matrix into each 3 x 3 transmissibility matrix: translational-input to translational-output, the rotational-input to translational-output, the translational-input to rotational-output, and the rotational-input to rotational-output (Figure 7.2) such that

$$\text{SVD}\left\{\begin{bmatrix} H_{Xx}(\omega) & H_{Xy}(\omega) & H_{Xz}(\omega) \\ H_{Yx}(\omega) & H_{Yy}(\omega) & H_{Yz}(\omega) \\ H_{Zx}(\omega) & H_{Zy}(\omega) & H_{Zz}(\omega) \end{bmatrix}\right\} = \mathbf{U}\boldsymbol{\Sigma}\mathbf{V}^{\mathrm{T}}$$

in which

$$\boldsymbol{\Sigma} = \begin{bmatrix} H_{11}(\omega) & 0 & 0 \\ 0 & H_{22}(\omega) & 0 \\ 0 & 0 & H_{33}(\omega) \end{bmatrix}$$

where $H_{11}(\omega)$, $H_{22}(\omega)$, and $H_{33}(\omega)$ represent three principal components in the orthogonal space. At each frequency, the principal diagonal components are transformed to a single number by using the maximum distortion energy theory (Equation 7.2).

7.3 Experimental Setup

The vibration response induced by whole-body vibration was measured in this work considering different vibration directions, postures, and vibration axes. Advanced methods of data collection and acceleration correction are used by DeShaw and Rahmatalla (2012) and are described later in this section.

7.3.1 Participants and Posture Conditions

Twelve healthy male participants that took part in the study had a mean age of 24.0 years (standard deviation of 2.7 years), a mean height of 180.1 cm (standard deviation of 5.9 cm), and a mean weight of 84.0 kg (standard deviation of 9.2 kg). Written informed consent, as approved by the University of Iowa Institutional Review Board, was obtained prior to testing (Appendix B). The participants were seated in a rigid seat coated with thin rubber mounted to a vibration platform. The thin rubber was used to increase friction and had negligible whole-body vibration effects on the participants. A footrest on the platform was adjusted so that the participants were comfortable and their thighs were close to horizontal. Each participant was tested in a simulated vibration environment for a maximum duration of one hour.

Four sitting postures were considered for this work: an upright seated posture with no backrest where the participants looked straight forward and their hands were in their laps (NB); a backrest-supported sitting posture where the participants looked forward and kept their hands in their laps (BS); a backrest-supported sitting posture where participants forearms rested on armrest supports (B+A); and a backrest-supported sitting posture where the participants used the armrest supports and rotated their heads to the side (B+A+R). An example of each of the four postures is shown in Figure 7.3. The

participants were asked to remain in each posture for the full 60 seconds of testing without making any movements that were not caused by the vibration itself.

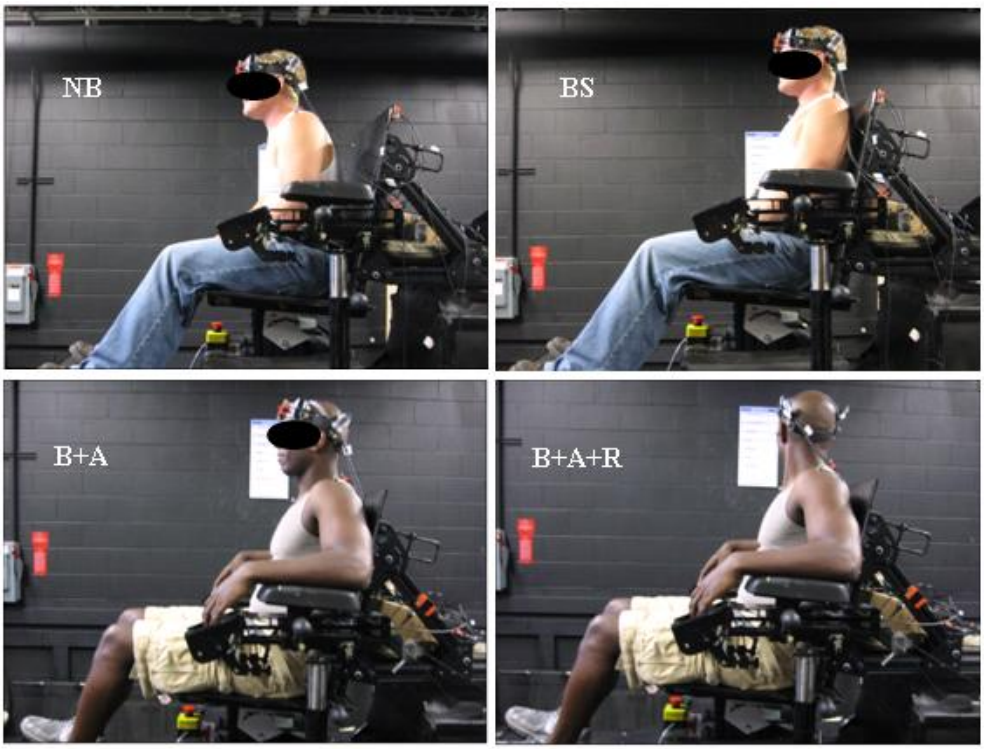

Figure 7.3 The four seating postures tested. The no-backrest condition (NB); the backrest-supported condition (BS); the backrest-supported and armrest-supported condition (B+A); and the backrest-supported, armrest-supported, and head-rotated condition (B+A+R).

7.3.2 Vibration Conditions

Vibration was generated using a six-degree-of-freedom man-rated motion simulator (Moog E-CU-624-1800, Moog-FCS, Ann Arbor, MI, USA) which is shown in Figure 7.4. The single-axis translational vibration conditions for this study included random fore-aft (X), lateral (Y), and vertical (Z) vibrations each from 0.5 to 12 Hz with each having an unweighted acceleration magnitude of approximately 1.8 m/s^2 RMS (root-mean-squared). The vibration files were created from white noise and band-pass filtered

to achieve the desired frequency range. Each participant experienced every one of the vibration conditions while undergoing each of the four postural conditions in a completely randomized ordering. Each vibration file lasted for a total of 60 seconds.

Three-dimensional and six-dimensional vibrations were also generated using the same simulator base (Figure 7.4). The vibrations were of random white noise from 0.5 to 12 Hz and at 1.8 m/s^2 RMS resultant acceleration for the translational directions (1.08 m/s^2 RMS per each direction) and 1.4 rad/s^2 RMS resultant acceleration for the rotational acceleration (0.8 rad/s^2 RMS per each direction). For the 3D and 6D vibrations, each component in translation and rotation was created of separate white noise and approximately equal in power. Each vibration file lasted for a total of 60 seconds and was again randomized between postures for each participant

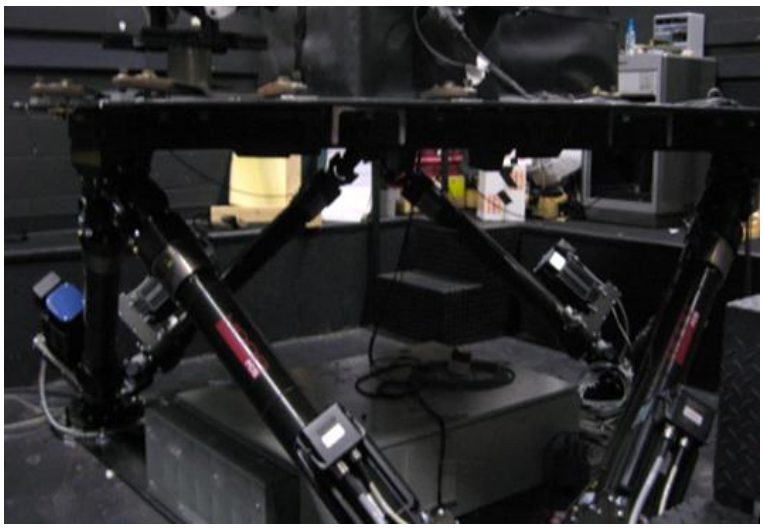

Figure 7.4 Motion simulator base used to generate single- and multi-axis vibrations

7.3.3 Data Collection

Similar to the instrumentation method presented by DeShaw and Rahmatalla

(2012), acceleration and gyroscope data were recorded for each participant during each posture and vibration combination. A methodology was used to correct the acceleration measurements from orientation errors in 3D space and errors from the acceleration effects from gravity. An inertial sensor (MTx inertial trackers, Xsens Technologies, Enschede, Netherlands) was attached to a ridged head-worn halo similar to a study by Wang and Rakheja (2006A) and DeShaw and Rahmatalla (2012). This inertial sensor recorded vibration data in the form of tri-axial acceleration data and tri-axial gyroscope data at 120 Hz. An additional motion -tracking inertial sensor was rigidly attached to the seat frame to use as a source of monitoring the input-vibration accelerations. Additional redundant sensors were placed on other locations on the seat frame and on the participant, with the additional data to be used for supplementary studies. The inertial sensors are shown in Figure 7.3. Each inertial sensor had a mass of 30g and a contact surface area of 20 cm^2. Initial experimentations showed that the inertial sensor has a natural frequency on the skin around 25 Hz, which is outside the frequency range under consideration.

7.4 Results

7.4.1 Single-Axis Random Vibration

Figure 7.5 shows the seat-to-head transmissibility during fore-aft vibration during the backrest posture. The graphs on the left show the individual transmissibility components due to the fore-aft, lateral, and vertical motions at the head. The fore-aft to fore-aft transmissibility (Xx) shows a peak at around 1.5 Hz which diminishes with higher frequencies. This is comparable to a study by Hinz et al. (2010). The cross-axis

lateral transmissibility shows near zero transmission to the head; however, the cross-axis vertical transmissibility shows a very large peak from 4 to 6 Hz.

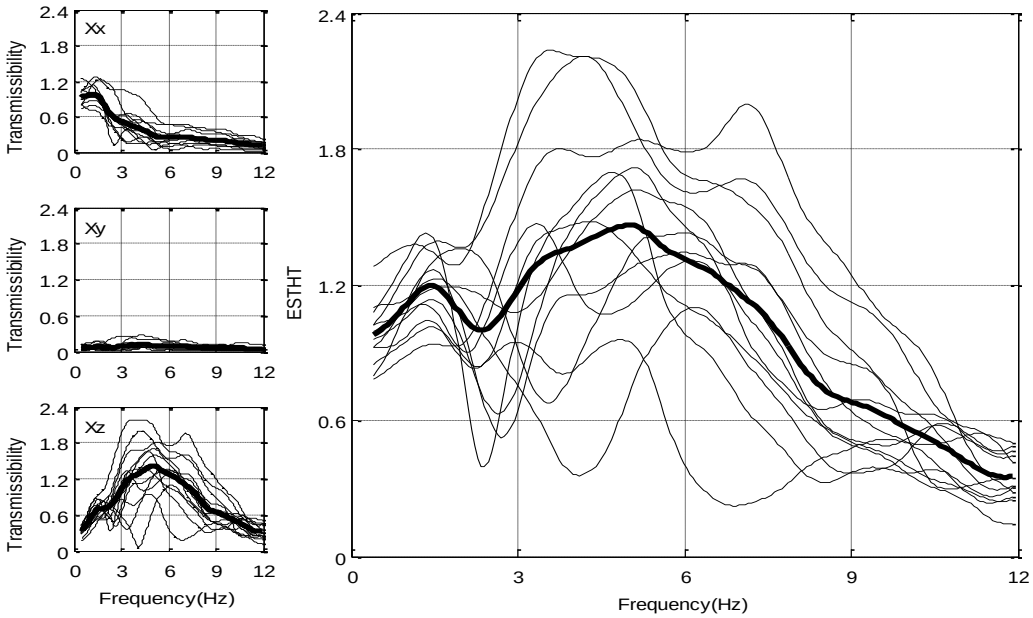

Figure 7.5 Example of three transmissibility components (1input-3output, located on left) reducing to one ESTHT graph for 12 participants in the backrest posture during fore-aft vibration. The bold line represents the average of the group.

This cross-axis component is also shown by others (Hinz et al., 2010; Paddan and Griffin, 1988B). The right graph in Figure 7.5 shows the effective seat-to-head transmissibility during fore-aft vibration. It shows a small peak around 1.5 Hz followed by a large peak at around 5 Hz. Both dominant peaks from individual transmissibility graphs are captured in the ESTHT graph.

Figure 7.6 shows the seat-to-head transmissibility during lateral vibration during the backrest posture. The graphs on the left show the individual transmissibility components due to the fore-aft, lateral, and vertical motions at the head. The lateral to

lateral transmissibility (Yy) shows a peak around 1.0 Hz, which diminishes with higher frequencies similar to Hinz et al. (2010).

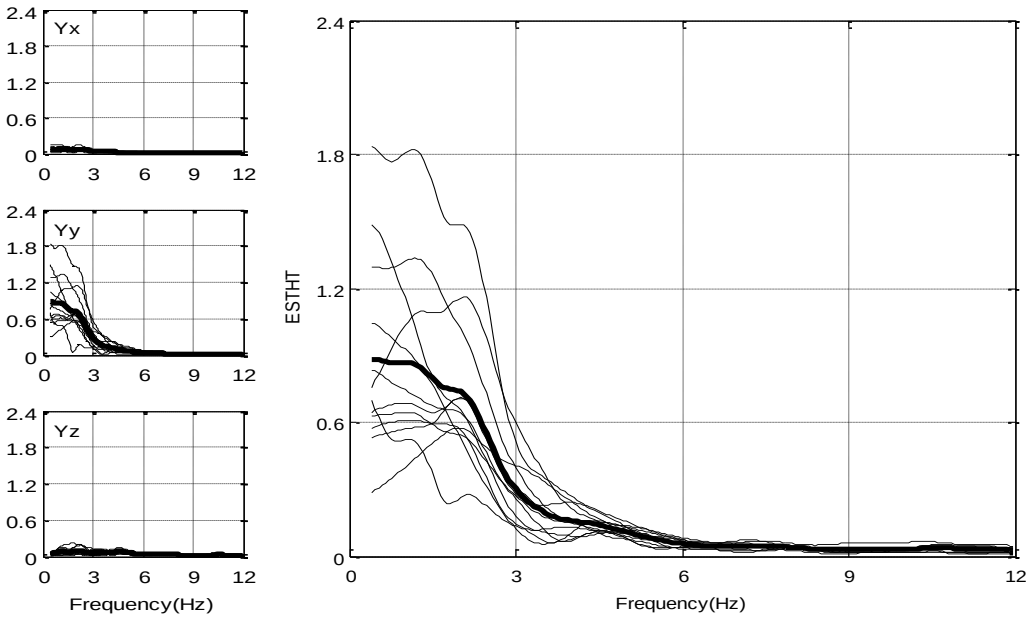

Figure 7.6 Example of three transmissibility components (1input-3output, located on left) reducing to one ESTHT graph for 12 participants in the backrest posture during lateral vibration. The bold line represents the average of the group.

The cross-axis fore-aft transmissibility shows near zero transmission as does the cross-axis vertical transmissibility. The graph on the right in Figure 7.6 shows the effective seat-to-head transmissibility during lateral vibration. It shows a peak at around 1.0 Hz that diminishes with higher frequencies. The ESTHT graph looks very similar to that of the lateral to lateral (Yy) transmissibility graph in this case.

Figure 7.7 shows the seat-to-head transmissibility during vertical vibration during the backrest posture. The graphs on the left show the individual transmissibility components due to the fore-aft, lateral, and vertical motions at the head. The vertical to

vertical transmissibility (Zz) shows a large peak around 5 Hz and is comparable to other studies (Hinz et al., 2010, Paddan and Grffin, 1988A). The cross-axis lateral transmissibility shows near zero transmission to the head; however, the cross-axis fore-aft transmissibility shows a moderate peak from 3 to 5 Hz. The graph on the right in Figure 7.7 shows the effective seat-to-head transmissibility during vertical vibration. It shows a large peak at around 5 Hz which compares very closely with that of the individual vertical to vertical (Zz) transmissibility component.

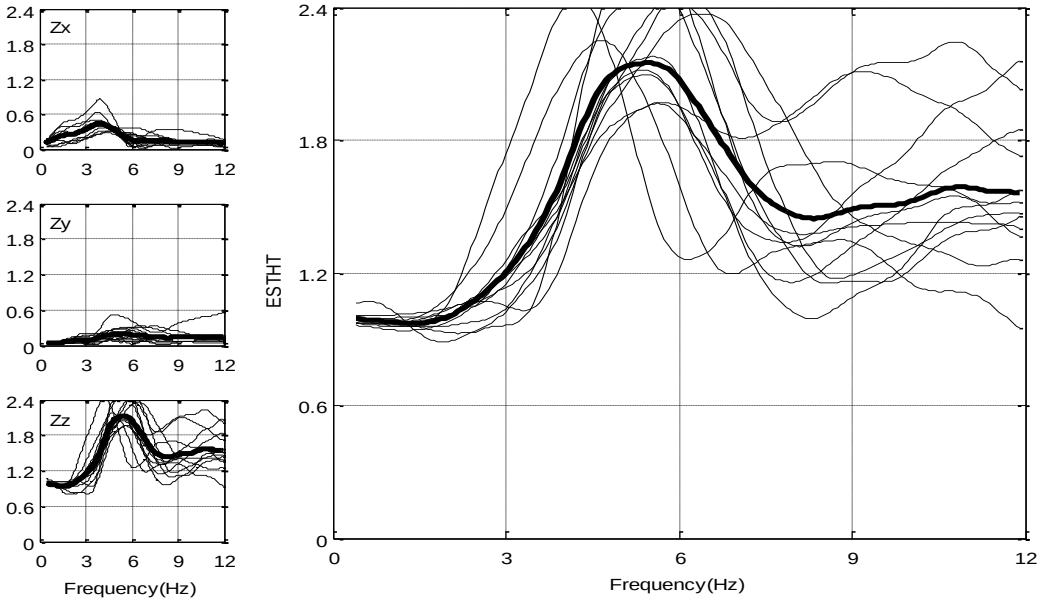

Figure 7.7 Example of three transmissibility components (1input-3output, located on left) reducing to one ESTHT graph for 12 participants in the backrest posture during lateral vibration. The bold line represents the average of the group.

While the previous graphs show differences between vibration directions in single-axis vibration (fore-aft, lateral, and vertical), Figure 7.8 shows the differences in effective seat-to-head transmissibility (ESTHT) between each of the four postures in consideration.

Figure 7.8a shows that the postures that contribute the greatest vibration transmission to the head in fore-aft vibration are the backrest (BS) and backrest with armrest (B+A) postures with peaks from around 4 to 5 Hz. This indicates that during fore-aft vibration, the armrest has little effect on vibration transmission. The no-backrest condition had the greatest effect on the ESTHT as the peak was reduced and shifted to around 2 Hz. As expected, this indicates that the backrest plays a large role in vibration transmission during fore-aft vibration. The posture with head rotation (B+A+R) had the same trend as the other backrest postures but was attenuated slightly. This could be due to the stiffening of the head-neck system or the effect from the head being out of alignment with the fore-aft coordinate axis.

Figure 7.8b shows the ESTHT for all the postures during lateral vibration. For this vibration direction, the posture with the head rotation (B+A+R) has the greatest transmissibility. This is likely due to the head being out of alignment with the lateral coordinate axis which relates to the ESTHT being lower for the B+A+R posture during fore-aft vibration (see Figure 7.5). Since the ESTHT are very similar between the NB, BS, and B+A postures, the results indicate that there is little backrest or armrest effect on vibration transmission to the head.

Figure 7.8c shows the ESTHT for all the postures during vertical vibration. During vertical vibration, the greatest ESTHT is found during the backrest-supported posture (BS) and at around 5 Hz. The addition of the armrest (B+A) seemed to attenuate the vibration as well as shift it to a higher frequency at around 6 Hz. The addition of head rotation drastically reduced the peak from the (B+A) posture but did not change the location of the peak. The no-backrest condition (NB) had the least ESTHT by far with a

peak around 4 Hz. The results indicate a strong importance of all postures during vertical vibration.

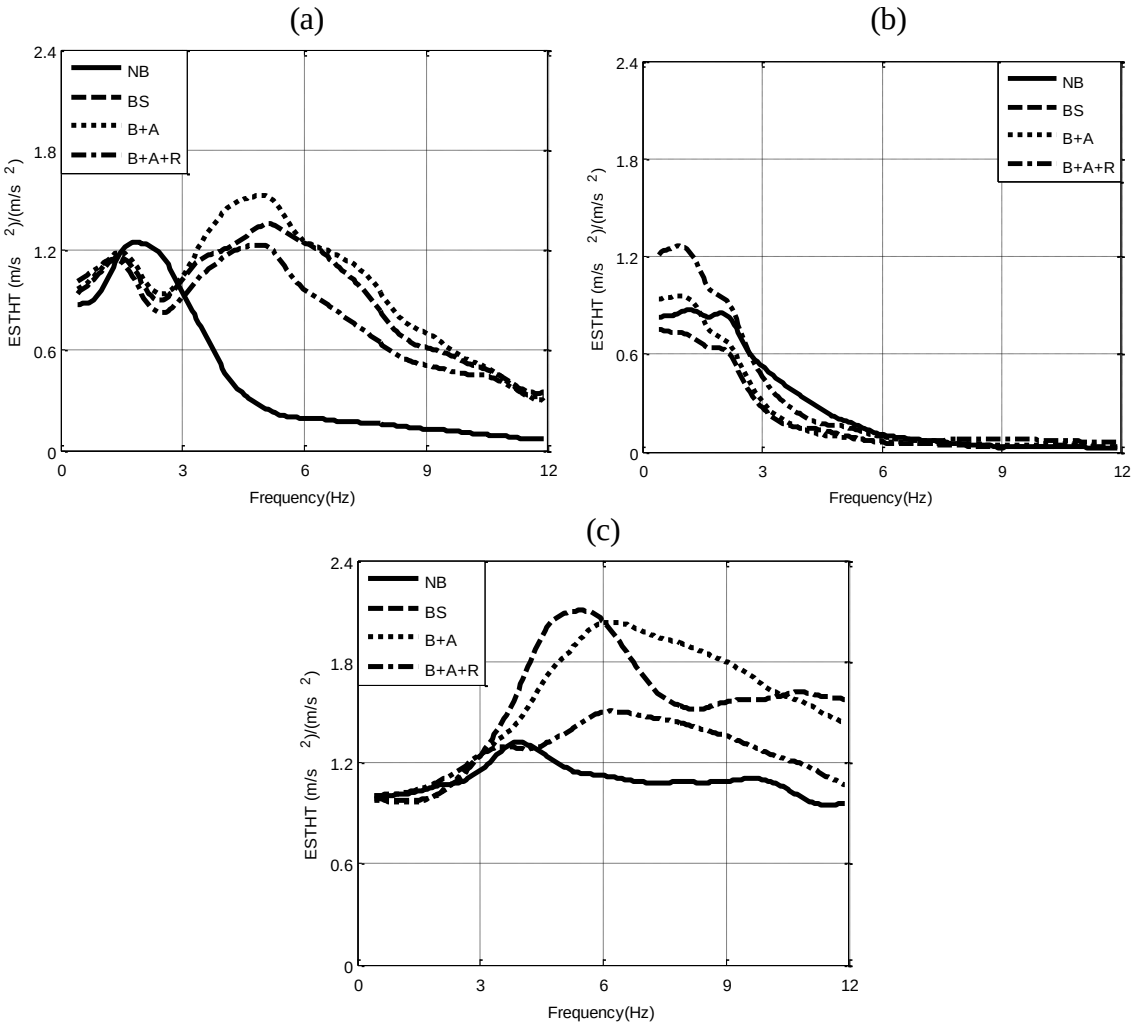

Figure 7.8 Average ESTHT of 12 participants for each of the four seated postures during (a) random fore-aft vibration (b) random lateral vibration and (c) random vertical vibration

7.4.2 Multiple-Axis 3D Random Vibration

The STHT matrix for the vertical single-input and multiple-output has three components. For the random multiple-input and multiple-output, the STHT matrix has nine components. Figure 7.9 shows the components for the B+A+R condition during 3D

random vibration. Because the B+A+R condition contains head rotation, many major contributions are seen in many different transmissibility components. Very large cross-axis contributions are seen in the Xz and Zx components due to the pitch motion of the head, while another large cross-axis contribution is seen in the Yx component due to the rotation of the head during the B+A+R posture.

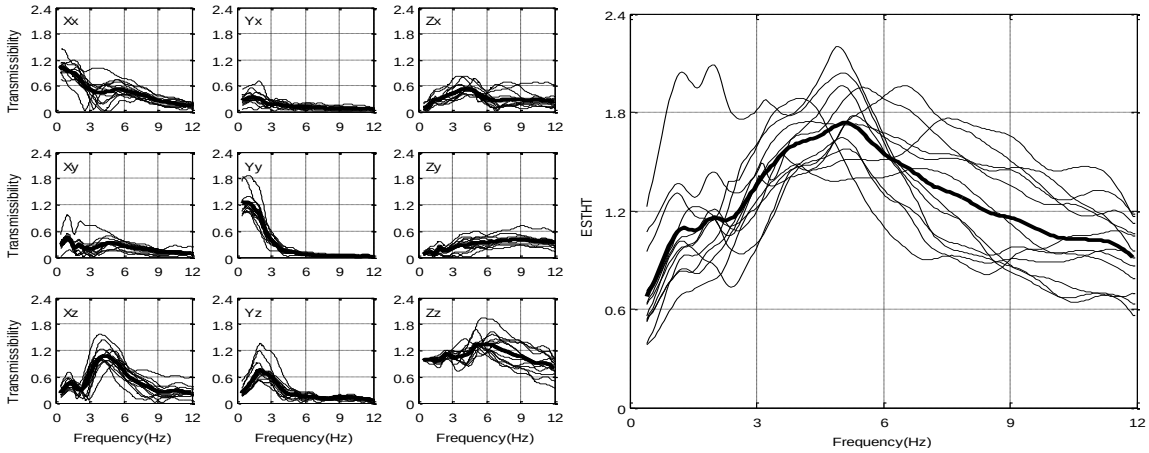

Figure 7.9 Example of nine transmissibility components (3input-3output) in a complicated posture, reducing to one ESTHT graph for 12 participants during the backrest + armrest + rotation posture. The bold line represents the average of the group.

In Figure 7.10, the ESTHT for four different postures during 3D random vibration is shown. The BS posture shows the largest peak at around 5.25 Hz. The B+A posture shows a reduced peak from that of the BS posture, while the B+A+R posture shows an even further reduced peak. This indicates that while the B+A+R posture may have output vibration in more directions, the overall energy to the output point on the head is reduced.

The NB posture showed by far the least magnitude and had a peak location at a much lower frequency than the other postures at around 2.5 Hz.

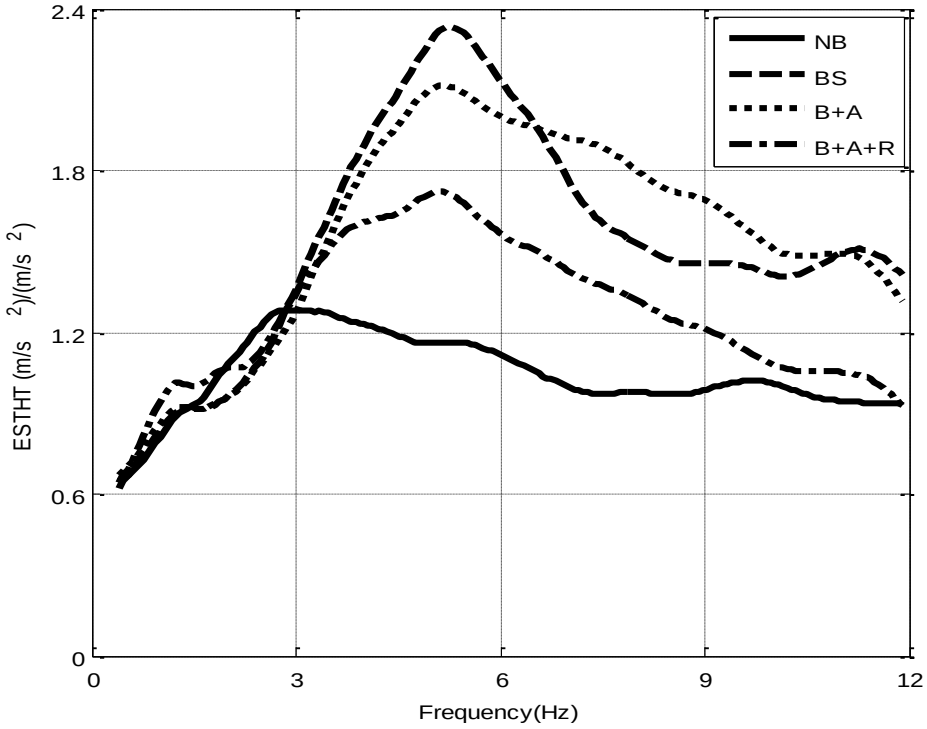

Figure 7.10 Average ESTHT of 12 participants during random 3D vibration during four seated postures

7.4.3 Multiple-Axis 6D Random Vibration

The STHT matrix for 3D multiple-input and multiple-output has nine components. For 6D multiple-input and multiple-output scenarios, the STHT matrix will now contain 36 components (3-translational-inputs plus 3-rotational-inputs by 3-translational-outputs plus 3-rotational-outputs). Input vibrations are noted by uppercase letters X,Y, and Z for translational motions and by RX, RY, and RZ for rotational motions Lowercase letter represent output motions. Figure 7.11 shows all 36 components

for the NB condition during 6D random vibration. The purely translational transmissibilities (upper-left 9 components) have units of m/s^2 / m/s^2, the purely rotational transmissibilities (lower-right 9 components) have units of rad/s^2 / rad/s^2, and the rotation-to-translational and translational-to-rotational transmissibilities have units of rad/s^2 / m/s^2 and m/s^2 / rad/s^2 respectively. As can be seen from Figure 7.11, because of the interaction between many different input and output components, useful information is difficult to interpret from the graphs. A large pitch (ry) association is seen between translational inputs X and Z as well as rotational input RY but other contributions are hard to evaluate. In order to utilize this complicated analysis the effective seat-to-head transmissibility (ESTHT) is calculated for each quadrant of the full 6 x 6 transmissibility matrix as shown in Figure 7.12.

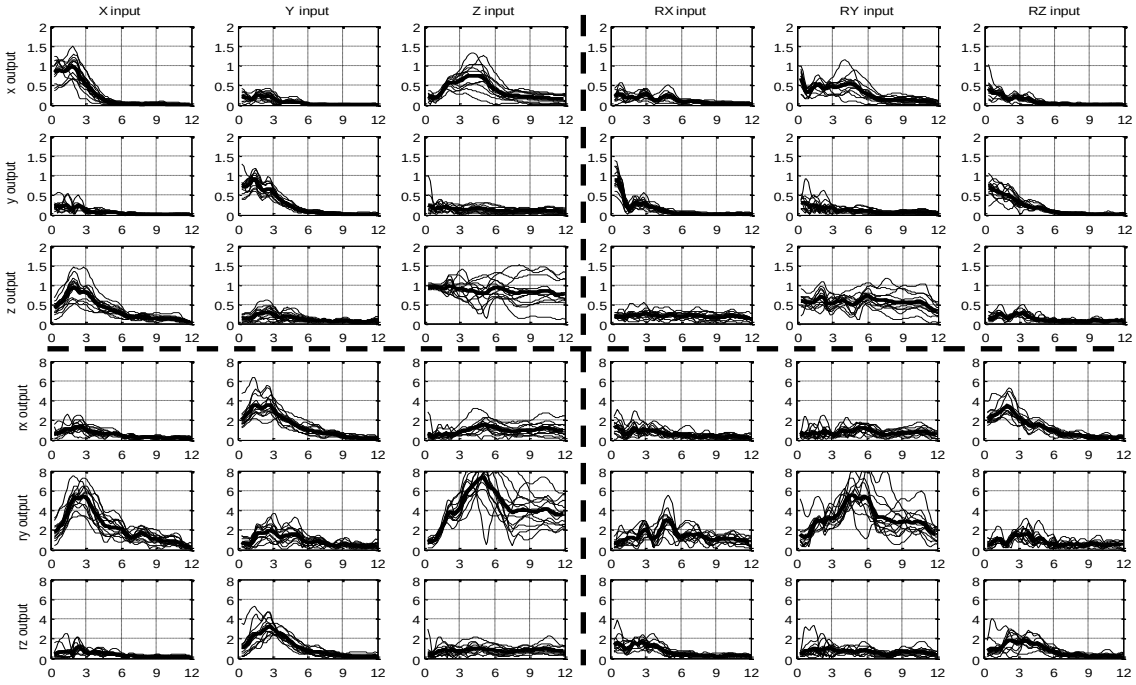

Figure 7.11 Example of each transmissibility component of a 6 x 6 matrix for the no-backrest posture (NB) during 6D vibration. Vertical and horizontal lines drawn distinguish between quadrants with like units.

While to the author's knowledge no studies have investigated 6-input-6-output transmissibilities directly, some have investigated 6D output vibrations with single-axis input vibrations (Paddan and Griffin, 1988A; Paddan and Griffin, 1988B; Paddan and Griffin, 1994; Paddan and Griffin, 2000). The individual transmissibility plots from these studies compare very well to the 6 x 6-transmissibility plot in Figure 7.11 for both peak magnitudes and peak resonance locations.

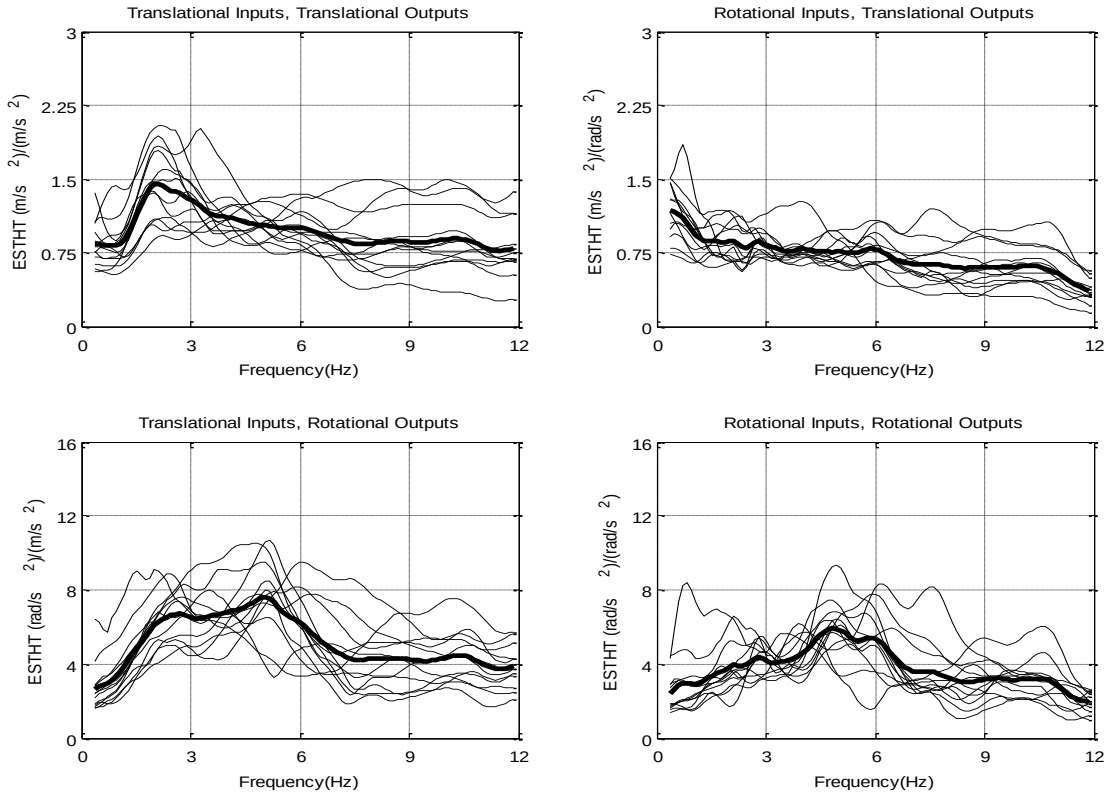

Figure 7.12 Example of the ESTHT during the no-backrest posture (NB) in 6D vibration. Each 3 x 3 transmissibility matrix is shown: translational-input to translational-output, the rotational-input to translational-output, the translational-input to rotational-output, and the rotational-input to rotational-output.

Figure 7.12 shows clearly the frequency range of importance for the no-backrest posture is 2 to 4 Hz for translational-input/translational-output motion, a range of

importance of 2 to 5 Hz for translational-input/rotational-output motion, and a range of importance of around 4 to 6 Hz for rotational-input/rotational-output motion. Interestingly, rotational-input/translational-output did not show a distinct peak indicating that rotational inputs cause very little translational motion at the head during a no-backrest posture.

Figure 7.13 shows the ESTHT of each partitioned quadrant of a complex 6 x 6 transmissibility matrix for each posture in consideration. The quadrants reduce to an individual ESTHT for translational-input to translational-output, rotational-input to translational-output, translational-input to rotational-output, and to rotational-input to rotational-output graphs. The results indicate that the addition of a backrest contributes greatly to increased transmissibility during translational input, while the rotation of the head decreases the translational motion at the head (Figure 7.13a). Additionally, the results show that little effect on translation motion is seen with the addition of the armrest. During rotational-input and translational-output (Figure 7.13b), the ESTHT is minimal except at low frequencies (less than 1 Hz for all posture and at 6 Hz for backrest postures), which indicates that rotational inputs cause very little amplification of translational motions at the head. Figure 7.13c shows the ESTHT from translational inputs to rotational outputs. The backrest condition (BS) has the largest peak at around 6 Hz while the B+A and B+A+R postures have similar responses with reduced peaks from that of the BS posture. The NB posture has a greatly reduced maximum range from around 2 to 5 Hz and approximately half the amplitude of the backrest-supported posture. These results indicate that during translational vibration the posture plays a large role in the rotational response at the head. Lastly, Figure 7.13d shows the ESTHT from purely

rotational input and output components. The backrest-supported posture (BS) has a very large peak around 4.5 Hz while the B+A and the B+A+R postures have smaller varied peaks from 3 to 6 Hz. The NB posture has a reduce amplitude from the BS posture with a peak around 4.5 Hz. Results from Figures 7.13c and 7.13d indicate that the backrest-supported posture is prone to rotational outputs.

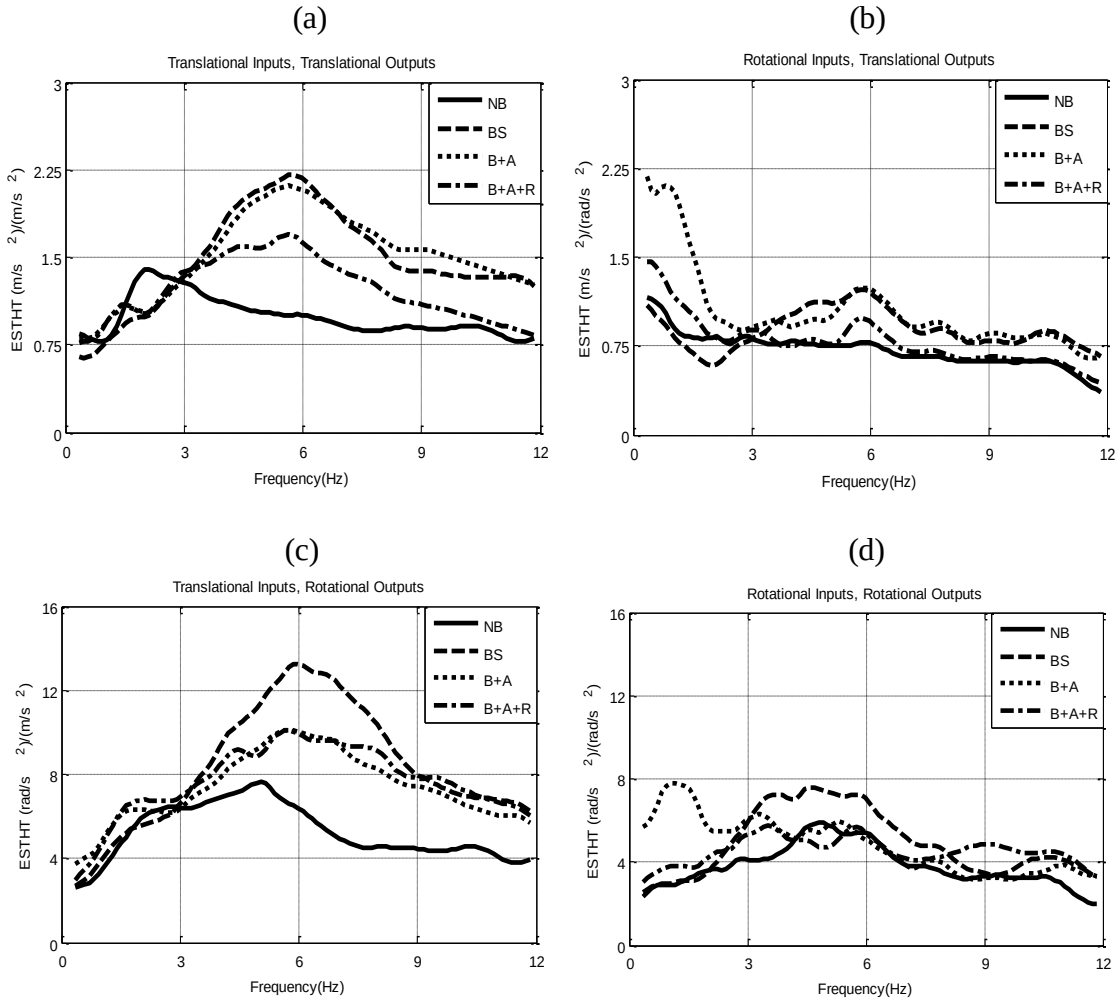

Figure 7.13 The ESTHT during each of the four postures in 6D vibration. Each 3 x 3 transmissibility matrix is shown: (a) the translational-input to translational-output, (b) the rotational-input to translational-output, (c) the translational-input to rotational-output, and (d) the rotational-input to rotational-output.

7.5 Discussion

The concept of ESTHT is introduced in this work, which represents an objective way to transform the multiple-input and multiple-output transmissibility matrix to a single graph similar to those of the single-input and single-output.

During single-axis vibration, the three transmissibility components in Figures 7.5 through 7.7 gave useful insights into what is happening in each component direction. When these components are combined, the effect is like a resultant, which is similar to methods by previous studies (Wang et al., 2008; Paddan and Griffin, 1998). When three inputs and three outputs are considered, the transmissibility matrix is more complex and needs to be rotated as cross-components affect each other (see Figure 7.9). This rotated matrix can then be combined using the maximum distortion energy theory (Hibbeler, 2008) to compute a resultant number that represents the effective transmissibility. This effective transmissibility then represents the total energy through the system and in the case of seat-to-head transmissibility, represents the energy to the head.

It can be seen (Figure 7.9) that during 3D vibration, it is difficult to infer an objective description from the nine transmissibility graphs from the combinations of input and output motions. This can be even more complicated if the input and the output motions each have six degrees of freedom as seen in Figure 7.11. In order to objectively quantify the effect of 6D vibrations, the ESTHT was calculated for each 3 x 3 transmissibility matrix of like quantities, including: translational-input to translational-output, rotational-input to translational-output, translational-input to rotational-output, and rotational-input to rotational-output. Using the ESTHT in such a manner allows a

seat designer or researcher to focus on the specific degrees of translation or rotation that cause motion and allow them to locate the critical frequencies based on those motions.

The results show that the proposed ESTHT concept presents an objective tool to assess relatively complicated input/output motions and gain insights into the effect of posture and the surrounding equipment on the biodynamic response of the operators. The results for the single-input and multiple-output for the fore-aft and vertical vibrations have similar characteristics to those in the literature (Rahmatalla et al., 2010; Mandapuram et al., 2011; Hinz et al., 2010; Paddan and Griffin, 1988A; Paddan and Griffin, 1988B). Additionally, the results presented for 3D-input-3D-output and 6D-input-6D-output motion show similarities with previous literature in translation motion (Hinz et al. 2010; Paddan and Griffin, 1988A; Paddan and Griffin, 1988B) and in rotational motion (Paddan and Griffin, 1994).

This study presents an objective tool to be used for WBV analysis but considers only four postures, therefore, the results for the multiple-input and multiple-output vibration need further investigations with more participants and seating conditions to be used effectively as guides for designing vehicle seating in WBV. This study is timely as advances in seat design for operators are increasingly important with the evolving armrests, backrest, and seat suspension systems. The utilization of an objective quantification method such as ESTHT, therefore, would be beneficial to the fields of seat/equipment design as well as human biomechanics studies.

CONCLUSION

The work in Chapter 1 introduced an acceleration measurement system for WBV studies in which a hybrid marker-accelerometer system overcomes current measurement difficulties, eliminates the need for multiple accelerometers, and can add accuracy when the vibration motion has multiple directions. The method presented has great potential for use in other labs, as it is easily reproducible and has the potential to extend to multiple rigid body segments to monitor human motion. Being able to decouple the acceleration of motions in any reference direction will also make it more accurate for defining single-directional transmissibility in any desired direction. The results also have demonstrated the flexibility in using the proposed systems by eliminating the gravity component from the accelerometer signals. With this proposed methodology, it becomes possible to investigate various biodynamic measures in any direction with a clear picture of the relationship between the direct and cross-components of the motion.

The work in Chapter 2 presented a methodology for the correction of acceleration measurements in WBV by utilizing the data from inertial based sensors to deal with inclined surfaces or when the motion has multiple directions. Current correction methodologies may work well with uni-axial direction WBV testing, with some precautions; however, they will encounter considerable errors under multiple-axis WBV. The method presented an objective measurement that can be used across labs and for standardization purposes.

Another challenge in the field of WBV is how to accurately predict human discomfort given a posture condition and vibration environment. Many occupations require people to use non-neutral postures to monitor their equipment while both the

person and the equipment are under vibration. Therefore, there is a great need for a straightforward predictive discomfort model that can address the issues of posture and vibration content. Chapters 3 and 4 examined the role of single-axis vibration on human discomfort and proposed predictive equations for that discomfort. The proposed discomfort quantifies whole-body musculoskeletal discomfort considering body posture, closeness of the joints to their limits, and severity of the angular acceleration at the joints. The predictive discomfort model was able to capture the trend of the discomfort and the shift in the peaks during sinusoidal fore-aft vibration for different non-neutral head postures and during different backrest conditions. Due to its dependency on the angular parameters, the proposed discomfort model is less sensitive to the locations of measurement sensors, and therefore, more easily reproduced.

In Chapter 5, the biomechanically based predictive discomfort measure was modified from the discrete frequency forms of Chapters 3 and 4 in order to evaluate discomfort from multiple seating postures and random vibration during single- and multi-axis WBV. The inability to capture discomfort levels from alternative postures is a severe limitation of the current standards. Current assessment methods for discomfort and injury prevention (such as the ISO 2631-1 standard) are calculated by using frequency-weighted accelerations at the body contact areas during WBV. While these assessment methods have some consistency during simple seating postures and vibration inputs, they are limited in complicated vibration and seating environments. Even as these weighting factors continue to improve, there will always be limitations to posture conditions that can be better addressed by using a biomechanically based model, such as the one in the current work. Because the predictive model in Chapter 5 utilizes equivalent Borg CR-10

units it is extremely useful for evaluating discomfort in real-world scenarios. Many of the standards and models exist to provide only general limits for exposure durations and are limited by how to describe the actual instantaneous perceptions due to WBV. In this study, relating all terms to a Borg CR-10 equivalent value allows for the direct comparison between posture and vibration conditions to that of an actual reference scale of accompanying anchor words indicating actual perceptions of discomfort. Additionally, with advances in computer modeling, the proposed predictive discomfort may provide efficient ways to assess discomfort in complicated environments and to develop reliable biodynamic models for design of equipment inside moving vehicles.

A widely used vibration assessment tool used to measure human biodynamic response is the seat-to-head transmissibility. The limitation of this measure occurs when there is more than one input or output motion at the seat and head. To resolve this issue, the concept of effective seat-to-head transmissibility is proposed in this thesis. Chapter 6 examined the ESTHT during single-axis sinusoidal, single-axis random, and multi-axis 3D vibrations during WBV. Chapter 7 investigated the ESTHT during single-axis random, 3D random, and 6D random vibrations. The ESTHT provides an objective way to transform the multiple-input and multiple-output transmissibility matrix to a single graph similar to those of the single-input and single-output. This is done by using the maximum distortion energy theory to compute a resultant number that represents the effective transmissibility. This effective transmissibility then represents the total energy through the system and in the case of seat-to-head transmissibility, represents the energy to the head. It can be inferred from the results of these works that the proposed ESTHT concept presents an objective tool to assess relatively complicated input/output motions

and to gain insights into the effect of posture and the surrounding equipment on the biodynamic response of the operators.

This thesis addresses the current issues and limitations in the field of WBV, (1) by introducing effective tools to measure human response to whole-body vibration in a more precise and comprehensive manner, (2) by introducing a new musculoskeletal-based predictive measure for the evaluation of discomfort in WBV with people in multiple postures and vibration axes, and (3) by developing a new seat-to-head transmissibility measure, called effective transmissibility, to investigate human response in complex multiple-axis whole-body vibration.

This thesis is timely as advances in seat design for operators are increasingly important with the evolving armrests, backrest, and seat suspension systems. The utilization of comprehensive measurement techniques, a predictive discomfort model, and the concept of ESTHT, therefore, would be beneficial to the fields of seat/equipment design as well as human biomechanics studies in WBV.

REFERENCES

1. Adams M.A.; Hutton, W.C. The effect of posture on the lumbar spine. *J. Bone Joint Surg.* **1986,** 67-B, 625-629.

2. Alan, J.C.; Alan, H.S.C. Ergonomics of grab unloaders for bulk materials handling. *International Journal of Industrial Ergonomics.* **1999,** 23, 61-66.

3. Baker, W.D.R.; Mansfield, N.J. Effects of horizontal whole-body vibration and standing posture on activity interference. *Ergonomics.* **2010,** 53, 365-374.

4. Basri, B.; Griffin, M.J. Predicting discomfort from whole-body vertical vibration when sitting with an inclined backrest. *Applied Ergonomics.* **2013,** 44, 423-434.

5. Beard, G.F.; Griffin, M.J. Discomfort during lateral acceleration: Influence of seat cushion and backrest. *Applied Ergonomics.* **2013,** In press.

6. Borg, G. A category scale with ratio properties for intermodal and interindividual comparisons."*In: H.G. Geissler and P. Petzold, Editors, Psychophysical Judgment and the Process of Perception,* Deutscher Verlag der Wissenschaften, Berlin **1982,** 25-33.

7. Boyer, K.A.; Nigg, B.M. Quantification of the input signal for soft tissue vibration during running. *Journal of Biomechanics.* **2007,** 40, 1877-1880.

8. British Standards BS 6841:1987. Measurement and evaluation of human exposure to whole-body mechanical vibration and repeated shock, **1987.**

9. Cereatti, A.; Groce, U.D.; Cappozzo, A. Reconstruction of skeletal movement using skin markers: comparative assessment of bone pose estimators. *Journal of Neuro Engineering and Rehabilitation***. 2006,** 3-7.

10. Chaffin, D.B.; Anderson, G.B.J.; Martin, B.J. *Occupational Biomechanics.* **1999**, Wiley-Interscience.

11. Chu, J.J.; Caldwell, G.E. Stiffness and damping response associated with shock attenuation in downhill running. *Journal of Applied Biomechanics.* **2004,** 20, 291-308.

12. Courtney, A.J.; Cahn, A.H.S. Ergonomics of grab unloaders for bulk materials handling. *International Journal of Industrial Ergonomics.* **1999,** 23, 61-66.

13. De Oliviera, C.G.; Nadal, J. Transmissibility of Helicopter Vibration in the Spines of Pilots in Flight. *Aviation, Space, and Environmental Medicine.* **2005,** 76, 576-580

14. Demic, M.; Lukic, J. Investigation of the transmission of fore and aft vibration through the human body. *Applied Ergonomics.* **2009,** 40, 622-629.

15. DeShaw, J.; Rahmatalla, S. Comprehensive measurement in whole-body vibration. *Journal of Low Frequency Noise, Vibration and Active Control.* **2012,** 31(2), 63-74.

16. DeShaw, J.; Rahmatalla, S. Predictive discomfort and seat-to-head transmissibility in low-frequency fore-aft whole-body vibration. *Journal of Low Frequency Noise, Vibration and Active Control.* **2011,** 30(3), 185-196.

17. Dickey, J.P.; Eger, T.R.; Oliver, M.L.; Boileau, P.E.; Trick, L.M.; Edwards, M. Multi-axis sinusoidal whole0body vibrations: Part II – Relationship between vibration total value and discomfort varies between vibration axes. *Journal of Low Frequency Noise, Vibration and Active Control.* **2007,** 26(3), 195-204.

18. Dickey, J.P.; Oliver, M.L.; Boileau, P.E.; Eager, T.R.; Trick, L.M.; Edwards, A.M. Multi-axis sinusoidal whole-body vibrations: Part 1 – How long should the vibration and rest exposures be for reliable discomfort measures? *Journal of Low Frequency Noise, Vibration and Active Control.* **2006,** 25, 175-184.

19. Ebe, K.; Griffin M.J. Quantitative prediction of overall seat discomfort. *Ergonomics.* **2000,** 43, 791-806.

20. Eger, T.R.; Stevenson, J.; Callaghan, J.P.; Grenier, S.; VibRG. Predictions of health risks associated with the operation of load-haul-dump mining vehicles: Part 2-Evaluation of operator driving postures and associated postural loading. *International Journal of Industrial Ergonomics***. 2008,** 38, 801-815.

21. Ewing, C.L.; Thomas, D.J. Human head and neck response to impact acceleration. *Naval Aerospace Medical Research Lab*: Pensacola, FL, **1972.**

22. Fairley, T.E.; Griffin. M.J. The apparent mass of the seated human body: vertical vibration. *Journal of Biomechanics.* **1989,** 22, 81-94.

23. Fard, M.A.; Ishihara, T.; Inooka, H. Dynamics of the head-neck complex in response to the Trunk horizontal vibration: modeling and identification. *ASME Journal of Biomechanical Engineering.* **2003,** 125, 533-539.

24. Fard, M.A.; Ishihara, T.; Inooka, H. Transmission of the translational trunk vibration to the head-neck complex. *JSME International Journal*. **2001,** 46, 116-122.

25. Fritz, M. Three-dimensional biomechanical model for simulating the response of the human body to vibration stress. *Med. Biol. Eng. Copmut*. **1998**, 36, 686-692.

26. Gal, J.; Herzog, W.; Kawchuk, G.; Conway, P. Measurements of vertebral translations using bone pins, surface markers and accelerometers. *Clinical Biomechanics*. **1997,** 12, 337-340.

27. Genaidy, A.M.; Karwowski, W. The effects of neutral posture deviation on perceived joint discomfort ratings in sitting and standing postures. *Ergonomics*. **1993,** 36, 785-792.

28. Griffin, M. *Handbook of Human Vibration*. **1990,** London, Academic Press.

29. Griffin, M. J.; Lewis, C.H.; Parsons, K.C.; Whitham, E.M. The biodynamic response of the human body and its application to standards. *AGARD Conference Proceedings (CP-253). In: Models and analogues for the evaluation of human biodynamic response, performance, and protection*, **1979,** Paris, France, (von Gierke, H.E., ed). Paper A28. Advisory Group on Aerospace Research and Development.

30. Griffin, M.J. Discomfort from feeling vehicle vibration. *Vehicle System Dynamics* **2007,** 45, 679-698.

31. Hacaambwa, T.M.; Giacomin, J. Subjective response to seated fore-and-aft direction whole-body vibration. *International Journal of Industrial Ergonomics* **2007,** 61-72.

32. Heath, M.T. *Scientific Computing: An Introductory Survey*. **1997,** McGraw–Hill Inc., Boston.

33. Hibbeler, R.C. *Mechanics of Materials, Seventh Editions*. **2008,** Pearson Prentice Hall, New Jersey.

34. Hinz, B.; Menzel, G.; Bluthner, R.; Seidel, H. Seat-to-head transfer function of seated men--determination with single and three axis excitations at different magnitudes. *Industrial Health*. **2010,** 48, 565-583.

35. Hinz, B.; Seidel, H. The Nonlinearity of the Human Body's Dynamic Response during Sinusoidal Whole Body Vibration. *Industrial Health*. **1987,** 25, 169-181.

36. Hinz, B.; Seidel, H.; Menzel, G.H.; Bluthner, R. Effects related to random whole-body vibration and posture on suspended seat with and without backrest, *Journal of Sound and Vibration*. **2002,** 253, 265-282.

37. Holmlund, P.; Lundstrom, R.; Lindberg, L. Mechanical impedance of the human body in vertical direction. *Applied Ergonomics*. **2000,** 31, 415-422.

38. Huang, Y.; Griffin, M.J. Nonlinearity in apparent mass and transmissibility of the supine human body during vertical whole-body vibration. *Journal of Sound and Vibration*. **2009,** 324, 429-452.

39. Hwang, C.L., Yoon, K., *Multiple Attribute Decision Making: Method and Application*. **1981,** Spring, New York.

40. Inman, D.J.; *Control of Vibrations, in Vibration with Control*, **2006,** John Wiley & Sons, Ltd, Chichester, UK.

41. International Organization for Standardization ISO 2631-1, Mechanical vibration and shock – evaluation of human exposure to whole-body vibration – part 1: general requirements, **1997.**

42. Jack, R.J.; Eger, T.R. The effects of posture on seat-to-head whole-body vibration transmission. *Journal of Low Frequency Noise, Vibration and Active Control.* **2008,** 27, 309-325.

43. Johanning, E.; Landsbergis, P.; Fischer, S.; Christ, E.; Göres, B.; Luhrman, R. Whole-body vibration and ergonomic study of US railroad locomotives. *Journal of Sound and Vibration***. 2006,** 298, 594-600.

44. Kaneko, C.; Hagiwara, T.; Maeda S. Evaluation of whole-body vibration by the category judgment method. *Industrial Health*. **2005,** 43, 221-232.

45. Kee, D.; Karwowski, W. LUBA: as assessment technique for postural loading on the upper body based on joint motion discomfort and maximum holding time. *Applied Ergonomics*. **2001,** 32, 357-366.

46. Kee, D.; Karwowski, W. Ranking systems for evaluation of joint and joint motion stressfulness based on perceived discomforts. *Applied Ergonomics*. **2003,** 34, 167-176.

47. Kitazaki, S.; Griffin, M.J. Resonance behavior of the seated human body and effects of posture. *Journal of Biomechanics*. **1998**, 31, 143-149.

48. Kitazaki., S.; Griffin, M.J. Correction method for surface measurement of vibration on the human body. *Journal of Biomechanics.***1995,** 28, 885-890.

49. Kittusamy, N.K.; Buchholz, B. Whole-body vibration and postural stress among operators of construction equipment: A literature review. *Journal of Safety Research*. **2004,** 35, 255-261.

50. Lucchetti, L.; Cappozzo, A.; Cappello, A.; Della Croce, U. Skin movement artefact assessment and compensation in the estimation of knee joint kinematics. *Journal of Biomechanics*. **1998,** 31, 977–984.

51. Madakashira-Pranesh, A. Experimental and Analytical Study of Transmission of Whole Body Vibration to Segments of the Seated Human Body. *PhD Thesis, Concordia University*. **2011.**

52. Maeda, S.; Mansfield, N.J.; Shibata, N. Evaluation of subjective response to whole-body vibration exposure: Effect of frequency content. *International Journal of Industrial Ergonomics*. **2008,** 38, 509-515.

53. Magnusson, M.L.; Pope, M.H; Wilder, D.G; Areskoug, B.M. Are occupational drivers at an increased risk for developing musculoskeletal disorders? *Spine*. **1996,** 21(6), 710-717.

54. Mandapuram, S.; Rakheja, S.; Boileau, P.E.; Maeda, S.; Shibata, N. Apparent mass and seat-to-head transmissibility responses of seated occupants under single and dual axis horizontal vibration. *Industrial Health*. **2010,** 48, 698-714.

55. Mandapuram, S.; Rakheja, S.; Marcotte, P.; Boileau, P-E. Analyses of biodynamic responses of seated occupants to uncorrelated fore-aft and vertical whole-body vibration, *Journal of Sound and Vibration*. **2011,** 330, 4064-4079.

56. Mansfield N.J.; Holmlund, P.; Lundstrom, R.; Lenzuni, P.; Nataletti, P. Effect of vibration magnitude, vibration spectrum and muscle tension on apparent mass and cross-axis transfer functions during whole body vibration exposure. *J. Biomechanics*. **2006,** 39, 3062-3070.

57. Mansfield, N.J. *Human Response to Vibration*, **2005A,** CRC Press LLC.

58. Mansfield, N.J. Impedance methods (apparent mass, driving point mechanical impedance and absorbed power) for assessment of the biomechanical response of the seated person to whole-body vibration. *Industrial Health*. **2005B,** 43, 378-389.

59. Mansfield, N.J.; Griffin, M.J. Non-linearities in apparent mass and transmissibility during exposure to whole-body vertical vibration, *Journal of Biomechanics*. **2000,** 33, 933-941.

60. Mansfield, N.J.; Holmlund, P.; Lundstorm, R. Comparison of subjective response to vibration and shock with standard analysis methods and absorbed power. *Journal of Sound and Vibration*. **2000,** 230, 477-491.

61. Mansfield, N.J.; Maeda, S. Effect of backrest and torso twist on the apparent mass of the seated body exposed to vertical vibration. *Industrial Health*. **2005,** 43, 413-420.

62. Mansfield, N.J.; Maeda, S. Subjective ratings of whole-body vibration for single- and multi-axis motion. *The Journal of the Acoustical Society of America*. **2011,** 130(6), 3723-3728

63. Mansfield, N.J.; Maeda, S. The apparent mass of the seated human exposed to single-axis and multi-axis whole-body vibration. *J. Biomechanics*. **2007**, 40, 2543-2551.

64. Marjanen, Y., Mansfield, N.J. Relative contribution of translational and rotational vibration to discomfort. *Industrial Health*. **2010,** 48, 519-529.

65. Marler, T.; Rahmatalla, S.; Shanhan, M.; Abdel-Malek, K. A new discomfort function for optimization-based posture prediction. *SAE Digital Human Modeling for Design and Engineering Conference. SAE. International.* **2005,** Iowa City, Iowa, USA.

66. Matsumoto, Y.; Griffin, M.J. Movement of the upper-body of seated participants exposed to vertical whole-body vibration at the principal resonance frequency. *Journal of Sound and Vibration*. **1998,** 215, 743-762.

67. McGill, S.M. The biomechanics of low back injury: implications on the current practice in industry and the clinic. *Journal of Biomechanics*. **1997,** 30, 465-475.

68. Miwa, T. Evaluation methods for vibration effect part 7. The vibration greatness of the pulses. *Industrial Health*. **1968,** 6, 143-164.

69. Morioka, M.; Griffin, M.J. Magnitude-dependence of equivalent comfort contours for fore-and-aft, lateral and vertical whole-body vibration. *Journal of Sound and Vibration*. **2006,** 298, 755–772.

70. Nawayseh, N.; Griffin, M.J. Non-linear dual-axis biodynamic response to fore-and aft whole-body vibration, *Journal of Sound and Vibration*. **2005,** 282, 831-862.

71. Newell, G.S.; Mansfield, N.J. Evaluation of reaction time performance and subjective workload during whole-body vibration exposure while seated in upright and twisted postures with and without armrests. *International Journal of Industrial Ergonomics*. **2008,** 38, 499-508.

72. Newland, D.E. *An Introduction to random vibrations and spectral analysis*. **1984,** Longman Inc., New York.

73. Niekerk, J.L.; Pielemeier, W.J.; Greenberg, J.A. The use of seat effective amplitude transmissibility (SEAT) values to predict dynamic seat comfort. *Journal of Sound and Vibration*. **2003**, 260, 867-888.

74. Okunribido, O.O.; Magnusson, M.; Pope, H.M. The role of whole body vibration, posture and manual materials handling as risk factors for low back pain in occupational drivers, *Ergonomics*. **2008,** 51, 308-329.

75. Olson, R.; Hahn, D.I.; Buckert, A. Predictors of severe trunk postures among short-haul truck drivers during non-driving tasks: An exploratory investigation involving video assessment and driver behavioral self-monitoring. *Ergonomics*. **2009,** 52, 707-722.

76. Paddan, G.S.; Griffin, M.J. A review of the transmission of translational seat vibration to the head. *Journal of Sound and Vibration*. **1998,** 215, 863-882.

77. Paddan, G.S.; Griffin, M.J. The transmission of translation seat vibration to the head – I. Vertical seat vibration. *J. Biomechanics*. **1988A,** 21, 191-197.

78. Paddan, G.S.; Griffin, M.J. The transmission of translation seat vibration to the head – II. Horizontal seat vibration. *J. Biomechanics*. **1988B,** 21, 199-206.

79. Paddan, G.S.; Griffin, M.J. The transmission of translational seat vibration to the head: the effect of measurement position at the head. *Proceedings of the Institute of Mechanical Engineers, Part H: Journal of Engineering in Medicine*. **1992,** 206, 159-168.

80. Paddan, G.S.; Griffin, M.J. Transmission of roll and pitch seat vibration to the head, *Ergonomics*. **1994,** 37(9), 1513-1531.

81. Paddan, G.S.; Griffin, M.J. Transmission of yaw seat vibration to the head, *Journal of Sound and Vibration*. **2000,** 229, 1077-1095.

82. Padgaonkar, A.J.; Krieger, K.W.; King, A.I. Measurement of angular acceleration of a rigid body using linear accelerometers. *Transactions of the ASME*. **1975,** 552-556.

83. Pope, M.H.; Wilder, D.G.; Magnusson, M.L. Possible mechanisms of low back pain due to whole-body vibration. *Journal of Sound and Vibration*. **1998,** 215(4), 576-586.

84. Preumont, A.; Horodinca, M.; Romanescu, I.; Marneffe, B.; Avraam, M.; Deraemaeker A.; Bossens, F.; Abu Hanieh, A. A six-axis single-stage active vibration isolator based on Stewart platform. *Journal of Sound and Vibration*. **2006**, 300, 644-661.

85. Qiu, Y.; Griffin, M.J. Transmission of fore-aft vibration to a car seat using field tests and laboratory simulation. *Journal of Sound and Vibration*. **2003,** 264, 135-155.

86. Qiu, Y.; Griffin, M.J. Transmission of vibration to the backrest of a car seat evaluated with multi-input models. *Journal of Sound and Vibration*. **2004,** 274, 297-321.

87. Rahmatalla, S.; DeShaw, J. Effective seat-to-head transmissibility in whole-body vibration: Effects of posture and arm position. *Journal of Sound and Vibration*. **2011,** 330(25), 6277-6286.

88. Rahmatalla, S.; DeShaw, J. Predictive Discomfort of Non-Neutral Head-Neck Postures in Fore-Aft Whole-Body Vibration. *Ergonomics*. **2011,** 54, 263-272.

89. Rahmatalla, S.; Smith, R.; Meusch, J.; Xia, T.; Marler, T.; Contratto, M. A quasi-static discomfort measure in whole-body vibration. *Industrial Health*. **2010,** 48, 645-653.

90. Rahmatalla, S.; Xia, T.; Contratto, M.; Kopp, G..; Wilder, D.; Frey-Law, L.; Ankrum, J. Three-dimensional Motion Capture Protocol for Seated Operators in Whole Body Vibration. *International Journal of Industrial Ergonomics*. **2008,** 38, 425-433.

91. Rahmatalla, S.; Xia, T.; Contratto, M.; Wilder, D.; Frey Law, L.; Kopp, G.; Grosland, N. 3D displacement, velocity, and acceleration of seated operators in a whole body vibration environment using optical motion capture systems. *In The Ninth International Symposium on the 3-D Analysis of Human Movement*. **2006,** Valenciennes, France.

92. Rakheja, S.; Boileau, P.E.; Stiharu, I. Seated occupant apparent mass characteristics under automotive postures and vertical vibration. *Journal of Sound and Vibration*. **2002,** 253, 57-75.

93. Rakheja, S.; Dong, R.G.; Patra, S.; Boileau, P.E.; Marcotte, P.; Warren, C. Biodynamics of the human body under whole-body vibration: Synthesis of the reported data. *International Journal of Industrial Ergonomics*. **2010,** 40, 710-732.

94. Rehn, B.; Nilsson, T.; Olofsson, B.; Lundstorm, R. Whole-Body Vibration exposure and non-neutral neck postures during occupational use of all-terrain vehicles. *The Annals of Occupational Hygiene*. **2005,** 49, 267-275.

95. Rehn, B.; Nilssonb, T.; Lundstro, R.; Hagbergd, M.; Burstro, L. Neck pain combined with arm pain among professional drivers of forest machines and the association with whole-body vibration exposure. *Ergonomics*. **2009,** 52, 1240-1247.

96. Sandover, J. Vibration, posture and low-back disorders of professional drivers. *Report Number DHS 402*, **1981,** Department of Human Sciences, University of Technology, Loughborough, England.

97. Schust, M.; Bluthner, R.; Seidel, H. Examination of perceptions (intensity, seat comfort, effort) and reaction times (brake and accelerator) during low-frequency vibration in x- or y-direction and biaxial (xy-) vibration of driver seats with activated and deactivated suspension. *Journal of Sound and Vibration*. **2006,** 298, 606-626.

98. Simoneaua, M.; Denninger, M.; Haind, T.C. Role of loading on head stability and effective neck stiffness and viscosity. *Journal of Biomechanics*. **2008,** 41, 2097–2103.

99. Smeathers, J. Measurement of transmissibility for the human spine during walking and running, *Clinical Biomechanics*. **1989,** 4, 34-40.

100. Smets, M.P.H.; Eger, T.; Grenier, S.G. Whole-body vibration experienced by haulage truck operators in surface mining operations: A comparison on various analysis methods utilized in the prediction of health risks. *Applied Ergonomics*. **2010,** 41, 763-770.

101. Smith, D.; Andrews, D.; Wawrow, P. Transmission characteristics of suspension seats in multi-axis vibration environment. *International Journal of Industrial Ergonomics*. **2008,** 38, 434-446.

102. Smith, S.D. The effects of head orientation on head/helmet vibration response. *SAFE Journal*. **2000,** 30, 114-125.

103. Subashi, G.H.M.J.; Nawayeh, N.; Matsumoto, Y.; Griffin, M.J. Nonlinear subjective and dynamic responses of seated participants exposed to horizontal whole-body vibration. *Journal of Sound and Vibration*. **2009,** 321, 416-434.

104. Thuresson, M.; Ang, B.; Linder, J.; Harms-Ringdahl, K. Mechanical load and EMG activity in the neck induced by different head-worn equipment and neck postures. *International Journal of Industrial Ergonomics* **2005,** 35, 13-18.

105. Verstraete, M.C.; Soutas-Little, R.W. A Method for Computing the Three-Dimensional Angular Velocity and Acceleration of a Body Segment From Three-Dimensional Position Data. *Transaction of the ASME*. **1990,** 112, 114-118.

106. Viviani, P.; Berthoz, A. Dynamics of the head-neck system in response to small perturbations. *Biol. Cybernetics*. **1975,** 19, 19-37.

107. Wang, W.; Rakheja, S.; Boileau, P.E. Effect of back support condition on seat to head transmissibilities of seated occupants under vertical vibration, *Journal of Low Frequency Noise, Vibration and Active Control*. **2006A,** 25, 239-259.

108. Wang, W.; Rakheja, S.; Boileau, P.E. Effects of sitting posture on biodynamic response of seated occupants under vertical vibration. *International Journal of Industrial Ergonomics*. **2004,** 34, 289-306.

109. Wang, W.; Rakheja, S.; Boileau, P.E. Relationship between measured apparent mass and seat-to-head transmissibility responses of seated occupants exposed to vertical vibration. *Journal of Sound and Vibration*. **2008,** 314, 907-922.

110. Wang, W.; Rakheja, S.; Boileau, P.E. The role of seat geometry and posture on the mechanical energy absorption characteristics of seated occupants under vertical vibration, *International Journal of Industrial Ergonomics*. **2006B,** 36, 171-184.

111. Waters, T.; Genaidy, A.; Viruet, H.B.; Makola, M. The impact of operating heavy equipment vehicles on lower back disorders. *Ergonomics*. **2008,** 51, 602-636.

112. Westhuizen, A.; Niekerk, J.L. Verification of seat effective amplitude transmissibility (SEAT) value as a reliable metric to predict dynamic seat comfort. *Journal of Sound and Vibration*. **2006,** 295, 1060-1075.

113. Whitham, E.M.; Griffin, M.J. The effects of vibration frequency and direction on the location of areas of discomfort caused by whole-body vibration. *Applied Ergonomics*. **1978,** 9, 231-239.

114. Wikstrom, B.O. Effects from twisted postures and whole-body vibration during driving. International Journal of Industrial Ergonomics. **1993,** 12, 61-75.

115. Wilder, D.G.; Pope, M.H. Epidemiological and aetiological aspects of low back pain in vibration environments – an update. *Clinical Biomechanics*. **1996,** 11(2), 61-73.

116. Wilder, D.G.; Pope, M.H; Magnusson, M. Mechical stress reduction during seated jolt/vibration exposure. *Seminars in Perinatology*. **1996,** 20, 54-60.

117. Wilder, D.G.; Woodworth, B.B.; Frymoyer, J.W.; Pope, M.H. Vibration and the Human Spine. *Spine*. **1982.** 7, 243-254.

118. Williams, E.J. Experimental designs balanced for the estimation of residual effects of treatments. *Australian Journal of Scientific Research*. **1949,** A2, 149-168.

119. Yoshimura, T.; Nakai, K.; Tamaoki, G. Multi-body Dynamics Modelling of Seated Human Body under Exposure to While-Body Vibration, *Industrial Health*. **2005,** 43, 411-447.

APPENDIX A: BORG CR-10 SCALE

Borg CR10 Scale	
0	Nothing at all
0.3	
0.5	Extremely Weak
0.7	
1	Very Weak
1.5	
2	Weak
2.5	
3	Moderate
4	
5	Strong
6	
7	Very Strong
8	
9	
10	Extremely Strong

Figure A.1 Borg CR-10 Scale used for measurement of self-reported discomfort. The scale ranges from 0 to 10 and has anchoring keywords with where higher values indicate higher exertion or discomfort. Because the reference value is zero at no vibration, the Borg CR-10 scale is an absolute scale and allows for the comparison between multiple postures and vibrational conditions.

APPENDIX B: INFORMED CONSENT DOCUMENT

FOR IRB USE ONLY
APPROVED BY: IRB-02
IRB ID #: 200811705
APPROVAL DATE: 11/20/12
EXPIRATION DATE: 07/14/13

INFORMED CONSENT DOCUMENT

Project Title: **Comfort Weighting Curve for Seated Machine Operators**

Principal Investigator: **Salam Rahmatalla**

Research Team Contact: **Salam Rahmatalla, 1 319 335-5614**
John Meusch
Jonathan DeShaw

This consent form describes the research study to help you decide if you want to participate. This form provides important information about what you will be asked to do during the study, about the risks and benefits of the study, and about your rights as a research subject.

- If you have any questions about or do not understand something in this form, you should ask the research team for more information.
- You should discuss your participation with anyone you choose such as family or friends.
- Do not agree to participate in this study unless the research team has answered your questions and you decide that you want to be part of this study.

WHAT IS THE PURPOSE OF THIS STUDY?

This is a research study. We are inviting you to participate in this research study because you are a healthy adult between the ages of 18 and 60 years old who does not have a history of muscle or bone disease or injury.

The purpose of this research study is to determine how operators move in whole-body vibration environments. These environments could include heavy machinery or simulated motion in a lab. Additionally, this study will try to relate the comfort you experience in the environment to the motion that is measured. The relationships found between comfort and motion will help seat manufacturers design more comfortable and safer seats.

The study may also investigate the motion of people in a supine position (laying down on back). People who are injured often need to be transported in emergency situations on a litter (stretcher type board and cot). This study will measure the motion of humans during vibration with the goal of achieving better designs to transport people in this laying down position.

Additionally, this study may investigate the motion and comfort of people seated in an agricultural tractor in the field. The information will help in understanding the best way to capture the motion of people in real life settings where there is vibration, such as when operating a tractor. The study can also provide important information about seat design for the equipment and potential health effects from the vibration itself.

HOW MANY PEOPLE WILL PARTICIPATE?

Approximately 100 people will take part in this study at the University of Iowa.

Figure B.1 Page 1 of Informed Consent Document

FOR IRB USE ONLY
APPROVED BY: IRB-02
IRB ID #: 200811705
APPROVAL DATE: 11/20/12
EXPIRATION DATE: 07/14/13

HOW LONG WILL I BE IN THIS STUDY?

If you agree to take part in this study, your involvement will last for 3-6 hours in a single visit with no follow-up. If there are technical problems, you may be scheduled for second visit to complete the study procedures.

WHAT WILL HAPPEN DURING THIS STUDY?

If you agree to participate, you will be scheduled to return to the Engineering Research Facility, 330 South Madison Street, Iowa City, Iowa the morning of the test day. Inside the facility, you will change into shorts and a tank-top so that the motion measurements can be obtained. The clothing will be supplied to you at the test site.

Preparation and Set-Up

Marker placement and calibration: Your body motion will be monitored using infrared cameras (VICON). Up to 90 reflective markers will be attached to your body. Each marker is about a half inch sphere attached to a soft rubber base of about 1 ½ inch x 1 ½ inch. The rubber base will be attached to your body using non-allergenic, double-sided tape. The markers on your head will be attached to an adjustable head band which you will wear on your head. Markers will be attached to your skin over bony landmarks, such as the elbow, the knee, the collar bone, or back bone. If you have considerable body hair, we will shave the small area of skin under each marker to minimize pain with removal of the markers. Markers may also be attached using athletic pre-wrap instead of adhesive tape. In some parts of the experiment, you may be dressed in a motion capture suit (a black cloth suit to which markers will be attached); in this case, the markers will be directly stuck to the suit instead of your skin.

Inertial sensors: Inertial sensors are devices that can measure acceleration in three and six directions. Inertial sensors are small devices that can sense movement. Inertial sensors will also be attached to your body at the same time the above markers are attached. Inertial sensors will be placed on you at up to 18 locations. You will be asked to wear a lycra-based suit which has spots for each sensor. For certain situations up to 5 inertial sensors may be attached to the skin using medical-grade, double-sided adhesive tapes, after cleaning the skin with rubbing alcohol.

The placement of the markers and inertial sensors will take about one to two hours.

In addition to the recordings for motion tracking, we will videotape the study procedure.

Testing

After this preparation stage, you will be instructed to sit on a chair or lay on a litter similar to those used in patient's transportation that is attached to a table that vibrates, called a shaker table. During the experiments, you will experience the physical conditions of a heavy construction machinery operator who is performing tasks in the real world or a person on a litter in an emergency transport vehicle.

Motion Capture Calibration: The first step in the motion capture process is to calibrate the system and ensure that the cameras see only the reflected markers (no artifact). The second step involves calibrating

Figure B.2 Page 2 of Informed Consent Document

FOR IRB USE ONLY
APPROVED BY: IRB-02
IRB ID #: 200811705
APPROVAL DATE: 11/20/12
EXPIRATION DATE: 07/14/13

you by having you stand still for 30 seconds. The motion capture system will use this information to obtain your measurements, such as the length of your legs and arms.

Task Simulation: In order for you to keep your attention focused, we may provide a task for you to work on.

Experimental Protocol:
You will be tested under one of the following conditions:

Condition A) You will be asked to sit in the shaker table chair. The experiments to be conducted will include using a shaker table to provide vibration typical of operation of common heavy equipment.

You may be tested under the following scenarios:

1. Back on seatback and hands on armrests
2. Back on seatback and hands on lap
3. Back on seatback and hands on steering wheel
4. Back off seatback and hands on lap, and looking back (twisted posture)
5. Back off seatback and hands on armrests, and looking back (twisted posture)
6. Back off seatback and hands on lap
7. Back off seatback and hands on steering wheel
8. Back off seatback and hands on armrests
9. In some of the above cases, you may be asked to sit on a seat with your trunk constrain to the seatback using a life-Vest jacket; however, your arms will be freely to move. The reason for these cases is to isolate your head-neck motion from your trunk motion. By doing this, we will be able to more accurately analyzing the contribution of your head-motion to your discomfort level.

In all above cases, your feet will remain on the ground/pedals.

Condition B) You will be asked to take a supine position on a litter with a backboard similar to those in patient's transportation.
The following procedure will be used as recommended by the Local EMS provider (Johnson County):

1. Apply an appropriate, effective and properly fitted/sized cervical collar.
2. Position participant on the long spine board and center.
3. Place straps in an x-pattern over the shoulders and under the armpits to secure the upper chest.
4. Additional straps are placed across the iliac crest and above the knees to prevent movement.
5. Normal Anatomical Alignment of the spine should be maintained.
6. Immobilize the head in the normal anatomical position. 1-1.5 inches of non-compressive occipital padding may be used.
7. Towel rolls or other bulky, lightweight material may be placed around the head to stabilize.
8. Place a wide strip of adhesive tape across the forehead to form an "X" securing the head.
9. Secure the feet with tape to prevent leg motion.

The following cases will be considered:

i. Using traditional backboard.
ii. Using traditional backboard with cushions.

Figure B.3 Page 3 of Informed Consent Document

FOR IRB USE ONLY
APPROVED BY: IRB-02
IRB ID #: 200811705
APPROVAL DATE: 11/20/12
EXPIRATION DATE: 07/14/13

Condition C) You will be asked to drive a large agricultural tractor pulling a tillage machine in an open field. The ground conditions will consist of corn stock stubble at approximately 1 foot tall. The tractor is equipped with all the standard safety measures such as seat belts for your use and a roll over protection cab.

You will be asked to maintain certain common postures during the study:

1. Facing forward with no backrest
2. Facing forward with use of backrest
3. Facing backward (to monitor equipment) with no backrest
4. Facing backward (to monitor equipment) with use of backrest
5. A dynamic posture (you will go between the seating positions)

We will conduct a series of tests to collect information about your body's responses to the movement of the shaker table seat and to test whether or not we are tracking the markers attached to you. You will experience up to 200 bouts of typical ride vibration on the shaker table each lasting up to 60 seconds with total of up to 100 minutes. The test will be repeated for each of the above two conditions. The "rides" will consist of vibration in one or multiple directions. Normally, up to 100 minutes (for each of the two above mentioned conditions) of that time will consist of exposure to typical "ride" vibration. If up to half of the tests need to be repeated, you could be exposed to up to 150 minutes of "ride" vibration.

In the event a test is stopped before all the data are collected or data are lost due to computer failure, the test will be repeated, up to a maximum of half of the possible tests. It is unlikely that more than one or two tests will actually require repetition, but all estimates of total daily vibration and shock exposure have included these additional tests. In the event data recording systems fail to acquire data during a test, the test will be repeated. This may take an additional six hours during a separate visit.

As mentioned above, it is possible that some tests may need to be further repeated in the event results are not stored properly (data lost due to computer error, etc.). The duration of the testing procedures should require no longer than 6 hours (with breaks). The expected total duration of exposure to the vibration is 100 minutes, but could be as high as 150 minutes in the event half of the tests require repeating.

During the tests, you will be asked by the investigators to rate your discomfort level either using verbal forms or paper based forms.

You may be asked to complete more visits if additional testing is required.

Audio/Video Recording or Photographs

One aspect of this study involves taking some pictures and video movies during the testing procedures. The motion capture cameras can only "see" infrared light reflected from markers. In addition to the motion capture camera images, we will take photographs and video of you using traditional still and video cameras to know where the markers are located on your body. The pictures and video movies will help us in identifying the location of the markers on the body during the experiments; otherwise, it would be very difficult to recognize the real markers' locations on the body by just looking to the

Figure B.4 Page 4 of Informed Consent Document

motion capture data. In the event these materials are used in reports or publications, the images will be altered so that no personally-identifiable information will appear.

These recordings and photographs will be used to document the test protocol. These recordings will not be erased or destroyed as they will provide valuable documentation of the study.

WHAT ARE THE RISKS OF THIS STUDY?

You may experience one or more of the risks indicated below from being in this study. In addition to these, there may be other unknown risks, or risks that we did not anticipate, associated with being in this study.

You may feel some irritation from the preparation for, the use of, and the removal of the reflective markers, and accelerometers. We will try to minimize this risk by using only medical-grade tape meant for use on human skin and shaving any areas that have substantial hair. We will try to make the time that the devices are attached as short as possible consistent with the data to be gathered. We will monitor you carefully by sight and by asking questions about how you feel. We will ask you if you are allergic to adhesive tape before placing the markers and accelerometers on your skin.

You may be at risk for developing dizziness. You will have a switch that will immediately stop the ride in the event you feel you need to stop. You can also take breaks as needed throughout the test protocol. We will monitor you carefully by sight and by asking questions about how you feel. If you are prone to motion sickness, have a history of vestibular (inner ear) problems, or do not tolerate simulation rides at Amusement Parks, you should not enroll in this study.

The vibration involved in this study may pose a risk for muscle or back pain with extended exposures. However, one day of testing is unlikely to result in any chronic vibration or shock injuries. The front to back vibrations you will experience should be no worse than those felt while riding a tractor on a rough field or operating typical heavy construction equipment for a period of time. We have analyzed the vibration for the conditions you will experience using international standards to be sure that the total exposure is within acceptable levels. If you have a history of neck or back pain, you should tell the researchers before enrolling in the study.

There is a risk that you could faint during the test. Sitting for extended periods of time, coupled with the simulated ride, could result in feeling like you could faint. Before fainting, people have reported experiencing weakness, lightheadedness, nausea, sweating, hyperventilation, blurred vision and/or impaired hearing. Sitting or lying down can reverse the symptoms. To minimize the risk of fainting, regular rest intervals are planned, where you will be asked to get up out of the seat and stand and move your arms and legs. Further you will be monitored closely for any signs of intolerance listed above, by sight and by asking questions about how you feel throughout the test. If you have any history of fainting or have a cardiac condition you should not enroll in this study.

If you have a history of neck or back pain, heart problems, neurological problems, balance problems or dizziness, motion sickness, or are taking over-the-counter drugs, prescribed drugs, or have consumed alcohol or recreational drugs within 24 hours of the study, you should not enroll in this study.

Figure B.5 Page 5 of Informed Consent Document

FOR IRB USE ONLY
APPROVED BY: IRB-02
IRB ID #: 200811705
APPROVAL DATE: 11/20/12
EXPIRATION DATE: 07/14/13

There is a risk that you may experience a fear of falling or being unable to maintain your balance in the seat. We will minimize this situation by monitoring you carefully by sight and by asking questions about how you feel. If you have any history of fear, then you should not enroll in this study.

If you participate in the field test condition, the noise from the tractor could pose a hearing risk or be distracting. To minimize this risk we will provide earplugs or ear muffs to reduce your sound exposure.

WHAT ARE THE BENEFITS OF THIS STUDY?

You will not benefit from being in this study. However, we hope that, in the future, other people might benefit from this study because the result of this study may help seat and machine designers to develop more comfortable seats for heavy machinery operators.

WILL IT COST ME ANYTHING TO BE IN THIS STUDY?

You will not have any cost for being in this research study.

WILL I BE PAID FOR PARTICIPATING?

You will be paid for being in this research study. You will need to provide your social security number (SSN) in order for us to pay you. You may choose to participate without being paid if you do not wish to provide your social security number (SSN) for this purpose. You may also need to provide your address if a check will be mailed to you. If your social security number is obtained for payment purposes only, it will not be retained for research purposes.

For the laboratory study, you will be paid at a rate of $12 per hour of a total of up to $72. The average amount per visit is $48.

For the field study, you will be paid at a rate of $15 per hour of a total of up to $90.

WHO IS FUNDING THIS STUDY?

The University and the research team are receiving no payments from other agencies, organizations, or companies to conduct this research study.

WHAT IF I AM INJURED AS A RESULT OF THIS STUDY?

- If you are injured or become ill from taking part in this study, medical treatment is available at the University of Iowa Hospitals and Clinics.
- No compensation for treatment of research-related illness or injury is available from the University of Iowa unless it is proven to be the direct result of negligence by a University employee.
- If you experience a research-related illness or injury, you and/or your medical or hospital insurance carrier will be responsible for the cost of treatment.

Figure B.6 Page 6 of Informed Consent Document

FOR IRB USE ONLY
APPROVED BY: IRB-02
IRB ID #: 200811705
APPROVAL DATE: 11/20/12
EXPIRATION DATE: 07/14/13

WHAT ABOUT CONFIDENTIALITY?

We will keep your participation in this research study confidential to the extent permitted by law. However, it is possible that other people such as those indicated below may become aware of your participation in this study and may inspect and copy records pertaining to this research. Some of these records could contain information that personally identifies you.

- federal government regulatory agencies,
- auditing departments of the University of Iowa, and
- the University of Iowa Institutional Review Board (a committee that reviews and approves research studies)

To help protect your confidentiality, we will assign you an identification number that does not include any personally identifiable information. All data will be stored on password-protected computer files using this number and not your name. Your name and personal information will be linked to your study identification number in a separate document and kept by the principal investigator in electronic and hard-copy formats separately from the rest of the data. All data will be kept in a locked lab or office or in password protected computer files, with appropriate backup. The motion data will be available to other researchers for future model development; however no personal identification of any kind will be linked to the data sets.

If we write a report or article about this study or share the study data set with others, we will do so in such a way that you cannot be directly identified.

IS BEING IN THIS STUDY VOLUNTARY?

Taking part in this research study is completely voluntary. You may choose not to take part at all. If you decide to be in this study, you may stop participating at any time. If you decide not to be in this study, or if you stop participating at any time, you won't be penalized or lose any benefits for which you otherwise qualify.

Will I Receive New Information About the Study while Participating?
If we obtain any new information during this study that might affect your willingness to continue participating in the study, we'll promptly provide you with that information.

Can Someone Else End my Participation in this Study?
Under certain circumstances, the researchers might decide to end your participation in this research study earlier than planned. This might happen because in our judgment it would not be safe for you to continue or because the funding for the research study has ended.

WHAT IF I HAVE QUESTIONS?

We encourage you to ask questions. If you have any questions about the research study itself, please contact: Salam Rahmatalla at (319) 335-5614 or salam-rahmatalla@uiowa.edu. If you experience a research-related injury, please contact Salam Rahmatalla at (319) 335-5614 or salam-rahmatalla@uiowa.edu. If you have questions, concerns, or complaints about your rights as a research subject or about research related injury, please contact the Human Subjects Office, 105 Hardin Library

Page 7 of 8

Figure B.7 Page 7 of Informed Consent Document

FOR IRB USE ONLY
APPROVED BY: IRB-02
IRB ID #: 200811705
APPROVAL DATE: 11/20/12
EXPIRATION DATE: 07/14/13

for the Health Sciences, 600 Newton Road, University of Iowa, Iowa City, IA 52242-1098, (319) 335-6564, or e-mail irb@uiowa.edu. General information about being a research subject can be found by clicking "Info for Public" on the Human Subjects Office web site, http://research.uiowa.edu/hso. To offer input about your experiences as a research subject or to speak to someone other than the research staff, call the Human Subjects Office at the number above.

This Informed Consent Document is not a contract. It is a written explanation of what will happen during the study if you decide to participate. You are not waiving any legal rights by signing this Informed Consent Document. Your signature indicates that this research study has been explained to you, that your questions have been answered, and that you agree to take part in this study. You will receive a copy of this form.

Subject's Name (printed): _____

Do not sign this form if today's date is on or after EXPIRATION DATE: 07/14/13 .

_____ _____
(Signature of Subject) (Date)

Statement of Person Who Obtained Consent

I have discussed the above points with the subject or, where appropriate, with the subject's legally authorized representative. It is my opinion that the subject understands the risks, benefits, and procedures involved with participation in this research study.

_____ _____
(Signature of Person who Obtained Consent) (Date)

Figure B.8 Page 8 of Informed Consent Document